SYNTHESIS AND CHARACTERIZATION OF ORGANIC SOLVENT AND CROSSLINKER FREE DRUG CARRIER NANOMATERIALS

A Thesis Submitted to
the Graduate School of
İzmir Institute of Technology
in Partial Fulfillment of the Requirements for the Degree of

DOCTOR OF PHILOSOPHY

in Materials Science and Engineering

by
Sümeyra Çiğdem SÖZER DEMİRDAŞ

December 2025
İZMİR

We approve the thesis of **Sümeyra Çiğdem SÖZER DEMİRDAŞ**

Examining Committee Members:

Prof. Dr. Yaşar AKDOĞAN
Department of Materials Science and Engineering, IZTECH

Assoc. Prof. Dr. Fatih TOPTAN
Department of Materials Science and Engineering, IZTECH

Assoc. Prof. Dr. Nermin Seda KEHR
Department of Chemistry, IZTECH

Assoc. Prof. Dr. Muhammed ÜÇÜNCÜ
Izmir International Biomedicine and Genome Institute, Dokuz Eylül University

Assoc. Prof. Dr. Gülşah EREL AKBABA
Department of Pharmaceutical Biotechnology, Izmir Katip Çelebi University

9 December 2025

Prof. Dr. Yaşar AKDOĞAN
Supervisor, Department of Materials Science and Engineering, IZTECH

Prof. Dr. Yaşar AKDOĞAN
Head of the Department of Materials Science and Engineering

Prof. Dr. Mehtap EANES
Dean of the Graduate School

ACKNOWLEDGEMENT

Firstly, I would like to express my sincere gratitude to my esteemed advisor, Prof. Dr. Yaşar Akdoğan, who has contributed significantly to my academic development throughout my graduate education, has been a constant companion with his scientific approach and guidance, and has shared his invaluable knowledge and experience with me since the very beginning of my graduate studies. I would also like to express my gratitude to Assoc. Prof. Dr. Fatih Toptan and Assoc. Prof. Dr. Nermin Seda Kehr, who served on my thesis monitoring committee and defence jury, for their invaluable contributions and guiding assessments during the thesis monitoring committee meetings we held throughout my doctoral studies. I would like to thank other members of the thesis committee, Assoc. Prof. Dr. Gülşah Erel Akbaba and Assoc. Prof. Dr. Muhammed Üçüncü for their valuable comments and suggestions.

I would like to thank Asst. Prof. Dr. Gülçin Çakan-Akdoğan from the Izmir International Biomedicine and Genome Institute (IBG, Dokuz Eylül University) for their scientific and technical contributions to the experimental stages of this study, as well as for their collaborative research and inspiring collaboration. Also, I would like to thank Özlem Erez for her contributions to the cell uptake and cell viability studies, and Aytül Gül-Mete for her support in the production and loading of mRNA, as well as their invaluable contributions to the conduct of the experiments.

I would like to thank Prof. Dr. Mustafa Muammer Demir and DEMİR's Lab for DLS and zeta analyses. I would like to thank Yekta Günay and Dr. Murat Delman from IZTECH, the biotechnology and bioengineering application and research center (BIYOMER) for their kind assistance with the experiments lyophilization and ATIR-FTIR experiments, respectively. I also thank Dr. Zehra Sinem Yılmaz, Duygu Oğuz Kılıç, and Mutlu Devran Yaman from IZTECH, the materials research center (MAM) for conducting the SEM analyses.

I would like to express my sincere gratitude for the financial support provided by the TÜBİTAK 2211-C Fellowship Program, which has significantly contributed to the progress and successful completion of this study. This work was financially supported by the Scientific and Technological Research Council of Turkey (TUBITAK) via the 1001 Program under grant 118Z341 and 1002 Program under grant 119Z136. Additional support was provided by the Izmir Institute of Technology Scientific Research Projects

Coordination Unit via the 2022IYTE-3-0035 and Health Institutes of Türkiye (TUSEB) via 2024-B-01-4001.

I would like to express my endless gratitude to my dear husband, Berat Demirdaş, who is my greatest source of support, companion, and motivation throughout my life and throughout this process, for his patience, love, and moral support throughout my academic life. I am so grateful to have you.

And my dear son, who holds a special place in my heart, whose presence I felt every day throughout the thesis writing process, who gave me great hope and meaning for the future, you give me strength even though you haven't joined us yet. Writing this thesis, while I eagerly await your arrival, has been the greatest motivation in my life. Thank you for inspiring me in this step I've taken to leave you a healthy and bright future.

I am eternally grateful to my family, who have always supported me unconditionally throughout this challenging doctoral process and stood by me with their love and belief. I extend my deepest gratitude to my mother, Gülşen Sözer, and my father, Ahmet Sözer, for their moral support and strength throughout this process. I would also like to express my gratitude to my dear sister, İpek Keleşoğlu, my brother, Haşim Keleşoğlu, who have supported me throughout my academic career and who have always been there for me, and to my nephew, Kemal Keleşoğlu, who has energized me and always brought me joy with his presence.

My dear laboratory colleagues and colleagues, with whom I worked throughout my PhD studies, who have always helped me with experiments, and who have made this process more supportable and enjoyable with their scientific conversations and support, I extend my heartfelt gratitude to my lab mates Cansu Akyol Karpuzcu, Eda Argıtekin and Kardelen Aytekin. Also, my dear colleagues Merve Karakaya, Ezgi Oğur, Tuğçe Özmen, Utku Hatipoğlu, and Oğuz Akkaş for their support, positive inputs and friendship throughout every stage of this process. My doctoral process was shaped much more effectively thanks to our scientific collaborations and the time we spent together. I'm so glad they were here.

ABSTRACT

SYNTHESIS AND CHARACTERIZATION OF ORGANIC SOLVENT AND CROSSLINKER FREE DRUG CARRIER NANOMATERIALS

Serum albumin is preferred to produce nanoparticles (NPs) in drug delivery systems due to its high biocompatibility and carrier capacity. Conventional albumin nanoparticle (NP) preparation methods, such as desolvation and emulsification, typically rely on toxic organic solvents and crosslinkers like glutaraldehyde, which limit water-insoluble drug loading and therapeutic potential. This thesis aimed to overcome these limitations by producing albumin–albumin polyelectrolyte complex nanoparticles (PEC NPs) via a green chemical process. In the first part, the solubility behaviour of drugs with different aqueous solubilities (salicylic acid (high), ibuprofen (low), and chlorambucil (none)) was investigated using electron paramagnetic resonance (EPR) spectroscopy. Results revealed that albumin NPs were significantly more effective than albumin proteins in dissolving hydrophobic drugs in water. Moreover, drug release could be directly monitored from NP pellet dissolution by EPR, offering an advantage over conventional techniques. In the second part, albumin PEC NPs were synthesized by electrostatic interaction of cationic and anionic albumins without solvents, crosslinkers, or specialized equipment. The obtained albumin PEC NPs (110 nm, +37 mV) enabled up to 17-fold higher chlorambucil loading compared to the desolvation, mainly due to avoiding drug loss to organic solvents. Chlorambucil loaded albumin PEC NPs also reduced Huh-7 cell viability to 44% within 24 h. In the third part, albumin PEC were further processed into hydrogel systems, demonstrating their potential for sustained release and local delivery applications. Overall, this study highlights albumin PEC NPs as a simple, green, and effective strategy for producing highly drug-loaded nanocarriers suitable for advanced drug delivery applications.

ÖZET

ORGANİK ÇÖZÜCÜ VE ÇAPRAZ BAĞLAYICI İÇERMEYEN İLAÇ TAŞIYICI NANOMALZEMELERİN SENTEZİ VE KARAKTERİZASYONU

Serum albümini, yüksek biyouyumluluğu ve taşıyıcı kapasitesi nedeniyle ilaç taşıyıcı sistemlerinde nanoparçacık (NP) üretmek için tercih edilmektedir. Desolvasyon ve emülsifikasyon gibi geleneksel albümin NP'leri hazırlama yöntemleri, genellikle suda çözünmeyen ilaç yüklemesini ve terapötik potansiyelini sınırlayan toksik organik çözücülere ve glutaraldehit gibi çapraz bağlayıcılara dayanır. Bu tez, yeşil kimyasal bir süreçle albümin-albümin polielektrolit kompleks nanoparçacıkları (PEC NP'leri) üreterek bu sınırlamaların üstesinden gelmeyi amaçlamıştır. İlk bölümde, farklı sulu çözünürlüklere sahip ilaçların (salisilik asit (yüksek), ibuprofen (düşük) ve klorambusil (hiç yok)) çözünürlük davranışları elektron paramanyetik rezonans (EPR) spektroskopisi kullanılarak incelenmiştir. Sonuçlar, albümin NP'lerinin hidrofobik ilaçları suda çözmede albümin proteininden önemli ölçüde daha etkili olduğunu göstermiştir. Ayrıca, ilaç salımı EPR ile NP pelet çözünmesinden doğrudan izlenebilmekte ve bu da geleneksel tekniklere göre bir avantaj sağlamaktadır. İkinci bölümde, albümin PEC NP'leri, çözücüler, çapraz bağlayıcılar veya özel ekipman olmadan katyonik ve anyonik albüminlerin elektrostatik etkileşimi ile sentezlenmiştir. Elde edilen albümin PEC NP'leri (110 nm, +37 mV), büyük ölçüde organik çözücülere ilaç kaybının önlenmesi nedeniyle, desolvasyon yöntemine kıyasla 17 kata kadar daha yüksek klorambusil yüklemesine olanak sağlamıştır. Klorambusil yüklü albümin PEC NP'leri ayrıca Huh-7 hücre canlılığını 24 saat içinde %44'e düşürmüştür. Üçüncü bölümde, albümin PEC hidrojel sistemlerine dönüştürülerek, sürekli salım ve lokal salım uygulamaları için potansiyel olarak uygulanabilirliğini göstermektedir. Genel olarak bu çalışma albümin PEC NP'lerini, yeşil kimya ile basit bir şekilde üreterek yüksek oranda ilaç yüklü nanotaşıyıcılar ve gelişmiş ilaç salım uygulamaları için uygun ve etkili bir strateji olduğu vurgulamaktadır.

TABLE OF CONTENTS

TABLE OF CONTENTS vii

LIST OF FIGURES x

LIST OF TABLES xx

CHAPTER 1. INTRODUCTION 1

1.1. Overview, Structure and Scope of Thesis 1

CHAPTER 2. WATER SOLUBILITY AND BINDING BEHAVIOR OF SPIN-LABELED DRUGS IN ALBUMIN-BASED SYSTEMS 3

2.1. Introduction 3

2.2.1. Materials 6

2.2.2. Preparation of cationic bovine serum albumin (cBSA) proteins 6

2.2.3. Preparation of cBSA and BSA nanoparticles 7

2.2.4. Characterizations of cBSA proteins, cBSA NPs and BSA NPs 7

2.2.5. Synthesis of spin labeled salicylic acid (SLSA) 8

2.2.6. Synthesis of spin labeled ibuprofen (SLIbf) 8

2.2.7. Synthesis of spin labeled chlorambucil (SLChl) 8

2.2.8. Solubility measurements of SLDrugs by EPR spectroscopy 9

2.2.9. Solubility measurements of SLDrugs by UV-Vis spectroscopy 9

2.2.10. SLSA Loading: Addition of drugs before desolvation and after NPs formation (incubation) 9

2.3. Results and Discussion 10

2.4. Conclusion 32

CHAPTER 3. A GREEN ROUTE TO ALBUMIN/ALBUMIN POLYELECTROLYTE COMPLEX NANOPARTICLES IN WATER WITH HIGH DRUG LOADING FOR DRUG DELIVERY 34

3.1. Introduction 34
3.2. Materials and Methods 37
3.2.1. Materials 37
3.2.2. Preparation of cationic bovine serum albumin protein (cBSA) 37
3.2.3. Preparation of albumin PEC NPs 37
3.2.3.1. Concentration Effect 38
3.2.3.2. Crosslinking Effect 39
3.2.3.3. Heating Effect 39
3.2.4. Characterization of albumin PEC NPs 39
3.2.5. Biodegradation test 40
3.2.6. Chlorambucil loading into albumin PEC NPs via incorporation method 40
3.2.7. Chlorambucil loading into albumin PEC NPs via incubation method 41
3.2.8. Chlorambucil loading into BSA NPs via desolvation method 41
3.2.9. Measuring the percentages of entrapment efficiency and drug loading 41
3.2.10. In vitro release of CHL from albumin PEC NPs 42
3.2.11. PEG Coating of Albumin PEC NPs 42
3.2.12. Cell Uptake and Imagining 43
3.2.13. Cell Viability Assay 43
3.2.14. mRNA Loading on albumin PEC NPs 44
3.3. Results and Discussion 45
3.4. Conclusion 64

CHAPTER 4. ALBUMIN POLYELECTROLYTE HYDROGEL COMPLEX FORMATION FOR THERAPEUTIC SYSTEMS 66

4.2. Materials and Methods 71
4.2.1. Materials 71
4.2.2. Preparation of cationic bovine serum albumin protein (cBSA) 71
4.2.3. Preparation of albumin PEC hydrogels 72
4.2.4. Characterization of albumin PEC hydrogels 72
4.2.4.1. Rheological Characterization 72

4.2.4.2. Fourier Transform Infrared Spectroscopy Measurements..... 73
4.2.4.3. Scanning Electron Microscopy 74
4.3. Results and Discussion 74
4.4. Conclusion 80

CHAPTER 5. CONCLUSION AND FUTURE DIRECTIONS..... 82

REFERENCES 84

LIST OF FIGURES

Figure **Page**

Figure 2.1. Molecular structures of spin labeled drugs: (A) spin labeled salicylic acid (SLSA), (B) spin labeled ibuprofen (SLIbf) and (C) spin labeled chlorambucil (SLChl) (Sozer and Akdogan, 2022). 5

Figure 2.2. EPR spectrum of 4.9 mM of SLIbf in the presence of 0.7 mM of BSA protein in water (black) and its corresponding simulation (dashed red) obtained upon addition of simulations of unbound, bound and undissolved SLIbf (red) spectra after multiplication with appropriate numbers (Sozer and Akdogan, 2022). 11

Figure 2.3. EPR spectra of 4.9 mM of 4-Amino Tempo, SLSA, SLIbf and SLChl in DMSO (A) and in water (B). The asterisks mark a broad spectral component (Sozer and Akdogan, 2022). 12

Figure 2.4. EPR spectra of 4.9 mM of 4-Amino Tempo, SLSA, SLIbf and SLChl (black) dissolved in DMSO and their corresponding simulations (red) (Sozer and Akdogan, 2022). 12

Figure 2.5. EPR spectra of 4.9 mM of (A) 4-Amino Tempo (black) and (B) SLSA (black) dissolved in water and their corresponding simulations (red) (Sozer and Akdogan, 2022). 14

Figure 2.6. (A) EPR spectra of 4.9 mM of SLIbf (black) and its total simulation (dashed red) obtained by combination of dissolved and undissolved SLSA EPR simulations (red) after multiplication with the appropriate numbers. (B) Double integrations of the spectra in (A). (C) EPR spectra of 0.5 mM SLIbf (black) and its total simulation (dashed red) obtained by combination of dissolved and undissolved SLSA EPR simulations (red) after multiplication with the appropriate numbers. (D) Double integrations of the spectra in (C) (Sozer and Akdogan, 2022). 15

Figure 2.7. EPR spectrum of 0.5 mM of SLChl in water (Sozer and Akdogan, 2022). 15

Figure **Page**

Figure 2.8. MALDI-TOF mass spectra of BSA (black) and cationic BSA (cBSA) (red) proteins (Sozer and Akdogan, 2022). 16

Figure 2.9. SEM images of BSA NPs (A) and cBSA NPs (B). Scale bar = 1 μm (Sozer and Akdogan, 2022). 17

Figure 2.10. EPR spectra of 4.9 mM of SLSA in water (bottom) and upon additions of 0.7 mM of BSA (middle) and BSA NPs (top) (A), and 0.7 mM of cBSA (middle) and cBSA NPs (top) (B) (Sozer and Akdogan, 2022). 18

Figure 2.11. (A) EPR spectra of 4.9 mM of SLSA in the presence of 0.7 mM BSA (black) and its total simulation (dashed red) obtained by combination of bound and unbound SLSA EPR simulations (red) after multiplication with the appropriate numbers. (B) % of double integrations of the spectra in (A). (C) 4.9 mM of SLSA in the presence of 0.7 mM BSA NPs (black) and its total simulation (dashed red) obtained by combination of bound and unbound SLSA EPR simulations (red) after multiplication with the appropriate numbers. (D) % of double integrations of the spectra in (C). They are normalized to the double integration of the experiment (Sozer and Akdogan, 2022). 19

Figure 2.12. (A) EPR spectra of 4.9 mM of SLSA in the presence of 0.7 mM cBSA (black) and its total simulation (dashed red) obtained by combination of bound and unbound SLSA EPR simulations (red) after multiplication with the appropriate numbers. (B) % of double integrations of the spectra in (A). (C) 4.9 mM of SLSA in the presence of 0.7 mM cBSA NPs (black) and its total simulation (dashed red) obtained by combination of bound and unbound SLSA EPR simulations (red) after multiplication with the appropriate numbers. (D) % of double integrations of the spectra in (C). They are normalized to the double integration of the experiment (Sozer and Akdogan, 2022). 20

Figure 2.13. EPR spectra of 4.9 mM of SLIbf in water (bottom) and upon addition of 0.7 mM of BSA (middle) and BSA NPs (top) (A), and 0.7 mM of cBSA (middle) and cBSA NPs (top) (B) (Sozer and Akdogan, 2022). 21

Figure **Page**

Figure 2.14. (A) EPR spectra of 4.9 mM of SLIbf in the presence of 0.7 mM BSA (black) and its total simulation (dashed red) obtained by combination of bound and unbound SLIbf EPR simulations (red) after multiplication with the appropriate numbers. (B) % of double integrations of the spectra in (A). (C) 4.9 mM of SLIbf in the presence of 0.7 mM BSA NPs (black) and its total simulation (dashed red) obtained by combination of bound and unbound SLIbf EPR simulations (red) after multiplication with the appropriate numbers. (D) % of double integrations of the spectra in (C). They are normalized to the double integration of the experiment (Sozer and Akdogan, 2022)..... 22

Figure 2.15. (A) EPR spectra of 4.9 mM of SLIbf in the presence of 0.7 mM cBSA (black) and its total simulation (dashed red) obtained by combination of bound and unbound SLIbf EPR simulations (red) after multiplication with the appropriate numbers. (B) % of double integrations of the spectra in (A). (C) 4.9 mM of SLIbf in the presence of 0.7 mM cBSA NPs (black) and its total simulation (dashed red) obtained by the combination of bound and unbound SLIbf EPR simulations (red) after multiplication with the appropriate numbers. (D) % of double integrations of the spectra in (C). They are normalized to the double integration of the experiment (Sozer and Akdogan, 2022)..... 23

Figure 2.16. EPR spectra of 1.4 mM of SLChl in water (bottom) and upon addition of 0.7 mM of BSA (middle) and BSA NPs (top) (A), and 0.7 mM of cBSA (middle) and cBSA NPs (top) (B) (Sozer and Akdogan, 2022)..... 24

Figure **Page**

Figure 2.17. (A) EPR spectra of 1.4 mM of SLChl in the presence of 0.7 mM BSA (black) and its total simulation (dashed red) obtained by combination of bound and unbound SLChl EPR simulations (red) after multiplication with the appropriate numbers. (B) % of double integrations of the spectra in (A). (C) 1.4 mM of SLChl in the presence of 0.7 mM BSA NPs (black) and its total simulation (dashed red) obtained by combination of bound and unbound SLChl EPR simulations (red) after multiplication with the appropriate numbers. (D) % of double integrations of the spectra in (C). They are normalized to the double integration of the experiment (Sozer and Akdogan, 2022). 25

Figure 2.18. (A) EPR spectra of 1.4 mM of SLChl in the presence of 0.7 mM cBSA (black) and its total simulation (dashed red) obtained by combination of bound and unbound SLChl EPR simulations (red) after multiplication with the appropriate numbers. (B) % of double integrations of the spectra in (A). (C) 1.4 mM of SLChl in the presence of 0.7 mM cBSA NPs (black) and its total simulation (dashed red) obtained by combination of bound and unbound SLChl EPR simulations (red) after multiplication with the appropriate numbers. (D) % of double integrations of the spectra in (C). They are normalized to the double integration of the experiment (Sozer and Akdogan, 2022). 26

Figure 2.19. UV-Vis spectra of 0.32 mM SLSA, SLChl and SLIbf in water:ethanol (1:1 v/v) mixture (Sozer and Akdogan, 2022). 27

Figure 2.20. Calibration curves and equations for SLSA (A), SLChl (B) and SLIbf (C) using UV-Vis spectroscopy in water:ethanol (1:1 v/v) solution (Sozer and Akdogan, 2022). 28

Figure **Page**

Figure 2.21. (A) SLSA loading was performed before desolvation: EPR spectra of 1.1 mM of SLSA in 0.15 mM of BSA NPs and 0.7 mM of SLSA in 0.1 mM of cBSA NPs solutions (mixtures), supernatant and pellet aqueous solutions, and their corresponding double integration values. (B) SLSA loading after nanoparticle formation via incubation method: EPR spectra of 0.7 mM of SLSA in 0.1 mM of BSA NPs or cBSA NPs solutions (mixtures), supernatant and pellet aqueous solutions, and their corresponding double integration values (Sozer and Akdogan, 2022). 30

Figure 2.22. (A) EPR spectra of SLSA loaded cBSA NPs aqueous solution in a dialyzer tube as a function of time at 37 °C. SLSA was loaded via incubation method. The initial loaded SLSA concentration is 0.49 mM in cBSA NPs (0.07 mM) aqueous solution. (B) The bound SLSA release profile of cBSA NPs with time upon taking double integrations of spectra in (A) (red). The bound SLSA did not release if the SLSA was added before nanoparticle formation (desolvation) (black) (Sozer and Akdogan, 2022). 31

Figure 3.1. Schematic representation of chlorambucil (CHL) loaded albumin polyelectrolyte complex (PEC) nanoparticles (NPs) synthesis in water, without using organic solvents and crosslinkers. BSA: Bovine serum albumin, cBSA: Cationic bovine serum albumin (Sozer-Demirdas, et al. 2025). 36

Figure 3.2. Schematic representation of cBSA:BSA polyelectrolyte complex (PEC) formation and PEC nanoparticle (PEC NP) synthesis under different conditions: (A) PEC formation by mixing BSA and cBSA proteins without crosslinking at room temperature (RT), (B) PEC NP synthesis via glutaraldehyde crosslinking at RT, and (C) PEC NP synthesis without crosslinking at 80°C. 38

Figure 3.3. The zeta potentials of BSA (black) and cationic BSA (cBSA) (red) proteins were measured in distilled water (Sozer-Demirdas et al., 2025). 45

Figure **Page**

Figure 3.4. Turbidity (100 - T%) versus molar ratios of a system containing cBSA:BSA in different molar ratios (Sozer-Demirdas et al., 2025)..... 46

Figure 3.5. SEM images of albumin PEC NPs producing with different albumin concentrations; (A) 3.2 mg/mL, (B) 12.2 mg/mL and (C) 24.6 mg/mL (Sozer-Demirdas et al., 2025)..... 46

Figure 3.6. (A) SEM image of albumin PEC NPs prepared in water without glutaraldehyde and organic solvents. (B) Hydrodynamic particle size distribution and (C) zeta potential of albumin PEC NPs obtained from DLS measurements. Sample was prepared with 1:3.5 molar ratio of cBSA:BSA at 6.5 mg/mL total albumin concentration (Sozer-Demirdas et al., 2025). 47

Figure 3.7. (A) SEM image of albumin PEC NPs crosslinked with glutaraldehyde in water system. (B) Particle size distribution and (C) zeta potential results of albumin PEC NPs obtained by DLS measurements. (1:3.5 molar ratio of cBSA:BSA, 6.5 mg/mL albumin concentration)..... 48

Figure 3.8. Images of albumin PEC NPs produced at different preparation temperatures (Sozer-Demirdas et al., 2025). 49

Figure 3.9. (A) SEM image of albumin PEC NPs and (B) particle size distribution obtained from the SEM image (A). (C) DLS results of the hydrodynamic size distribution of albumin PEC NPs in PBS at pH 7.4. (D) Zeta potential of the albumin PEC NPs in water. Albumin PEC NPs were prepared at 80 °C (Sozer-Demirdas et al., 2025). 49

Figure 3.10. (A) SEM images of albumin PEC NPs prepared at 60 °C, 70 °C, and 90 °C. (B) Hydrodynamic particle size distribution and (C) zeta potential of albumin PEC NPs prepared at 60 °C, 70 °C and 90 °C. Samples were prepared with 1:3.5 M ratio of cBSA:BSA at 6.5 mg/mL total albumin concentration (Sozer-Demirdas et al., 2025)..... 50

Figure 3.11. DLS results of hydrodynamic size distributions, PDI and zeta potential values of albumin PEC NPs produced at 80 °C in water at different pH values; 3.0 (A, B), 7.0 (C, D) and 9.0 (E, F) within 28 days (Sozer-Demirdas et al., 2025). 51

Figure **Page**

Figure 3.12. (A) The concentrations of the albumin PEC NPs (μg/mL) in PBS (black line) and in trypsin (50 μg/mL) containing PBS (red line) within 27 hours. (B) Calibration curve obtained from the turbidity results of albumin PEC NPs at different concentrations at 565 nm using UV-Vis absorption spectroscopy (Sozer-Demirdas et al., 2025). 52

Figure 3.13. (A) CHL encapsulation efficiency (wt%) results and (B) CHL loading (wt%) results of albumin PEC NPs and classical BSA NPs (blue) with respect to the initial mole ratio of albumin:CHL. CHL loading was performed via incorporation (black) or incubation (red) methods. (C) SEM image of CHL loaded albumin PEC NPs prepared via incorporation method at albumin:CHL molar ratio 1:5. (D) The cumulative percentages of CHL released from the albumin PEC NPs (black) prepared via incorporation method with the 1:5 (albumin:CHL) molar ratio and the cumulative percentages of free CHL release (red) after 30 h (Sozer-Demirdas et al., 2025)..... 53

Figure 3.14. (A) Hydrodynamic size distribution and (B) zeta potential value of conventional BSA NPs (black) and CHL loaded conventional BSA NPs (red) produced by desolvation method followed by glutaraldehyde crosslinking (Albumin:CHL molar ratio 1:5) (Sozer-Demirdas et al., 2025). 54

Figure 3.15. SEM images of CHL loaded albumin PEC NP preparation with incorporation method; (A) 1:1 molar ratio, (B) 1:3 molar ratio, (C) 1:5 molar ratio, and with incubation method; (D) 1:1 molar ratio, (E) 1:3 molar ratio, (F) 1:5 molar ratio (Sozer-Demirdas et al., 2025). 55

Figure 3.16. DLS results of albumin PEC NPs and CHL loaded albumin PEC NPs prepared with incorporation method (A) and incubation method (C). Zeta potential results of albumin PEC NPs and CHL loaded albumin PEC NPs prepared with incorporation method (B) and incubation method (D) (Sozer-Demirdas et al., 2025). 56

Figure **Page**

Figure 3.17. DLS results showing the hydrodynamic size distribution of (A) albumin PEC NPs (black) and PEG coated albumin PEC NPs (red), (B) CHL loaded albumin PEC NPs using incorporation method (black) and PEG coated CHL loaded albumin PEC NPs using incorporation method (red), (C-D) Corresponding zeta potential values of (Alb:CHL molar ratio 1:5). SEM images of PEG coated albumin PEC NPs (E) and PEG coated CHL loaded albumin PEC NPs using incorporation method (Albumin:CHL molar ratio 1:5) (F) (Sozer-Demirdas et al., 2025)..... 58

Figure 3.18. (A) Huh-7 cellular uptake of 12.5 μg/mL PEG coated CHL loaded FITC labeled albumin PEC NPs (green) for 24 h of treatment. Huh-7 cells were stained with CM-Dil (red) vital dye. At the end of the treatment, cell nuclei were stained with DAPI (blue). Scale bar = 50 μm. (B) Huh-7 cell viability and (C) HEK293T cell viability upon addition of PEG coated albumin PEC NPs (black), PEG coated CHL loaded albumin PEC NPs via incorporation method (red), or the free CHL in the same amount as that carried by the albumin PEC NPs based on the drug loading efficiency of 6.4 wt% (blue) at different concentrations after 24 h of incubation. Error bars represent ± SD, ns: non-significant, * $P \leq 0.05$, ** $P \leq 0.01$, *** $P \leq 0.001$, **** $P \leq 0.0001$ (Sozer-Demirdas et al., 2025)..... 59

Figure 3.19. (A) Huh-7 cellular uptake of 12.5 μg/mL PEG coated FITC labeled albumin PEC NPs (green) for 24 h of treatment. (B) Huh-7 cellular uptake of 12.5 μg/mL FITC labeled BSA NPs (green) prepared via desolvation method for 24 h of treatment. Huh-7 cells were stained with CM-Dil (red) vital dye. At the end of the treatment, cell nuclei were stained with DAPI (blue). Scale bar = 50 μm. The arrows point the NPs (Sozer-Demirdas et al., 2025). 60

Figure **Page**

Figure 3.20. MCF-7 cell viability upon addition of PEG coated albumin PEC NPs (black), PEG coated CHL loaded albumin PEC NPs via incorporation method (red), or the free CHL in the same amount as that carried by the albumin PEC NPs based on the drug loading efficiency of 6.4 wt% (blue) at different concentrations after 24 h of incubation. Error bars represent ± SD, ns: non-significant, * P ≤0.05, ** P ≤0.01, *** P ≤0.001, **** P ≤0.0001 (Sozer-Demirdas et al., 2025). 61

Figure 3.21. DLS results showing the hydrodynamic size distribution of (A) albumin PEC NPs (black) and mRNA loaded albumin PEC NPs (266:1 mol ratio) (red), (C) mRNA loaded albumin PEC NPs at different molar ratios; 26:1 (blue), 13:1 (pink) and 2.6:1 (green), and albumin PEC NPs (black) (B and D) Corresponding zeta potential values. 64

Figure 4.1. Gelation behavior of cBSA:BSA (1:1, pH 6) complex solutions under different conditions; (A) Liquid form of 20 wt% albumin PEC sample at room temperature, (B) Hydrogel form of the same sample after 2 hours of incubation at 37 °C, (C) Comparison of gelation of samples prepared at 15, 17.5 and 20 wt% total protein ratios after 2 hours of incubation at 37 °C. 75

Figure 4.2. (A) Frequency-dependent variation of storage modulus (G′) and loss modulus (G″) of 20 wt% albumin PEC hydrogel, plotted as a function of logarithmic frequency (Hz). (B) The loss ratio, tan(δ) and (C) Complex viscosity (η*) as a function of logarithmic frequency. (D) Comparison of average Young's modulus values in the 1-10 Hz and 10–100 Hz logarithmic frequency ranges. 77

Figure 4.3. SEM images obtained from 20 wt% albumin PEC hydrogel solution at pH 6 and incubated for 2 hours at 37 °C. (A, B) Microstructure showing the porous and layered morphology of the hydrogel (C) nanometer-scale smooth surface regions and transitional pore structure (A portion of the sample was cut and dried at RT for 24h). 79

Figure **Page**

Figure 4.4. The FTIR spectra of BSA (black), cBSA (red) and albumin PEC (blue) hydrogel powder. 79

LIST OF TABLES

Table **Page**

Table 2.1. Simulated EPR parameters of 4-Amino Tempo, SLSA, SLIbf and SLChl dissolved in DMSO (4.9 mM) (Sozer and Akdogan, 2022). 13

Table 2.2. Simulated EPR parameters of 4-Amino Tempo, SLSA and SLIbf dissolved in water (4.9 mM) (Sozer and Akdogan, 2022). 14

Table 2.3. Percentages of undissolved, dissolved-unbound and dissolved-bound 4.9 mM of SLSA and SLIbf, and 1.4 mM of SLChl in water, and upon addition of 0.7 mM of BSA, BSA NPs, cBSA or cBSA NPs determined by EPR spectroscopy (Sozer and Akdogan, 2022). 33

Table 3.1. Encapsulation efficiencies of mRNA loaded albumin PEC NPs obtained by Nanodrop spectrophotometer. 62

Table 4.1. Areas of use of albumin-based hydrogels in cancer treatment. 68

Table 4.2. Areas of use of albumin-based hydrogels in tissue regeneration engineering. 69

ABBREVIATIONS

BSA	Bovine Serum Albumin
cBSA	Cationic Bovine Serum Albumin
BSA NPs	Bovine Serum Albumin Nanoparticles
cBSA NPs	Cationic Bovine Serum Albumin Nanoparticles
PEC NPs	Polyelectrolyte Complex Nanoparticles
CHL	Chlorambucil
SLChl	Spin Labelled Chlorambucil
SLSA	Spin Labelled Salicylic Acid
SLIbf	Spin Labelled Ibuprofen
EPR	Electron Paramagnetic Resonance Spectroscopy
PEG	Polyethylene Glycol
SEM	Scanning Electron Microscopy
UV-Vis	Ultraviolet-Visible
ATR-FTIR	Attenuated Total Reflectance-Fourier Transform Infrared
DLS	Dynamic Light Scattering

CHAPTER 1

INTRODUCTION

1.1. Overview, Structure and Scope of Thesis

There has been considerable interest in using nanoparticles (NPs) as carriers in drug delivery systems. They offer several advantages, including gradual and controlled release, preservation of pharmaceutical activity, and efficient targeting of hydrophilic and hydrophobic drugs. According to the Nanotechnology Initiative (NNI), nanotechnology is typically defined within the range of 1 to 100 nanometers, although this can be extended up to 1000 nanometers. Specific targeting, controlled drug release, non-toxicity, and biodegradability are key characteristics of an ideal nanoparticle-based delivery system.

Albumin based nanocarrier systems have long attracted attention in drug delivery applications owing to their biocompatibility, biodegradability, and high drug binding capacity (Elzoghby et al., 2012). Serum albumin is a suitable platform for controlled-release systems due to the presence of numerous binding sites that can bind both hydrophilic and hydrophobic drugs (Ghuman et al., 2005). In addition, the amino, thiol, and carboxyl groups on its surface are amenable to functionalization, allowing the addition of targeting ligands (Singh et al., 2012). Conventional methods for albumin nanoparticle synthesis include desolvation and emulsification, which are among the most widely applied approaches (Langer et al., 2003). Nevertheless, the use of organic solvents such as ethanol, methanol, acetone, and crosslinkers (glutaraldehyde) in these methods imposes significant limitations in terms of biocompatibility and drug loading efficiency (Von Storp et al., 2012). The use of organic solvents often leads to poorly soluble drugs to remain in the solvent phase rather than being incorporated into albumin, thereby reducing loading efficiency. Similarly, toxic crosslinkers such as glutaraldehyde limit the use of nanoparticles in biomedical applications (Elzoghby et al., 2012).

To overcome these problems, alternative methods that do not involve organic solvents or toxic crosslinkers have been studied in recent years. One such method is the development of albumin based polyelectrolyte complex (PEC) nanoparticles.

Polyelectrolyte complexation occurs through electrostatic interactions between oppositely charged polymers, allowing the formation of stable complexes without requiring additional chemical additives (Achazi et al., 2021). This approach allows NPs to be obtained in aqueous environments by exploiting the charge properties of the polymers themselves. The polyampholytic nature of albumin makes it suitable for PEC formation, allowing for both cationic and anionic modifications under appropriate pH conditions (Mandel, 1988; Kayitmazer et al., 2013). Although numerous studies on PEC nanoparticles formed from albumin and other polymers exist in the literature, no reports exist on PEC NPs based on two albumin proteins. This thesis fills this gap in the literature by generating albumin–albumin PEC NPs for the first time by combining modified albumins with different surface charges via polyelectrolyte complexation. In the initial phase of the study, the binding behavior of drugs with different solubility properties to both free albumin proteins and albumin NPs was investigated using electron paramagnetic resonance (EPR) analysis. In the subsequent phase, albumin–albumin PEC NPs were produced and loaded with a model hydrophobic drug and their drug loading, release behavior, cytotoxicity, and cellular uptake were thoroughly investigated. This study also investigated the loading of therapeutic mRNA onto the albumin PEC NPs. The green synthesis method for albumin PEC NPs provides a safer and more biocompatible approach for mRNA delivery compared to other carrier systems. Furthermore, the albumin PEC system was also transformed into a hydrogel form under mild conditions (37 °C, pH 6), without requiring high temperatures or harsh processing, thereby providing an additional platform for sustained drug delivery applications. The final chapter of this thesis summarizes the overall findings and outlines potential directions for future studies on the biomedical applications of albumin-based PEC nanoparticles and their hydrogel derivatives.

CHAPTER 2

WATER SOLUBILITY AND BINDING BEHAVIOR OF SPIN-LABELED DRUGS IN ALBUMIN-BASED SYSTEMS

2.1. Introduction

Drug solubility in the aqueous medium is one of the restriction for the pharmaceutical development process. Most of the available drugs have hydrophobic characteristics since drug binding sites in the proteins are usually hindered from the aqueous environment (Williams et al., 2013; Cisneros et al., 2017). Therefore, improvements of solubility and bioavailability of the hydrophobic drugs are crucial especially for oral drug delivery (Kanikkannan, 2018). To enhance the water solubility of the drugs, several methods are available in the literature. This includes physical methods (e.g. particle size reduction), chemical methods (e.g. derivatization, salt formation) and carrier technologies (e.g. polymeric micelles, nanoparticles) (Savjani et al., 2012; Serajuddin, 2007; Hwang et al.,2020).

Nanotechnology has provided different types of nano- carriers made of polymers, lipids, proteins, ceramics, metals, etc. for various drug delivery applications (Sahoo et al., 2007). Besides increasing the solubility of hydrophobic drugs, nanocarriers protect them from degradation and improve intracellular penetration and distribution (Patra et al., 2018; Fu et al., 2017). Moreover, controlled and sustained drug delivery could be achieved by the use of nanocarriers (Shah et al., 2021). Protein based nanoparticles have been frequently preferred over other nanoparticles due to their nontoxic and non-antigenic features, high water solubility and easy surface modifications (Verma et al., 2018). Among the proteins that are used to prepare nanoparticles, serum albumin protein has been preferred often due to its rich drug transportation ability (Spada et al.,2021).

Serum albumin consists of three domains with two principal ligand binding sites, known as Sudlow's sites I and II (Sudlow et al., 1975). Furthermore, weak drug binding sites were also observed including several fatty acid binding sites (Ghuman et al., 2005). Both hydrophilic and hydrophobic drugs can be transported in the body by binding to the

specific drug binding sites of albumin protein. At physiological condition, pH 7.4, albumin surface is negatively charged (Sozer et al., 2020). Yet, negatively charged drugs could bind to serum albumin protein efficiently (Ghuman et al., 2005). On the other hand, modified serum albumin e.g. cationic serum albumin can bind to anionic drugs more efficiently via electrostatic interactions (Akdogan et al., 2016). While maximum 7 spin labeled salicylic acids (SLSA) which are negatively charged can bind to bovine serum albumin (BSA), almost 20 SLSA can bind to cationic BSA (cBSA) (Akdogan et al., 2016). This shows the strong impact of electrostatic interactions in addition to the hydrogen bonding and hydrophobic interactions on the drug binding mechanisms of serum albumin. Consequently, the rich drug binding ability of serum albumin protein has inspired the making of nanoparticles from it.

Albumin nanoparticles can be prepared with different ways including desolvation, emulsification, thermal gelation, nano spray drying, etc. (Elzoghby et al., 2012; Storp et al., 2012; Demirkurt et al., 2019; Demirkurt et al., 2018; Lee et al., 2011). Among these methods, desolvation has been preferred often because of its easy, cheap and rapid procedure. In this method, addition of desolvating agents e.g. ethanol, acetone or acetonitrile to the aqueous albumin solution reduces the albumin solubility, and leads to nano- particle formation in the presence of crosslinker. Although, the size of nanoparticles are affected by various parameters which include desolvating agent type, albumin concentration, desolvating agent/water ratio, pH, stirring rate, etc., the stable albumin nanoparticles are obtained mostly in the size range of 150–280 nm (Langer et al., 2003). The surface charge of BSA NPs has been found between 20 and 50 mV depending on the used desolvating agent (Sozer et al., 2020).

In the literature, different types of drugs such as aspirin, naproxen, salicylic acid, albendazole, doxorubicin and paclitaxel have been incorporated into albumin NPs using desolvation method (Sozer et al., 2020; Das et al., 2005; Bronze-Uhle et al., 2017; Tang et al., 2016; Onafuye et al., 2019). Differently, modified serum albumin NPs have been also prepared to improve the drug transportation ability of albumin NPs. For example, in the previous study, cationic BSA (cBSA) proteins were prepared via ethylenediamine conjugation, and then cBSA NPs were prepared with a simple desolvation method (Sozer et al., 2020). The obtained cBSA NPs have a surface charge between + 20 and + 50 mV at pH 7.4 depending on the used desolvating agent. Therefore, cationization of albumin increased the anionic spin labeled salicylic acid loading capacity and slowed release of it compared to the native albumin NPs. In another study, doxorubicin loaded NPs were

prepared using cationic and mannose modified human serum albumins with a desolvation method for dual targeting in brain tumors (Byeon et al., 2016).

Herein, both native and cationic BSA proteins in addition to their NPs were used to enhance the drug solubility in water. Three types of drugs including salicylic acid (SA), ibuprofen (Ibf) and chlorambucil (Chl) with different water solubility e.g. high, low and none, respectively, were studied. There are various methods for drug solubility measurements in the literature, which include high performance liquid chromatography (HPLC) (Glomme et al., 2005; Bergström et al., 2002), potentiometric titration (Thapa et al., 2017), turbidimetry (Glomme et al., 2005), dynamic methods (Wang et al., 2008), last crystal disappearance method (Hao et al., 2005), and laser monitoring technique (Li et al., 2006). As an alternative technique to observe the effect of proteins and NPs on the solubility of drugs, we used continuous wave (cw) electron paramagnetic resonance (EPR) spectroscopy. In order to monitor drugs with EPR spectroscopy, spin labeled drugs (SLSA, SLIbf and SLChl) were synthesized using stable Tempo (2,2,6,6-tetramethylpiperidine- 1-oxyl) based nitroxide radicals (Fig 2.1) (Elzoghby et al., 2012; Torricella et al., 2021; Hauenschild et al., 2016). This technique has already been used to investigate ligand and drug bindings to albumin proteins (Elzoghby et al., 2012; Hauenschild et al., 2016; Tatlidil et al., 2015; Akdogan et al., 2011). However, according to our knowledge, spin labeled drug binding to any nanoparticles has not been studied with EPR spectroscopy yet.

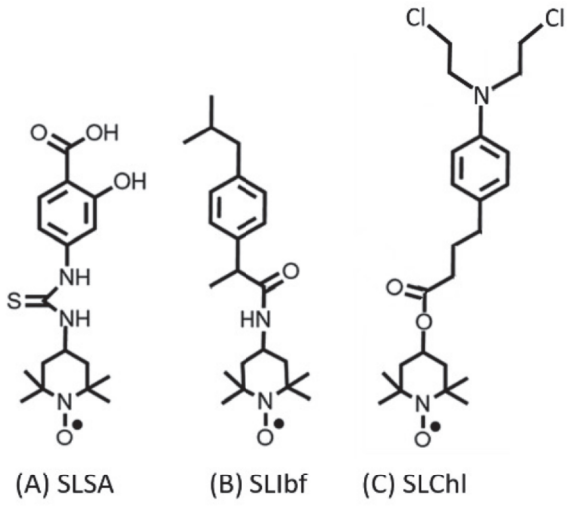

Figure 2.1. Molecular structures of spin labeled drugs: (A) spin labeled salicylic acid (SLSA), (B) spin labeled ibuprofen (SLIbf) and (C) spin labeled chlorambucil (SLChl) (Sozer and Akdogan, 2022).

The major advantage of using EPR spectroscopy is the ability to measure the undissolved drugs, dissolved (free) drugs and dissolved but bound drugs to proteins or nanocarriers in the same solution simultaneously. EPR spectroscopy can discriminate the bound and unbound (free) drugs due to its sensitivity to the rotational dynamics of the radical centers. Bound drugs have broad signals stemming from restricted rotational motion and unbound drugs have sharp signals originating from the freely tumbling motion (Hauenschild et al., 2016; Tatlidil et al., 2015). On the other hand, undissolved drugs in the solution can be identified with a single signal. The close interaction between the radical centers in the drug aggregates causes dipolar and exchange interactions that yield a single broad EPR signal (Hauenschild et al., 2016; Tatlidil et al., 2015; Akdogan et al., 2011; Babcock and Kattnig, 2020). Thus, all the forms of drugs can be monitored which can provide more accurate results for the drug solubility and drug loading.

2.2. Materials and Methods

2.2.1. Materials

Bovine serum albumin (lyophilized powder, MW: 66.5 kDa), N- (3-Dimethylaminopropyl)- N′- ethylcarbodiimide hydrochloride (EDC), ethylenediamine (EDA), glutaraldehyde solution (8% (v/v) in H2O), dimethyl sulfoxide (DMSO), 4-Amino salicylic acid, ibuprofen, chlorambucil, 4-Amino Tempo, 4-Hydroxy Tempo, dichloromethane, trimethylamine, methanol, and ethyl acetate were purchased from Sigma-Aldrich. Acetonitrile and thiophosgene were purchased from Merck. Without any further purification, all chemical materials and solvents were used. All the solvents were analytical reagent quality. Distilled water was used to make all the aqueous solutions.

2.2.2. Preparation of cationic bovine serum albumin (cBSA) proteins

Cationic bovine serum albumin (cBSA) protein was prepared as described in our publication (Sozer et al., 2020). 50 mg of BSA was dissolved in 500 μL of distilled water, and then 9.5 mL of ethylenediamine/water aqueous solution 1.3/1 (v/v) with a pH of 4.75 was added to the BSA solution. 14.5 mg of EDC dissolved in 15 mL of distilled water was added drop by drop into the mixture of ethylenediamine and BSA. The reaction was

continued with stirring at 750 rpm for 2 hours. The reaction was terminated by using 1 mL of 4 M acetate buffer (pH 4.75). For the elimination of unreacted and excess ethylenediamine and EDC, the solution was washed twice with acetate buffer (0.1 M, pH 4.75) and three times with distilled water in an Amicon Ultra (50 kDa MWCO) centrifuge tube at 13,000 rpm for 3 minutes. The product of cBSA was lyophilized and preserved at 4 °C. The yield of the product was approximately 70%.

2.2.3. Preparation of cBSA and BSA nanoparticles

30 mg of lyophilized cBSA (or BSA) was dissolved in 1000 mL of water for 20 minutes at 750 rpm stirring. Then, 4 mL of acetonitrile was added dropwise to the aqueous solution of albumin at a rate of 1 mL/min with a syringe pump. After that, 18 μL of glutaraldehyde solution (8% in H2O) was added to the nanoparticle suspension. The solution was stirred at 750 rpm for 4 hours. Aliquots NP solutions were precipitated by centrifugation at 14,000 rpm for 45 min. Pellets were washed with distilled water to eliminate desolvating agents, unreacted cBSA (or BSA) and glutaraldehyde. For the yield calculations, pellets of cBSA and BSA NPs were lyophilized. The yields of BSA NPs and cBSA NPs formations were approximately 82% and 55%, respectively.

2.2.4. Characterizations of cBSA proteins, cBSA NPs and BSA NPs

The zeta potential and molecular weight of the obtained cBSA were obtained in distilled water by a Malvern dynamic light scattering (DLS) Nano-ZS instrument (Worcestershire, UK) and a mass spectrometer using Bruker Autoflex-III (smartbeam) MALDI TOF/TOF system, respectively. The size and shape of NPs were analyzed by the scanning electron microscope (SEM, FEI QUANTA 250 FEG) and dynamic light scattering (DLS, Malvern, Worcestershire, UK). For the SEM measurements, dissolved NPs were diluted 50 times with distilled water from their dissolved NP solutions. 5 μL solutions were dropped on an aluminium foil and samples were left for the drying for one day. Then, dried samples were coated with gold using EMITECH K550X in a vacuum for SEM imagining. The accelerating voltages were 5–7 kV. DLS measurements of NPs were analyzed at a wavelength of 632 nm. The scattering angle was set at 1730. The zeta

potentials of NPs were determined by a Malvern dynamic light scattering (DLS) Nano-ZS instrument.

2.2.5. Synthesis of spin labeled salicylic acid (SLSA)

Spin labeled salicylic acid (SLSA) was prepared as described in our group previous publication (Tatlidil et al., 2015). To protect anionic feature of salicylic acid, 4-Amino salicylic acid was used. 0.01 mol of 4-Amino salicylic acid was dissolved and acidified with 3.4 mL of HCl (12.2 M) in 32 mL of distilled water. Then, 0.044 mol of thiophosgene was added to the solution. The mixture was stirred for 1 hour at 0 °C, then for 2.5 hours at 25 °C. After filtering the mixture, the solution was vacuum-dried to produce 4-isothiocyanate salicylic acid. The product was obtained with approximately 50% yield. 0.46 mmol 4-isothiocyanate salicylic acid and 0.625 mmol 4-Amino Tempo were dissolved in 20 mL of DCM. Then a few drops of triethylamine were added to the mixture and stirred at 25 °C for overnight. The product was purified by column chromatography (ethyl acetate: methanol 15:1, 13:1, 12:1, and 10:1). The product was obtained with approximately 45% yield.

2.2.6. Synthesis of spin labeled ibuprofen (SLIbf)

Spin labeled ibuprofen (SLIbf) was prepared as described in our group's previous publication (Akdogan et al., 2016). Ibuprofen (0.2 M), 4-Amino Tempo (0.2 M), and 1-ethyl-3-(3-dimethylaminopropyl) carbodiimide (EDC) (0.2 M) were stirred in DCM under argon for 18 hours at 25 °C. The product spin labeled ibuprofen (SLIbf) was purified with column chromatography (hexane:ethyl acetate 5:1, 4:1, 3:1 and 2:1). The yield was approximately 70%.

2.2.7. Synthesis of spin labeled chlorambucil (SLChl)

Spin labeled chlorambucil (SLChl) was prepared as described according to Hauenschild et al. (Hauenschild et al., 2016). 0.29 mmol of chlorambucil, 0.44 mmol of 4-Hydroxy Tempo and 0.04 mmol of DMAP were dissolved in 15 mL of dry DCM at 25 °C. The solution was cooled to 0°C. After that, 0.38 mmol of DCC in 3 mL of dry DCM

was added drop by drop to the mixture and stirred for 2 h at 0°C and 24 h at 25 °C. The side product DCU was removed by filtering. The filtrate was concentrated to 4 mL. The product spin labeled chlorambucil (SLChl) was purified with column chromatography (DCM:ethyl acetate 10:1). The yield was approximately 75%.

2.2.8. Solubility measurements of SLDrugs by EPR spectroscopy

4 mg of BSA (or cBSA) proteins or BSA (or cBSA) NPs were dissolved in 80 µL of distilled water and mixed with 2 µL of SLSA (196 mM), SLIbf (196 mM) or SLChl (56 mM) prepared in DMSO for 1 hour. The ratio of SLSA and SLIbf to albumin was 7:1, and the SLChl to albumin was 2:1. For EPR measurements, 7 µL of samples were measured directly on a CMS 8400 (Adani) benchtop X-band EPR spectrometer with a TE102 resonator cavity at room temperature. Measurements were performed in quartz capillary sample tubes. EPR spectra were simulated with the Matlab-based Easyspin 4.5.5 software package (Gulsun et al., 2009).

2.2.9. Solubility measurements of SLDrugs by UV-Vis spectroscopy

The calibration curves of SLSA, SLIbf and SLChl were obtained in water:ethanol (1:1, v/v) mixture. The samples were prepared as same as in the EPR measurements. The drugs- BSA NPs mixtures (80 µL) were centrifuged and the supernatants were diluted to 2 mL with water:ethanol (1:1, v/v) solution for UV-Vis measurements. Also, the unbound drugs from the drugs-BSA protein mixtures were analyzed after ultrafiltration and dilution to 2 mL with water:ethanol.

2.2.10. SLSA Loading: Addition of drugs before desolvation and after NPs formation (incubation)

Before desolvation: 30 mg of lyophilized BSA (or cBSA) was dissolved in 480 µL of water, at pH 9.0 (at pH 7.0 for cBSA), and mixed with 12.5 µL, 212 mM SLSA (8.25 µL, 212 mM SLSA for cBSA) for 20 minutes at 750 rpm stirring. Then, 1920 µL of acetonitrile was added dropwise to the aqueous solution of albumin at a rate of 1 mL/min with a syringe pump. After that, 18 µL of glutaraldehyde solution (8% in H_2O) was added

to nanoparticle suspension. The solution was stirred at 750 rpm for 4 hours. After that 7 μL samples were taken out for EPR measurements.

Since the NP formation yields were 82% and 55% for BSA NPs and cBSA NPs, respectively, the final SLSA:Albumin ratios were kept 7:1. Aliquots NP solutions were precipitated by centrifugation at 10,000 rpm for 10 min. The supernatant and the obtained NP pellet dissolution with a same volume of water measured with EPR spectroscopy. Incubation. In order to have the same final SLSA:Albumin ratio of 7:1, 4 mg of BSA (or cBSA) NPs were dissolved in 560 μL of distilled water and then mixed with 7.0 μL of SLSA (58.33 mM) prepared in DMSO for 1 hour. Aliquots NP solutions were directly measured by EPR spectroscopy. After precipitation at 10,000 rpm for 10 minutes, the supernatant and the NP pellet dissolution with a same volume of water measured with EPR spectroscopy.

2.3. Results and Discussion

Most of the drugs exhibit poor water solubility (Thapa et al., 2017; Di et al., 2012). Yet, addition of water soluble carriers such as albumin proteins or albumin nanoparticles can enhance the solubility of drugs. The dissolved drugs either bind to carriers or stays unbound, which depends on the binding strength between drugs and the carriers. EPR spectroscopy allows distinguishing spin-labelled drugs in the solution such as dissolved drugs including unbound and bound forms, and undissolved drugs. Instantaneous detection of these three forms of drugs by EPR spectroscopy presents accurate results since they are all monitored at the same time. Here, we studied three different drugs with different water solubility; salicylic acid (SA) (high), ibuprofen (Ibf) (low) and chlorambucil (Chl) (none). They were spin labeled to be monitored by EPR spectroscopy. For example, EPR measurement of SLIbf in the BSA aqueous solution yielded three different EPR signals belong to unbound, bound and undissolved drugs in one spectrum. Combining simulations of these signals yielded the experimental result (Figure 2.2).

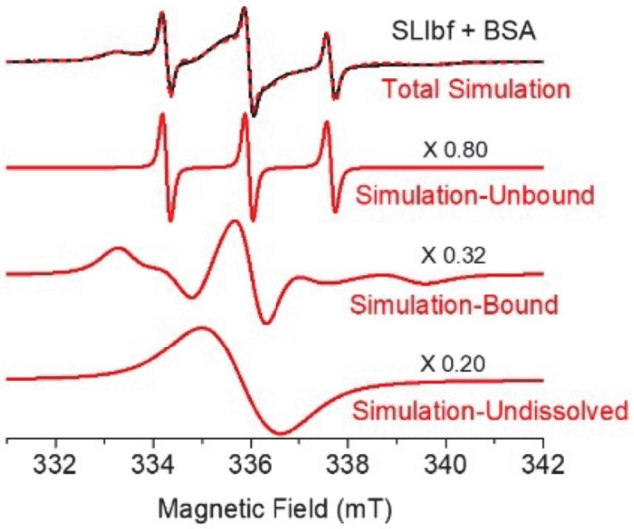

Figure 2.2. EPR spectrum of 4.9 mM of SLIbf in the presence of 0.7 mM of BSA protein in water (black) and its corresponding simulation (dashed red) obtained upon addition of simulations of unbound, bound and undissolved SLIbf (red) spectra after multiplication with appropriate numbers (Sozer and Akdogan, 2022).

Undissolved spin labeled drugs could be easily distinguished from the dissolved ones by the effects of dipolar coupling and spin exchange interactions observed in the clustered molecules (Hauenschild et al., 2016; Babcock and Kattnig, 2020). Without electron spin-spin interactions, the freely tumbling motion of unpaired electron belongs to the paramagnetic center yields sharp signals. Therefore, well-dispersed spin labeled drugs in the nonviscous solution have sharp EPR signals. Figure 2.3 (A) shows EPR spectra of 4.9 mM of 4-Amino Tempo (spin label) and three spin labeled drugs; SLSA, SLIbf and SLChl dissolved in DMSO. Since DMSO is effective in dissolution of a number of polar and non-polar molecules, their EPR signals are very similar. All have sharp three signals with slightly different rotational correlation times (τR) due to the different interactions with DMSO. The simulations of these spectra and their corresponding EPR parameters were shown in Figure 2.4 and Table 2.1, respectively.

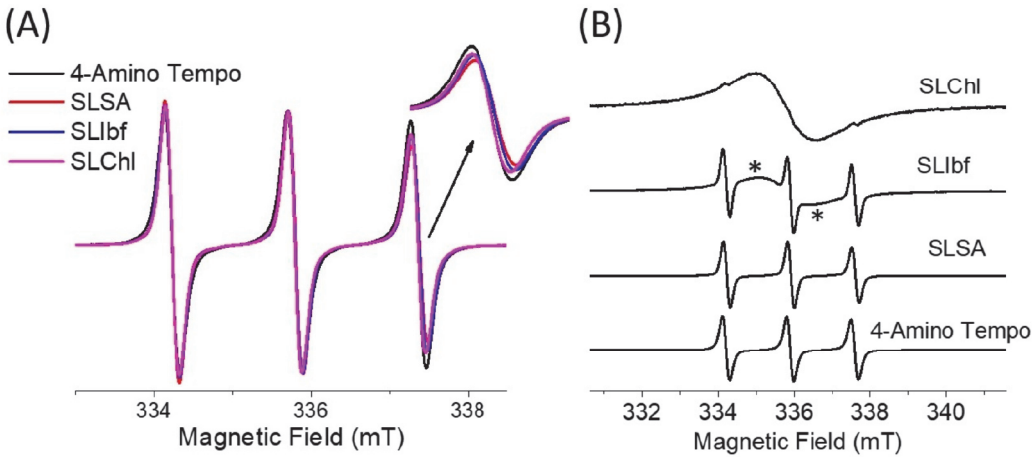

Figure 2.3. EPR spectra of 4.9 mM of 4-Amino Tempo, SLSA, SLIbf and SLChl in DMSO (A) and in water (B). The asterisks mark a broad spectral component (Sozer and Akdogan, 2022).

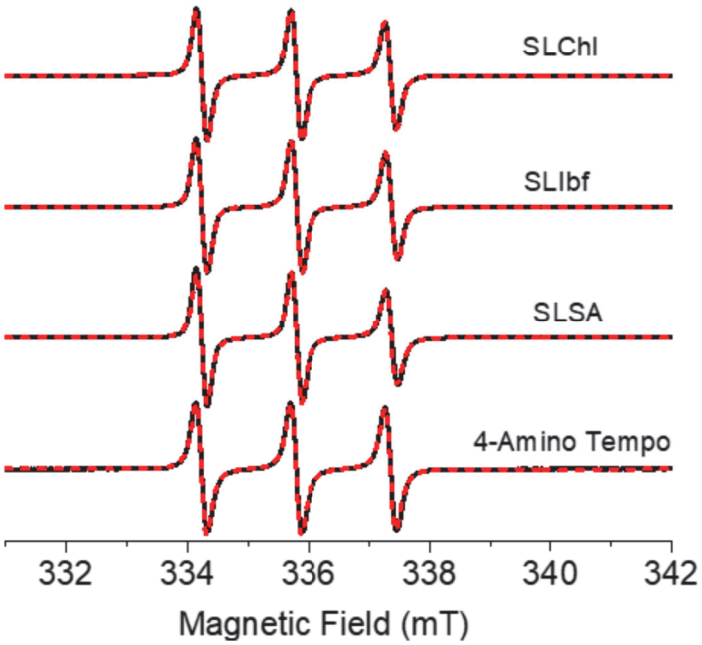

Figure 2.4. EPR spectra of 4.9 mM of 4-Amino Tempo, SLSA, SLIbf and SLChl (black) dissolved in DMSO and their corresponding simulations (red) (Sozer and Akdogan, 2022).

Table 2.1. Simulated EPR parameters of 4-Amino Tempo, SLSA, SLIbf and SLChl dissolved in DMSO (4.9 mM) (Sozer and Akdogan, 2022).

	g_{zz}	g_{yy}	g_{zz}	A_{xx} (mT)	A_{yy} (mT)	A_{zz} (mT)	τ_{Rot} (ps)
4-Amino Tempo	2,0104	2,0072	2,0040	0,64	0,64	3,43	27
SLSA	2,0102	2,0074	2,0038	0,64	0,64	3,44	104
SLIbf	2,0104	2,0070	2,0040	0,64	0,64	3,45	70
SLChl	2,0104	2,0040	2,0040	0,64	0,64	3,42	70

On the other hand, these drugs at 4.9 mM concentrations have different solubility in water. Figure 2.3 (B) shows that SLSA can be dissolved well in water. Therefore, EPR spectra of SLSA and 4-Amino Tempo have similar sharp signals. The simulations of these spectra and their corresponding EPR parameters were shown in Figure 2.5 and Table 2.2, respectively. However, the solubility of SLIbf is very limited in water. The EPR spectrum of SLIbf has mainly a broad signal in addition to sharp signals (Figure 2.3 (B)). The areas under the broad signal and sharp signals obtained from double integrations of the corresponding simulations are proportional with the numbers of undissolved and dissolved drugs, respectively. Simulation of the EPR spectrum of SLIbf provided that only 5 % of SLIbf was dissolved, and 95 % of SLIbf was not dissolved in water (Figure 2.6 (A, B)). This broad signal arises from the spin-spin interactions in the undissolved SLIbf. For a diluted 0.5 mM of SLIbf solution, a broad signal originating from the undissolved SLIbf was still observed but with a less ratio, 60 % (Figure 2.6 (C, D)). Different from SLSA and SLIbf, SLChl could not be dissolved in water at 4.9 mM concentration and even at 0.5 mM concentration. A broad signal again due to the spin-spin interactions in SLChl aggregates covers the whole spectrum (Figure 2.3 (B) and Figure 2.7).

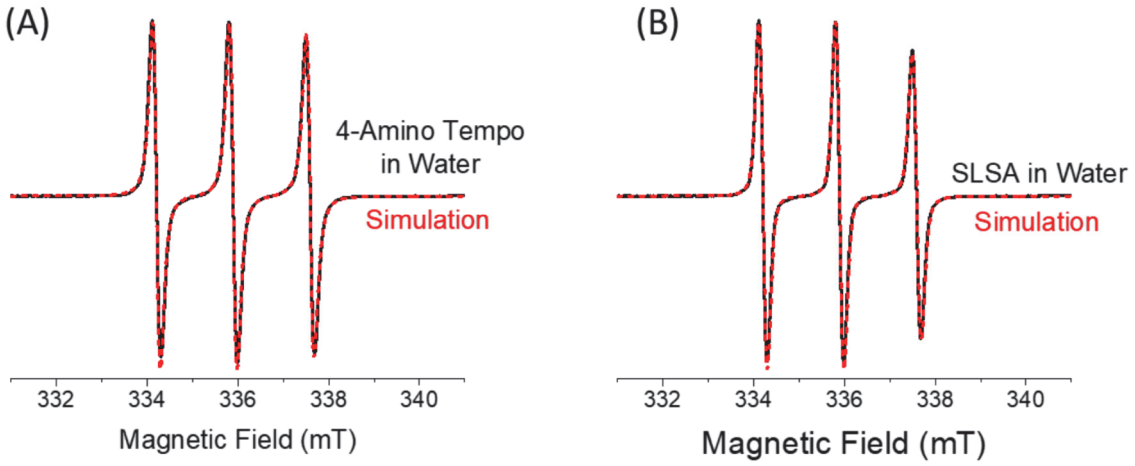

Figure 2.5. EPR spectra of 4.9 mM of (A) 4-Amino Tempo (black) and (B) SLSA (black) dissolved in water and their corresponding simulations (red) (Sozer and Akdogan, 2022).

Table 2.2. Simulated EPR parameters of 4-Amino Tempo, SLSA and SLIbf dissolved in water (4.9 mM) (Sozer and Akdogan, 2022).

	g_{zz}	g_{yy}	g_{zz}	A_{xx} (mT)	A_{yy} (mT)	A_{zz} (mT)	τ_{Rot} (ps)
4-Amino Tempo	2,0098	2,0068	2,0032	0,76	0,78	3,55	30
SLSA	2,0096	2,0066	2,0030	0,76	0,78	3,55	220
SLIbf	2,0098	2,0068	2,0028	0,76	0,78	3,55	77

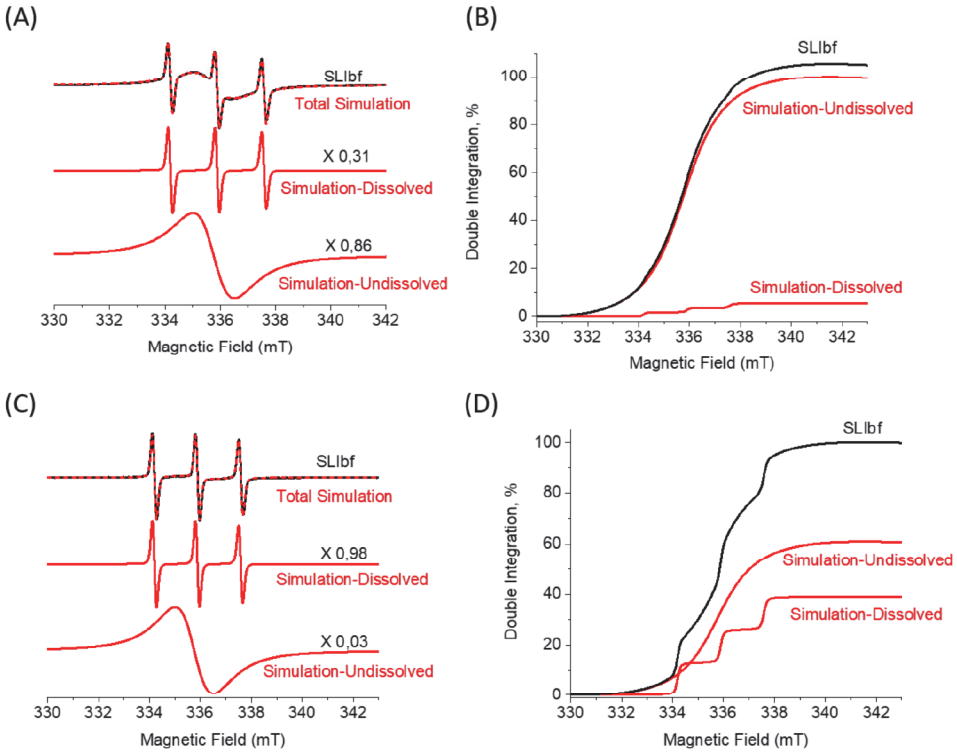

Figure 2.6. (A) EPR spectra of 4.9 mM of SLIbf (black) and its total simulation (dashed red) obtained by combination of dissolved and undissolved SLSA EPR simulations (red) after multiplication with the appropriate numbers. (B) Double integrations of the spectra in (A). (C) EPR spectra of 0.5 mM SLIbf (black) and its total simulation (dashed red) obtained by combination of dissolved and undissolved SLSA EPR simulations (red) after multiplication with the appropriate numbers. (D) Double integrations of the spectra in (C) (Sozer and Akdogan, 2022).

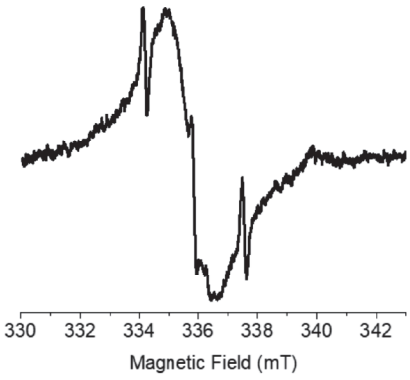

Figure 2.7. EPR spectrum of 0.5 mM of SLChl in water (Sozer and Akdogan, 2022).

In order to increase the drug solubility in water and compare the loading capacity of albumin proteins and nanoparticles, spin labeled drug molecules (SLSA, SLIbf and SLChl) were mixed with BSA, BSA NPs, cBSA and cBSA NPs separately. The previous study was followed to obtain cBSA protein, BSA NPs and cBSA NPs (Sozer et al., 2020). By addition of ethylenediamine to BSA in the presence of the crosslinker (EDC), the molecular weight of BSA increased from approximately 66650 g/mol to 68700 g/mol, which indicates that on average 49 ethylenediamine are conjugated with BSA (Figure 2.8). Ethylenediamine conjugation with the available carboxylic acid side chains of aminoacids (Asp and Glu) results in decreasing the negative charge of BSA. In addition, free amine groups of conjugated ethylenediamine contribute positive charge to the BSA. As a result, the surface charge varied from -11mV to +25mV at pH 7.0.

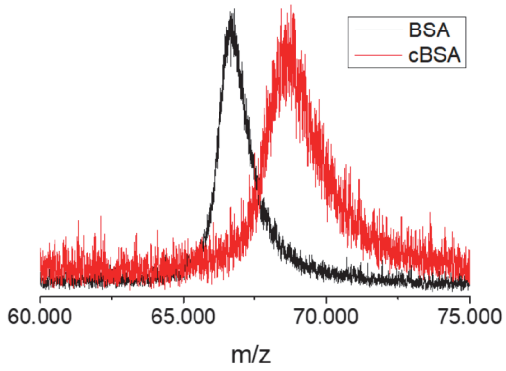

Figure 2.8. MALDI-TOF mass spectra of BSA (black) and cationic BSA (cBSA) (red) proteins (Sozer and Akdogan, 2022).

BSA NPs and cBSA NPs were prepared by a simple desolvation method. In the previous study, it has been shown that a significant amount of cBSA NPs (with a 55% yield) was obtained when acetonitrile was used as a desolvating agent (Sozer et al., 2020). Therefore, both BSA NPs and cBSA NPs were prepared using acetonitrile. The sizes of BSA and cBSA NPs were characterized using SEM and DLS. Figure 2.9 shows the SEM images of well dispersed spherical BSA NPs and cBSA NPs with similar particle sizes around 200 nm. Their hydrodynamic diameters are also very similar average sizes around 200 nm with PDI values less than 0.2 indicating a narrow size distribution. In addition, the zeta potentials of the obtained BSA NPs and cBSA NPs are -35 mV and + 38 mV, respectively.

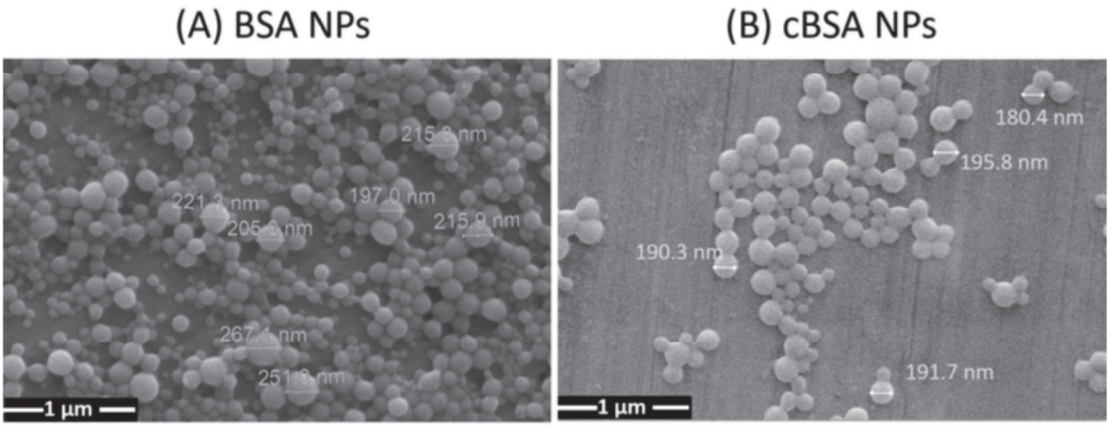

Figure 2.9. SEM images of BSA NPs (A) and cBSA NPs (B). Scale bar = 1 µm (Sozer and Akdogan, 2022).

0.7 mM albumin solutions in the forms of both anionic (BSA and BSA NPs) or cationic (cBSA and cBSA NPs) were mixed individually with SLSA at a ratio of 1:7 (albumin:drug). Since SLSA was already dissolved well in water, amorphous aggregate structure of SLSA was not observed upon addition of albumins too. Bound and unbound (free) types of SLSA were determined by EPR measurements. In order to compare bound and unbound types, the EPR spectrum of free SLSA was put in the Figure 2.10 (bottom) and the positions of EPR signals of bound SLSA were shown with dashed lines in Figure 2.10 (top and middle). After simulations of bound and unbound signals separately, the collective EPR spectrum was obtained (Figure 2.11 (A) and (C)). The percentage of bound SLSA can be calculated from the areas under EPR signals obtained by double integrations of simulated bound and unbound EPR spectra (Eq. 2.1) (Figure 2.11 (B) and (D)).

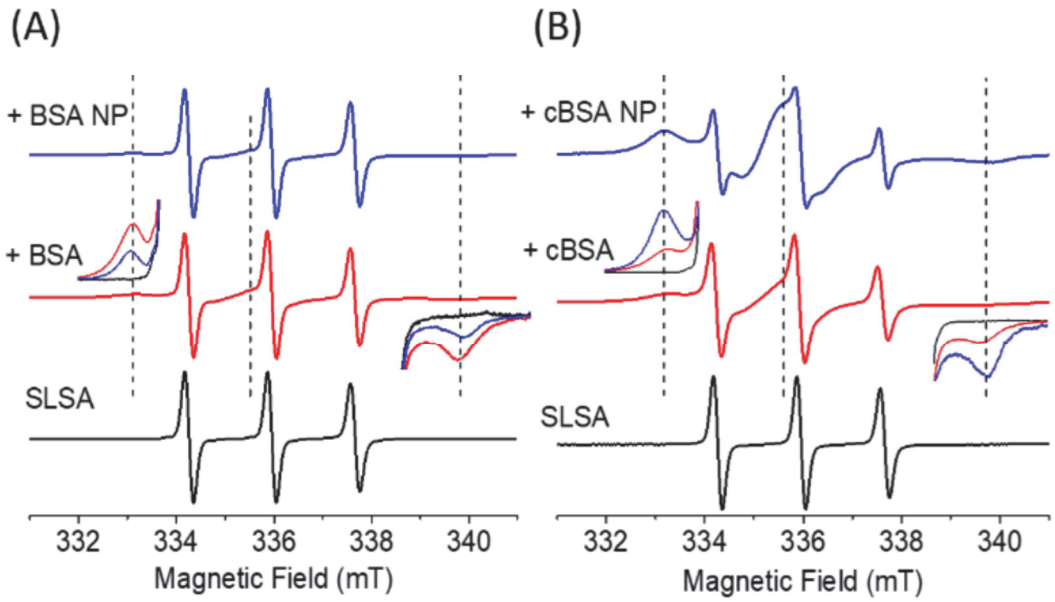

Figure 2.10. EPR spectra of 4.9 mM of SLSA in water (bottom) and upon additions of 0.7 mM of BSA (middle) and BSA NPs (top) (A), and 0.7 mM of cBSA (middle) and cBSA NPs (top) (B) (Sozer and Akdogan, 2022).

$$\%\ of\ Bound\ Drug = \frac{Area\ of\ Bound\ Drug}{Area\ of\ Bound\ Drug + Area\ of\ Unbound\ Drug} \quad (2.1)$$

After addition of 0.7 mM of BSA protein or BSA NPs to SLSA aqueous solution (with a SLSA/BSA ratio of 7), 71% and 52% of SLSA were bound to BSA proteins and BSA NPs, respectively (Fig. 2.10 (A) and Fig. 2.11). The water-soluble drug of SLSA bound to BSA more than BSA NPs because SLSA can be loaded into the several binding pockets of BSA protein (Akdogan et al., 2016) but most of these specific sites were damaged during the nanoparticle formation step. Drug binding to the specific binding sites is expected to be stronger than the binding of SLSA to the surface of BSA NPs. Anionic SLSA could bind to anionic BSA NPs through hydrogen bonds, van der Waals interactions and aromatic interactions. In addition, the surface charge of BSA NPs is about -35 mV, which is much higher than the charge of BSA protein -11 mV. Therefore, the electrostatic repulsion between anionic SLSA and BSA NPs is higher than the electrostatic repulsion between SLSA and BSA protein. These two reasons could decrease the binding of SLSA to BSA NPs compared to BSA protein. Moreover, since salicylic acid is a hydrophilic drug it dissolves well in water. Therefore, some parts of the salicylic acids prefer to be dissolved in water too. On the other hand, SLSA bound to cBSA and

cBSA NPs with 85% and 96%, respectively, at a SLSA/cBSA ratio of 7 (Fig. 2.10 (B) and Fig. 2.12). In comparison to BSA and BSA NPs, SLSA bound to cBSA and cBSA NPs much higher due to the strong electrostatic attractive interaction between the anionic residue of SLSA (-COOH) and cationic serum albumin. In addition, SLSA bound to cBSA NPs more than cBSA proteins since the higher positive surface charge of cBSA NPs (+38 mV *vs* +25 mV) became more effective to keep more anionic drugs on it.

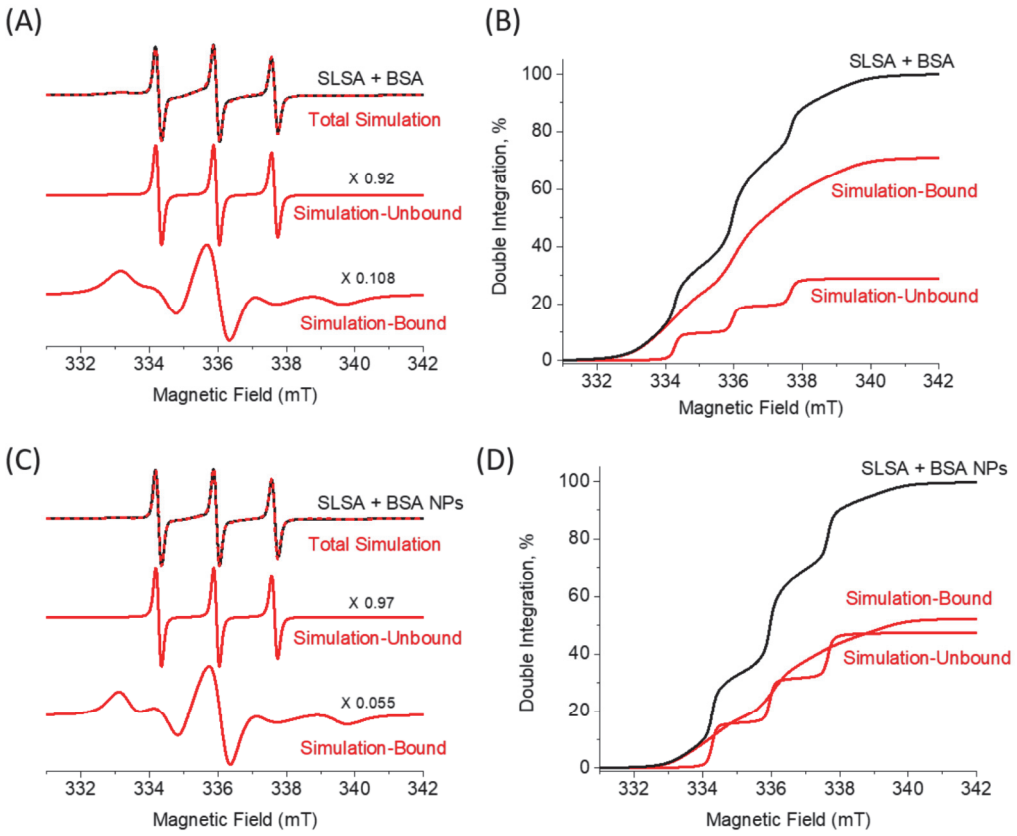

Figure 2.11. (A) EPR spectra of 4.9 mM of SLSA in the presence of 0.7 mM BSA (black) and its total simulation (dashed red) obtained by combination of bound and unbound SLSA EPR simulations (red) after multiplication with the appropriate numbers. (B) % of double integrations of the spectra in (A). (C) 4.9 mM of SLSA in the presence of 0.7 mM BSA NPs (black) and its total simulation (dashed red) obtained by combination of bound and unbound SLSA EPR simulations (red) after multiplication with the appropriate numbers. (D) % of double integrations of the spectra in (C). They are normalized to the double integration of the experiment (Sozer and Akdogan, 2022).

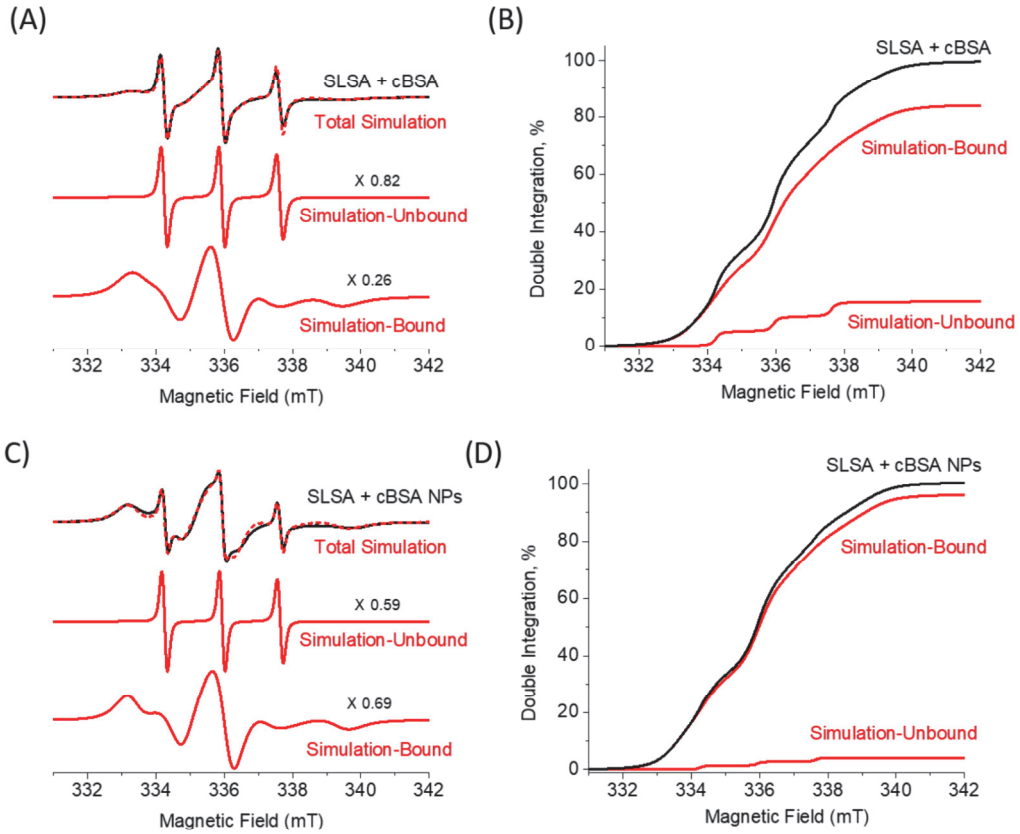

Figure 2.12. (A) EPR spectra of 4.9 mM of SLSA in the presence of 0.7 mM cBSA (black) and its total simulation (dashed red) obtained by combination of bound and unbound SLSA EPR simulations (red) after multiplication with the appropriate numbers. (B) % of double integrations of the spectra in (A). (C) 4.9 mM of SLSA in the presence of 0.7 mM cBSA NPs (black) and its total simulation (dashed red) obtained by combination of bound and unbound SLSA EPR simulations (red) after multiplication with the appropriate numbers. (D) % of double integrations of the spectra in (C). They are normalized to the double integration of the experiment (Sozer and Akdogan, 2022).

Although, solubility of SLIbf is very limited in water, addition of albumin proteins (BSA and cBSA) or nanoparticles (BSA NPs and cBSA NPs) increased the solubility of SLIbf. The simulation of EPR spectrum of 4.9 mM of SLIbf in water showed that 95% of SLIbf contributed to form aggregates in water (Fig. 2.6 (A, B)). Only 5% of them were dissolved in water. However, in the presence of BSA proteins or BSA NPs, the amount of dissolved SLIbf increased from 5% to 52% and 96%, respectively, at a SLIbf/BSA ratio of 7 (Fig. 2.13 (A) and Fig. 2.14). BSA or BSA NPs could extract SLIbf from the

amorphous aggregate structure and then bind them to themselves. As a result, 46% and 84% of SLIbf in the water solution were bound to BSA proteins and BSA NPs, respectively (Fig. 2.14). These results showed that BSA NPs could be loaded much more SLIbf than BSA proteins at the same BSA concentrations. Since ibuprofen water solubility is much lower compared to salicylic acid, its hydrophobic nature favors interaction with BSA NPs (84%). Similarly, addition of cBSA or cBSA NPs disturbed the undissolved SLIbf (Fig. 2.13 (B) and Fig. 2.15). They decreased the amount of SLIbf contributed into the amorphous aggregates. Thus, in the presence of cBSA proteins or cBSA NPs, the amount of dissolved SLIbf increased from 5% to 50% and 76%, respectively, at a SLIbf/cBSA ratio of 7.

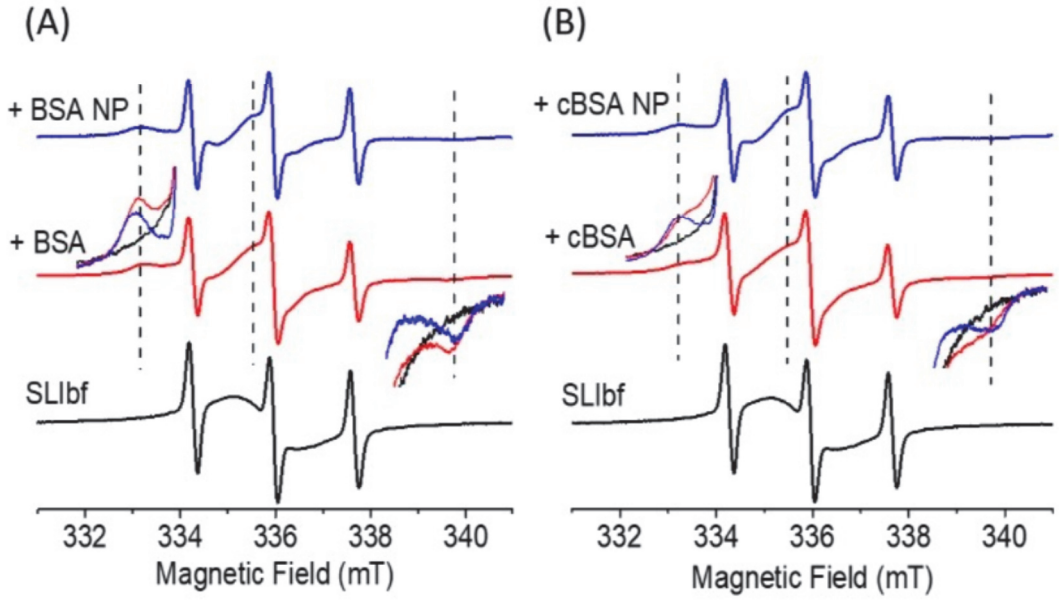

Figure 2.13. EPR spectra of 4.9 mM of SLIbf in water (bottom) and upon addition of 0.7 mM of BSA (middle) and BSA NPs (top) (A), and 0.7 mM of cBSA (middle) and cBSA NPs (top) (B) (Sozer and Akdogan, 2022).

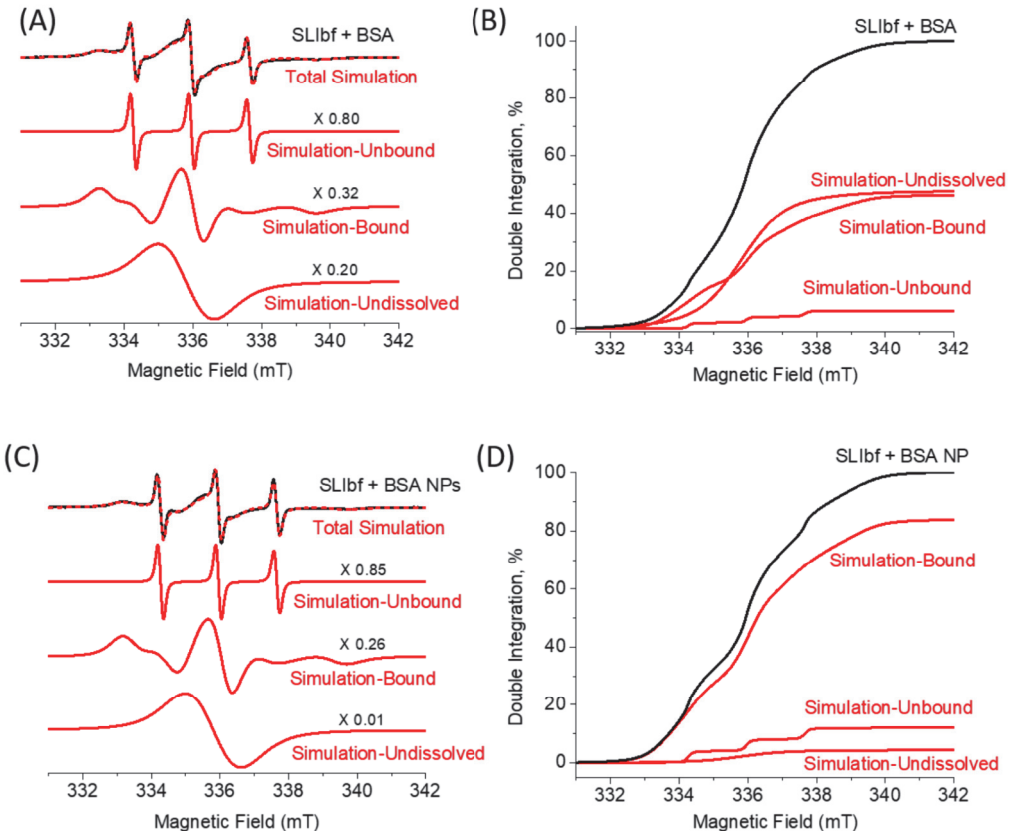

Figure 2.14. (A) EPR spectra of 4.9 mM of SLIbf in the presence of 0.7 mM BSA (black) and its total simulation (dashed red) obtained by combination of bound and unbound SLIbf EPR simulations (red) after multiplication with the appropriate numbers. (B) % of double integrations of the spectra in (A). (C) 4.9 mM of SLIbf in the presence of 0.7 mM BSA NPs (black) and its total simulation (dashed red) obtained by combination of bound and unbound SLIbf EPR simulations (red) after multiplication with the appropriate numbers. (D) % of double integrations of the spectra in (C). They are normalized to the double integration of the experiment (Sozer and Akdogan, 2022).

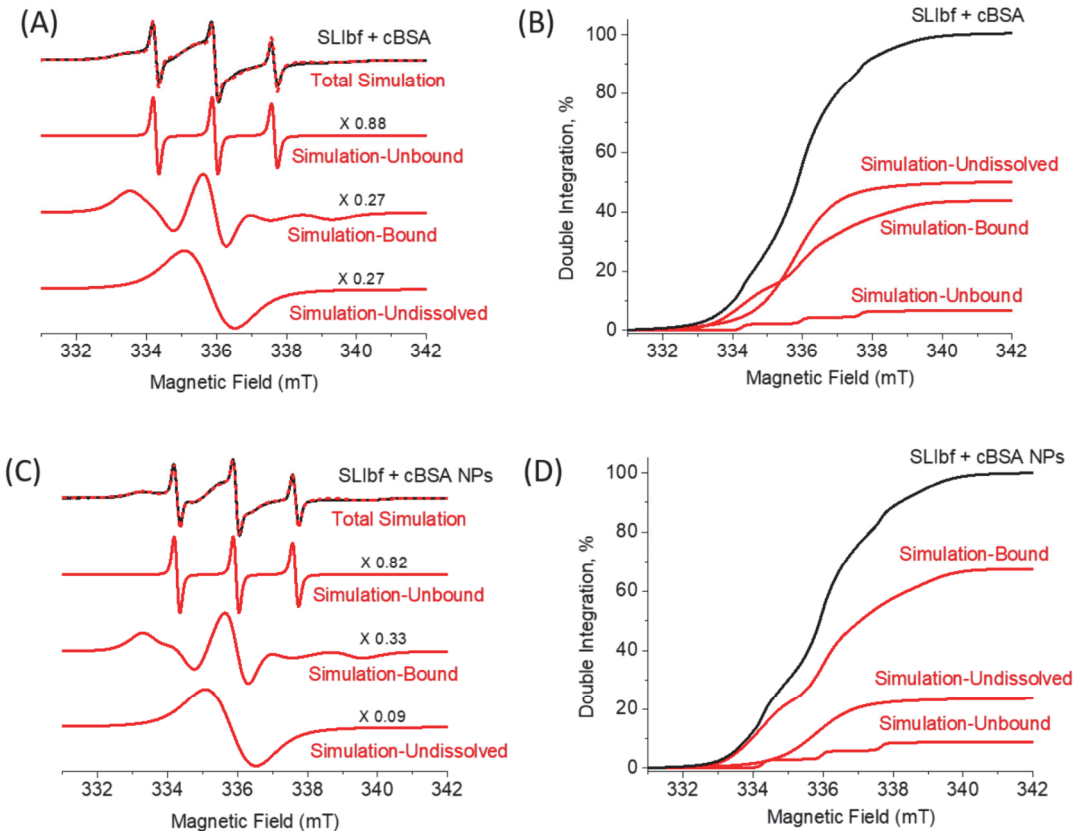

Figure 2.15. (A) EPR spectra of 4.9 mM of SLIbf in the presence of 0.7 mM cBSA (black) and its total simulation (dashed red) obtained by combination of bound and unbound SLIbf EPR simulations (red) after multiplication with the appropriate numbers. (B) % of double integrations of the spectra in (A). (C) 4.9 mM of SLIbf in the presence of 0.7 mM cBSA NPs (black) and its total simulation (dashed red) obtained by the combination of bound and unbound SLIbf EPR simulations (red) after multiplication with the appropriate numbers. (D) % of double integrations of the spectra in (C). They are normalized to the double integration of the experiment (Sozer and Akdogan, 2022).

Extraction of SLIbf from aggregate structure resulted in binding 43% and 67% of total SLIbf in solution to cBSA and cBSA NPs, respectively (Fig. 2.15). Similar to the results of BSA and BSA NPs, cBSA NPs carried more SLIbf than cBSA proteins. These results showed that albumins in the form of nanoparticles highly dissociate SLIbf clusters compared to albumin proteins. Binding of 4-Amino Tempo to ibuprofen leads to amid formation therefore ibuprofen loses its carboxyl acid side group and becomes neutral at

pH 7.0. Therefore, electrostatic interactions between SLIbf- cBSA are not as effective as in the case of SLSA-cBSA binding.

SLChl can not be dissolved in water, therefore a broad EPR signal covers the spectrum (Fig. 2.16). However, the presence of 0.7 mM albumin proteins or nanoparticles at a SLChl/BSA ratio of 2 increased the solubility of SLChl in water (Fig. 2.16 (A)). The aggregate concentration decreases from 100% to about 58% and 38% when BSA proteins and BSA NPs were added, respectively. Consequently, almost all the dissolved SLChl were bound to the BSA and BSA NPs with about 42% and 61% of total SLChl, respectively (Fig. 2.17). Since chlorambucil is not soluble in water, unbound fraction of spin labeled chlorambucil aggregated in water very quickly. Therefore, BSA NPs can not extract the chlorambucil drugs from the core of drug aggregates which decreases the chlorambucil loading.

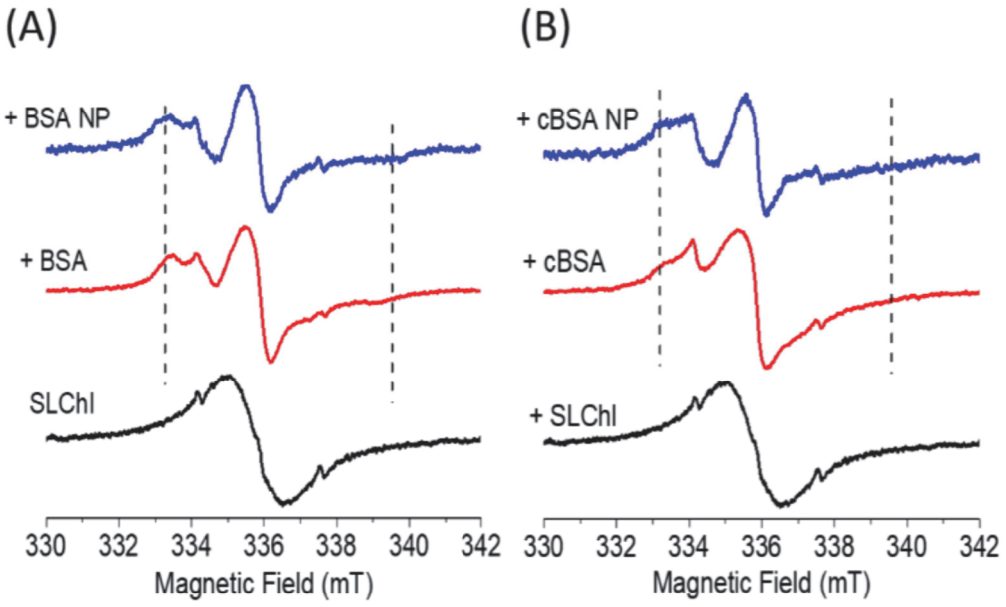

Figure 2.16. EPR spectra of 1.4 mM of SLChl in water (bottom) and upon addition of 0.7 mM of BSA (middle) and BSA NPs (top) (A), and 0.7 mM of cBSA (middle) and cBSA NPs (top) (B) (Sozer and Akdogan, 2022).

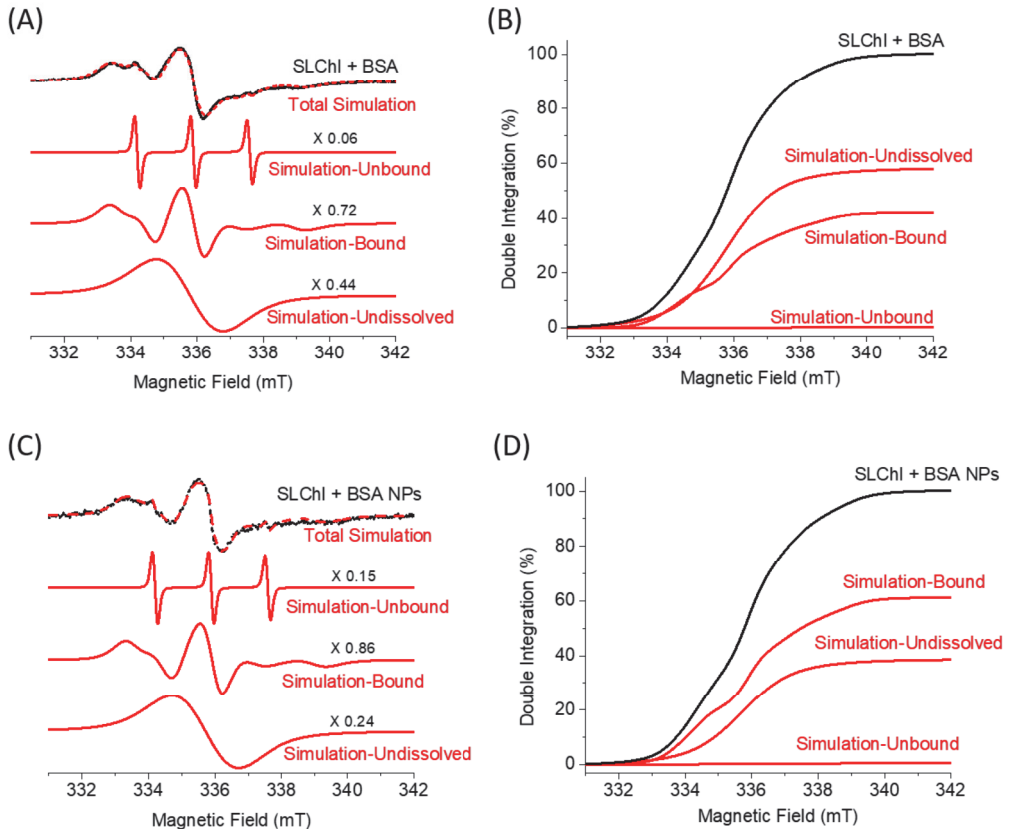

Figure 2.17. (A) EPR spectra of 1.4 mM of SLChl in the presence of 0.7 mM BSA (black) and its total simulation (dashed red) obtained by combination of bound and unbound SLChl EPR simulations (red) after multiplication with the appropriate numbers. (B) % of double integrations of the spectra in (A). (C) 1.4 mM of SLChl in the presence of 0.7 mM BSA NPs (black) and its total simulation (dashed red) obtained by combination of bound and unbound SLChl EPR simulations (red) after multiplication with the appropriate numbers. (D) % of double integrations of the spectra in (C). They are normalized to the double integration of the experiment (Sozer and Akdogan, 2022).

The cBSA proteins and cBSA NPs also favored SLChl solubility in water (Fig. 2.16 (B)). The aggregate concentration decreases from 100% to about 73% and 35% when cBSA proteins and cBSA NPs were added, respectively. As a result, about 26% and 64% of total SLChl bound to the cBSA and cBSA NPs, respectively (Fig. 2.18). Similar to the solubility and binding results of SLIbf, albumin in the form of nanoparticles dissociate SLChl clusters more than albumin proteins.

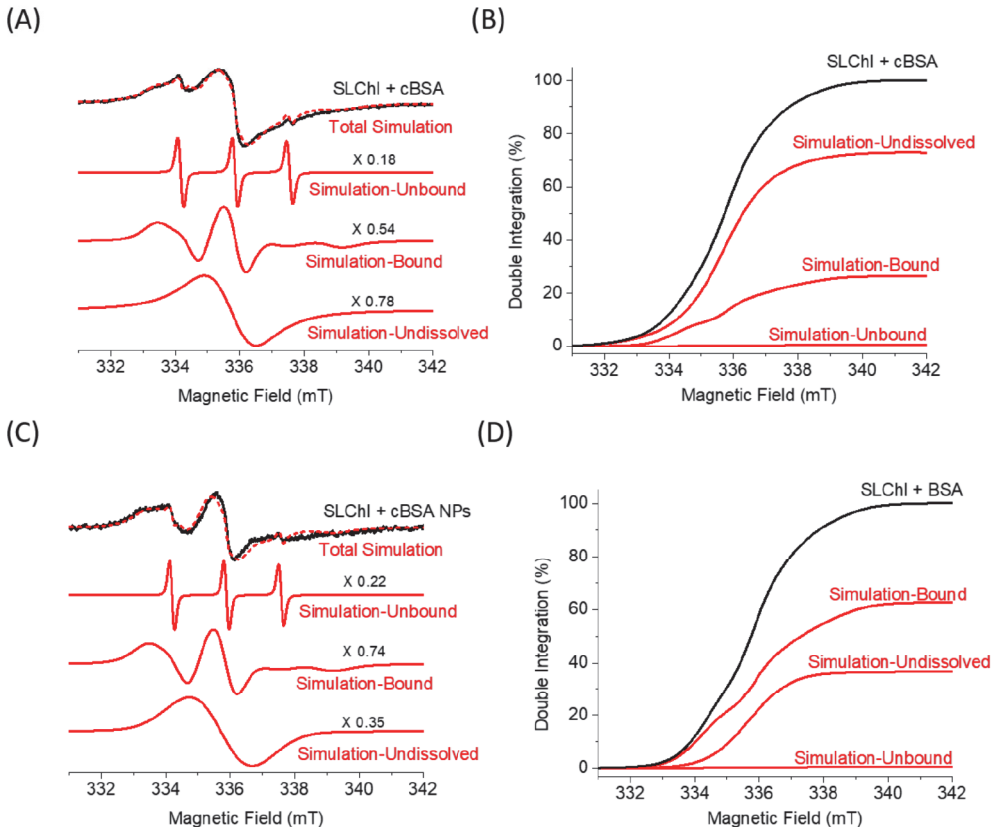

Figure 2.18. (A) EPR spectra of 1.4 mM of SLChl in the presence of 0.7 mM cBSA (black) and its total simulation (dashed red) obtained by combination of bound and unbound SLChl EPR simulations (red) after multiplication with the appropriate numbers. (B) % of double integrations of the spectra in (A). (C) 1.4 mM of SLChl in the presence of 0.7 mM cBSA NPs (black) and its total simulation (dashed red) obtained by combination of bound and unbound SLChl EPR simulations (red) after multiplication with the appropriate numbers. (D) % of double integrations of the spectra in (C). They are normalized to the double integration of the experiment (Sozer and Akdogan, 2022).

In order to clarify the accuracy and sensitivity of EPR spectroscopy, we used UV-Vis spectroscopy to find out the percentages of free (unbound) drugs in the albumin mixtures after centrifugation (for NPs) or ultrafiltration (for protein). UV-Vis spectroscopy is a very sensitive quantitative technique that is used commonly to determine the drug loading (Sozer et al., 2020). The UV-Vis spectra of SLSA, SLIbf and SLChl were shown in Fig. 2.19. Three overlapped signals at 254, 280 and 303 nm were

observed for SLSA. A strong signal at 257 nm and a weak signal at 304 nm were detected for SLChl. However, a broad weak signal between 250 and 280 nm was obtained for SLIbf. Supernatant of drug loaded albumin NPs and filtrate of drug loaded albumin proteins were collected and analyzed by the UV-Vis spectroscopy to calculate the % of free drugs (Eq. 2.2). Therefore, at first calibration curves of SLSA, SLIbf and SLChl were obtained with known concentrations in the same solvent system water:ethanol (1:1, v/v). The calibration curves and equations were shown in Fig. 2.20.

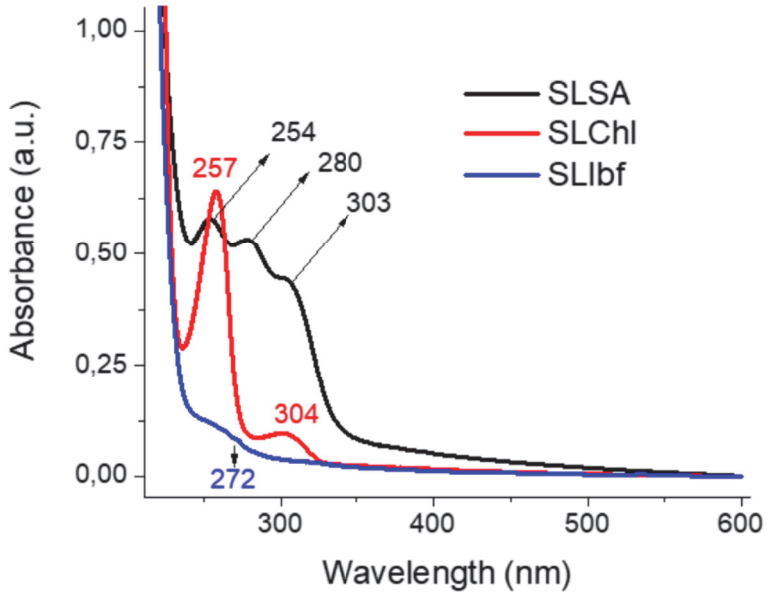

Figure 2.19. UV-Vis spectra of 0.32 mM SLSA, SLChl and SLIbf in water:ethanol (1:1 v/v) mixture (Sozer and Akdogan, 2022).

$$\text{Free Drug (\%)} = \frac{\text{Concentration from the Calibration Equation}}{\text{Initial Concentration}} \times 100 \qquad (2.2)$$

The UV-Vis absorption signal intensity of supernatant of drug BSA NPs or filtrate of drug-BSA solution was converted to corresponding concentration using the calibration equations. The ratio of calculated concentration with the initial drug concentration gives the free drug percentage in the solution. The free (unbound) fraction of SLSA in the BSA NPs solution was obtained by the analysis of its supernatant using the calibration equations of free SLSA in Fig. 2.20 (A) and Eq. 2.2. The UV-Vis result is as same as the result obtained with EPR spectroscopy (48%). Moreover, the obtained percentage of free (unbound) SLSA in the BSA protein solution after ultrafiltration is as same as the result

obtained with the EPR spectroscopy (29%). The same results were also obtained from EPR and UV-Vis spectroscopies when the experiments were repeated with cBSA and cBSA NPs too. This shows the eligibility of EPR spectroscopy in spin labeled drug monitoring. In addition, as explained above EPR spectroscopy can distinguish the rest of drugs e.g. bound and aggregated in the same solution, but it is not possible with UV-Vis spectroscopy, HPLC or turbidimetry.

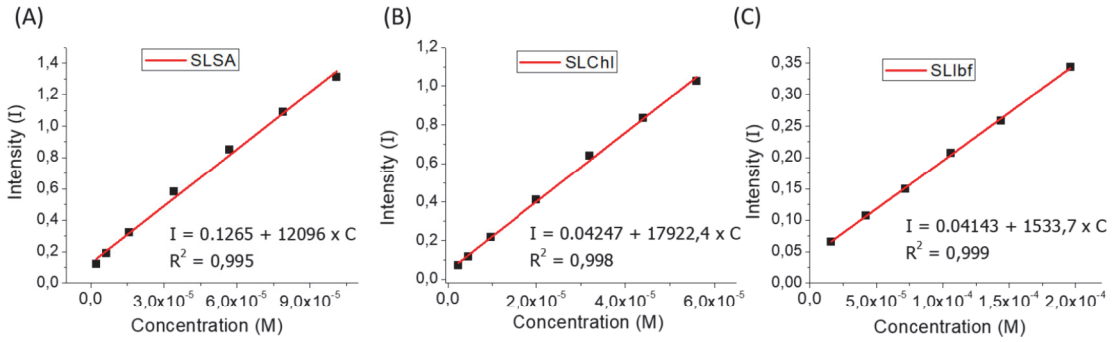

Figure 2.20. Calibration curves and equations for SLSA (A), SLChl (B) and SLIbf (C) using UV-Vis spectroscopy in water:ethanol (1:1 v/v) solution (Sozer and Akdogan, 2022).

For SLChl, EPR measurements showed that less than 1% of SLChl are free upon addition of BSA protein and BSA NPs. Similarly, the absorption signal of SLChl was not observed by measuring the samples with UV-Vis spectroscopy. Although EPR measurements revealed that 6% and 12% of SLIbf were free in the mixture of SLSA-BSA and SLSA-BSA NPs, respectively, their UV-Vis absorption signals could not be detected. This could be explained by the very weak absorption signal of SLIbf (Fig. 2.19).

Drugs can be loaded to albumin nanoparticles in two different ways. Firstly, drugs were incorporated into the albumin solution before the desolvation process (nanoparticle formation). The amount of added SLSA is higher for BSA experiments compared to cBSA experiments since the formation of BSA NPs (82%) is higher than that of cBSA NPs (55%) via desolvation method. Secondly, drugs were incubated with the obtained albumin nanoparticles in water within such a period of time. For both methods, EPR measurements were carried out in three different steps. Figure 2.21 shows the EPR spectra of SLSA in these steps; drug-nanoparticle mixture before the precipitation, in the supernatant of the mixture after precipitation, and in the albumin NPs pellet aqueous solution. Double integrations (*D.I.*) of these EPR spectra showed that total radical concentration in the

drug- nanoparticle mixture before the precipitation was almost equal to the sum of the radicals in the supernatant of the mixture after precipitation, and in the albumin NPs pellet aqueous solution (Eq. 2.3). By this way, drug loading can be directly calculated from pellet aqueous solution or indirectly after subtraction of supernatant result from the result of mixture.

$$\text{D. I. of EPR of Mixture} = \text{D. I. of EPR of Supernatant} + \text{D. I. of EPR of Pellet Dissolution} \quad (2.3)$$

For both drug loading methods, the loading of SLSA in cBSA NPs was higher compared to that in BSA NPs due to the electrostatic attractive interaction between cationic BSA and anionic SLSA. For example, SLSA incorporation before the desolvation process (first method) yielded about 4% of SLSA loading in BSA NPs but about 50% of SLSA loading in cBSA NPs (Fig. 2.21 (A)). On the other hand, addition of drug via incubation method (second method) led to an increase in the drug loadings to 15% and 93% for BSA NPs and cBSA NPs, respectively (Fig. 2.21 (B)). Obtaining lower drug loadings when drugs were incorporated before desolvation could be explained with the effect of desolvating agent in the albumin solution. An extensive electrostatic interaction between acetonitrile and albumin nanoparticles, together with the hydrogen bonding shielded nanoparticle surface and avoids further drugs binding. However, drug loading via incubation method was applied in water. Without any solvent interference, more anionic SLSA molecules are able to bind to cBSA NPs. For BSA NPs, drug loading was also favored via incubation but subsequent dissolution in water released the SLSA from BSA NPs. This showed that weaker interactions caused drug loading to BSA NPs during incubation in water.

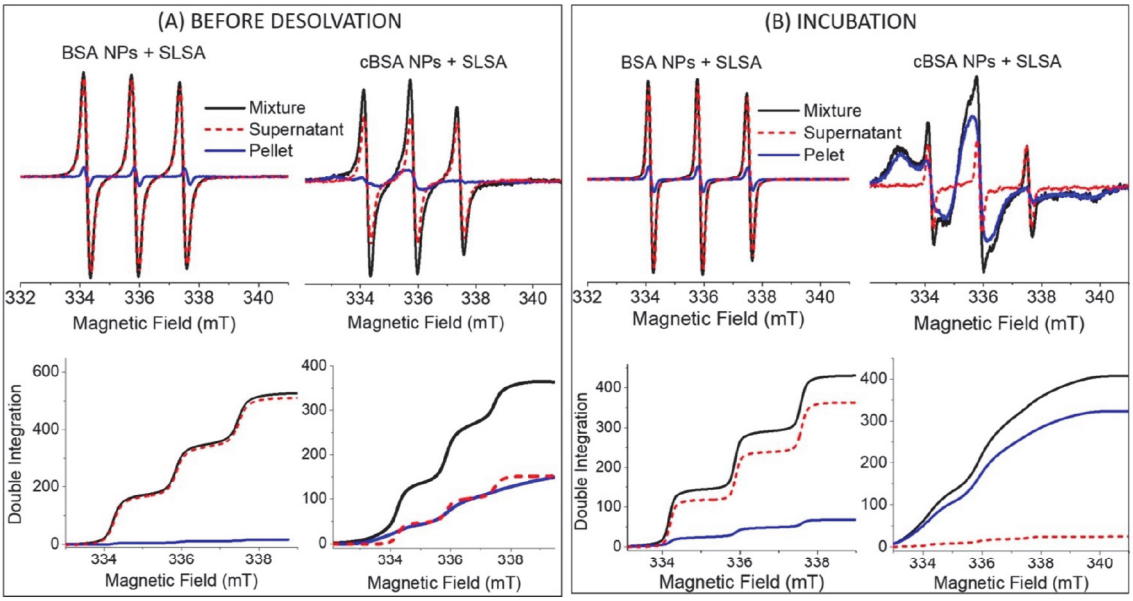

Figure 2.21. (A) SLSA loading was performed before desolvation: EPR spectra of 1.1 mM of SLSA in 0.15 mM of BSA NPs and 0.7 mM of SLSA in 0.1 mM of cBSA NPs solutions (mixtures), supernatant and pellet aqueous solutions, and their corresponding double integration values. (B) SLSA loading after nanoparticle formation via incubation method: EPR spectra of 0.7 mM of SLSA in 0.1 mM of BSA NPs or cBSA NPs solutions (mixtures), supernatant and pellet aqueous solutions, and their corresponding double integration values (Sozer and Akdogan, 2022).

In figure 2.21, the highest SLSA loading values of 50% and 93% were obtained when SLSA was added to cBSA before desolvation, and after cBSA nanoparticle formation (incubation method), respectively. The released amounts of SLSA with time from cBSA NPs prepared from these two methods were also studied. In the dialyzer tube, the initial loaded SLSA concentration is 0.49 mM in cBSA NPs (0.07 mM) aqueous solution. The drug loaded NPs samples were taken from the dialyzer tube with time and measured by EPR spectroscopy. Therefore, the bound SLSA (remained) could be measured directly every time. For the incubation method, the EPR signal intensity decreased with time since the loaded SLSA was released continuously (Fig. 2.22 (A)). Double integrations of these spectra showed an initial rapid release followed by a slower release. Up to 40% of loaded SLSA was released within 4 hours in water at 37 °C. At the end of 30 hours, the total SLSA release from cBSA NPs was found to be around 50% (Fig. 2.22 (B)). On the other hand, addition of SLSA before nanoparticle formation

(desolvation) prevents the SLSA from being released. The signal intensity did not change with time therefore double integrations of the EPR spectra remained constant (Fig. 2.22 (B)). Note that after release experiments, both SLSA loaded cBSA NPs prepared via addition of SLSA before desolvation and after nanoparticle formation (incubation) carried the similar amount of SLSA, 50% after 30 hours. These results showed that there are two types of SLSA binding to cBSA NPs. Strong binding was obtained when SLSA was added to cBSA aqueous solution before desolvation. This type of binding inhibits the release of SLSA. Therefore, initial 50% of drug loading was well preserved. On the other hand, both types of binding, strong and weak were observed with the incubation method. An initial rapid release around 40% within 4 hours provided the presence of weakly bound SLSA. Yet, around 50% of loaded SLSA were still inside the cBSA NPs.

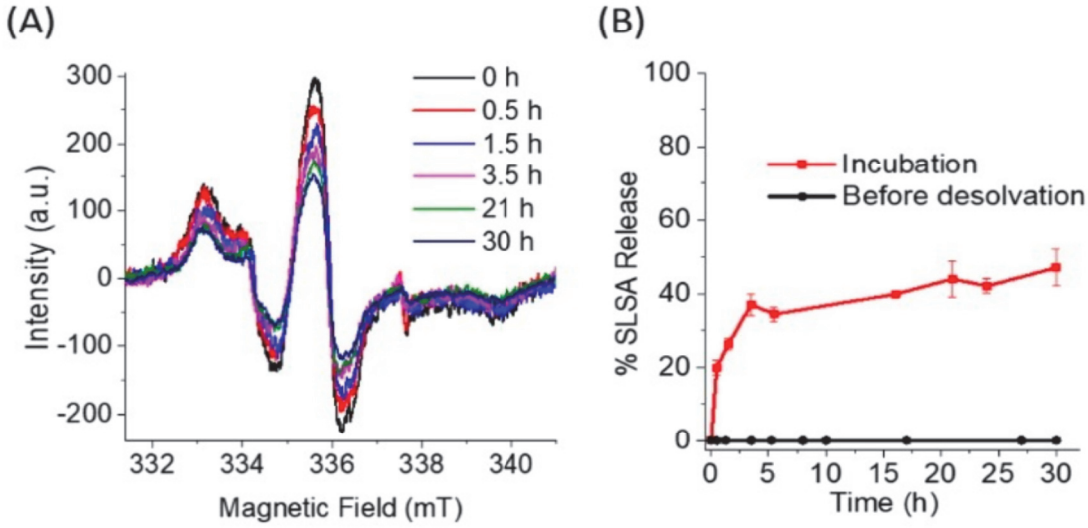

Figure 2.22. (A) EPR spectra of SLSA loaded cBSA NPs aqueous solution in a dialyzer tube as a function of time at 37 °C. SLSA was loaded via incubation method. The initial loaded SLSA concentration is 0.49 mM in cBSA NPs (0.07 mM) aqueous solution. (B) The bound SLSA release profile of cBSA NPs with time upon taking double integrations of spectra in (A) (red). The bound SLSA did not release if the SLSA was added before nanoparticle formation (desolvation) (black) (Sozer and Akdogan, 2022).

2.4. Conclusion

Water soluble albumin proteins and nanoparticles could be used to enhance water solubility of hydrophobic drugs. Several drug binding sites in albumin make various water insoluble drugs transportation possible. Inspiring by this fact, hydrophobic drugs could be transported with albumin nanoparticles.

Here, we compared the effects of BSA proteins and nanoparticles on the solubility of hydrophobic drugs in water. Moreover, as an alternative technique, we used EPR spectroscopy to investigate the drug solubility in addition to binding to and release from albumin proteins and nanoparticles. Spin labeling (SL) of diamagnetic drugs allows monitoring of these drugs directly. In the aqueous solution, the EPR spectroscopy is very sensitive to the spin-spin interactions. Therefore, SLdrugs weather found in the undissolved state or in the free form can be distinguished clearly. Our results showed that albumin nanoparticles are much more effective than albumin proteins in dissolving hydrophobic drugs including SLIbf and SLChl in water (Table 2.3). This suggests that nanoparticles could disturb undissolved SLIbf and SLChl aggregates more than proteins. However, well-dissolved SLSA prefers to bind to BSA protein binding pockets more than BSA NPs. Unbound fractions of SLdrugs were also determined by a well known technique of UV- Vis spectroscopy. Although UV-Vis results of unbound fractions of SLSA and SLChl are as same as the results of EPR measurements, the absorption signals of SLIbf could not be detected by UV-Vis spectroscopy due to its low absorption signal.

In addition, EPR spectroscopy can distinguish whether dissolved SLdrugs are bound to transporter or not due to its sensitivity to the rotational dynamics of the radical center. For example, in the presence of albumin proteins or nanoparticles, the dissolved hydrophobic SLIbf and SLChl preferred to bind to these carriers very highly. In addition, cationization of albumin provides much more anionic drug (SLSA) loading via electrostatic interactions (Table 2.3). Also, the higher cationic surface charge of cBSA NPs compared to that of cBSA protein provided more SLSA loading to NPs.

Furthermore, we compared two drug loading methods by EPR spectroscopy; addition of drug before desolvation or via incubation. SLSA can be loaded to cBSA NPs with 50% and 93% via addition of SLSA before desolvation and after NPs formation (incubation), respectively. Different from other techniques, drug loading could be measured directly from the NPs pellet dissolution. In addition, it could be measured

indirectly from measuring the radical concentrations in initial mixture and the supernatant. Yet, both measurements must provide the same drug loading result. Moreover, different from other techniques, drug release can be monitored from the NPs pellet dissolution. The remained drug in the NPs can be measured directly by EPR spectroscopy. In conclusion, the results suggested that EPR spectroscopy can be used as an alternative technique to obtain reliable drug solubility, drug loading and release data.

Table 2.3. Percentages of undissolved, dissolved-unbound and dissolved-bound 4.9 mM of SLSA and SLIbf, and 1.4 mM of SLChl in water, and upon addition of 0.7 mM of BSA, BSA NPs, cBSA or cBSA NPs determined by EPR spectroscopy (Sozer and Akdogan, 2022).

SLDrugs	in water (%)	+ BSA (%)	+ BSA NPs (%)	+ cBSA (%)	+ cBSA NPs (%)
SLSA					
Undissolved	0	0	0	0	0
Unbound	100	29	48	15	4
Bound	0	71	52	85	96
SLIbf					
Undissolved	95	48	4	50	24
Unbound	5	6	12	7	9
Bound	0	46	84	43	67
SLChl					
Undissolved	100	58	38	73	35
Unbound	0	0	1	1	1
Bound	0	42	61	26	64

CHAPTER 3

A GREEN ROUTE TO ALBUMIN/ALBUMIN POLYELECTROLYTE COMPLEX NANOPARTICLES IN WATER WITH HIGH DRUG LOADING FOR DRUG DELIVERY

3.1. Introduction

Green chemistry plays a vital role in eliminating the use of traditional organic solvents, stabilizers, and crosslinkers, which pose an environmental hazardous and biosafety risks during the production of drug carriers and may be associated with toxic side effects of the final product (Kanwar et al., 2019). Polyelectrolyte complexes (PEC) can be formed in water alone; due to the strong electrostatic attraction between oppositely charged molecules (Buriuli et al., 2017). Therefore, PEC formation method not only surpasses the need for organic solvents, initiators, stabilizers, catalysts or crosslinkers, it also provides a relatively easy protocol without need for specialized instrumentation (Lankalapalli et al., 2009; Durmaz et al., 2020). PECs have a wide range of clinical and industrial applications, including enzyme immobilization (Kokufuta et al., 1992), antigen transport for immunoprotection (Andrianov et al., 2005), cell micropatterning (Kumar et al., 2003), biosensor design (Chaniotakis et al., 2004), protein purification (Dubin et al., 1994), food product stabilization (Tuinier and de Kruif, 2002), and drug delivery (Wu et al., 2020).

Serum albumin protein is a valuable component in the development of drug nanocarriers due to its high drug-carrying capacity, biocompatibility and biodegradability (Spada et al., 2021; Argitekin et al., 2023; Solanki et al., 2021). Therefore, several methods have been applied for the preparation of albumin nanoparticles (NPs), emulsification and desolvation methods being the most frequently used ones (Langer et al., 2003; Qu et al., 2024; Argitekin et al., 2025; Srivastava et al., 2020; Akdogan et al., 2022; Ghosh et al., 2022; Cakan-Akdogan et al., 2022; Solanki et al., 2024). Challenges encountered with these methods include the use of organic solvents, surfactants, and

crosslinkers that may be toxic, and the requirement for specialized equipment such as high-pressure, ultrasonic or high-speed homogenizers. Organic solvents can also affect the size, size distribution, and stability of albumin NPs, as well as the solubility and albumin NP binding affinity of the drugs (Von Storp et al., 2012). The most commonly used crosslinker, glutaraldehyde has toxic properties and was shown to have undesirable interactions with cargo molecules through primary amines or thiol groups (St Clair et al., 1991; Fürst et al., 2005; Okuda et al., 1991; Migneault et al., 2004).

The intrinsic polyelectrolyte properties of serum albumin have been utilized for the preparation of NPs in conjunction with other polyelectrolytes. In the literature, cationic chitosan polysaccharide and anionic bovine serum albumin (BSA) proteins formed PEC NPs with a size around 235 nm, which was used to carry Resveratrol, a chemo-preventive agent (Ghorbani et al., 2018). Differently, PECs formed with cationic BSA (cBSA) and plasmid DNA were tested as gene transfection agent (Eisele et al., 2010). Also, coacervate structures were obtained by the mixture of cationic BSA and anionic polysaccharides, including pectin and gum acacia (Ferreira et al., 2021). However, to date, no albumin/albumin PECs have been reported. Here, the native BSA protein (isoelectric point (pI) = 5.0) was used as polyanions, while, cationic BSA (cBSA) obtained upon conjugating with ethylenediamine was used as polycations (pI =10.1) (Sozer et al., 2020). Although, ethylenediamine presents potential health risks, including irritation to the skin and eyes as well as respiratory sensitization, it was used only for the cationization of reactant BSA proteins, and all subsequent purification steps were performed to remove unreacted ethylenediamine before further use. After cBSA protein was obtained, a green method for synthesizing albumin PEC NPs was developed. This method relies on attractive electrostatic interactions between water-soluble albumin molecules, without the need for organic solvents (e.g. methanol, ethanol, acetone), crosslinkers (glutaraldehyde) and specialized equipment.

Another advantage of using PECs in drug delivery studies may be to achieve higher drug loading. In emulsification or desolvation methods, water-insoluble drugs prefer to remain in the organic solvent environment rather than albumin nanoparticles, resulting in lower drug entrapment efficiency and drug loading. Here, drug loading and release properties of albumin PEC NPs with chlorambucil (CHL) were studied. CHL, an anticancer drug, was employed to evaluate the drug-loading capacity of the albumin PEC NPs. CHL is an alkylating antineoplastic drug that acts by attacking DNA, and is used in the treatment of advanced ovarian and breast cancers, leukemia, lymph cancer, and

Hodgkin lymphoma (Saha et al., 2019; Bielawski et al., 2011; Zhang et al., 2004; Antonio et al., 2014). Due to its poor water solubility, low hydrolytic stability, and the need for improved specificity toward cancer cells (Saha et al., 2019; Yordanov et al., 2010; Zhang et al., 2017). In the previous chapter, water-insoluble drug of CHL could not be encapsulated by albumin nanoparticles during the desolvation method because the hydrophobic CHL preferred to be solvated in the organic solvent (Sozer and Akdogan, 2022). On the other hand, if drug encapsulation could be completed in water during the nanoparticle formation, the drugs will move into the nanoparticles.

Also, CHL has been investigated using various nanocarrier systems. These include butylcyanoacrylate polymers prepared via emulsion polymerization (Yordanov et al., 2010), albumin/liposome hybrid systems formed through a microemulsion process with a high-pressure homogenizer (Zhang et al., 2017), and albumin NPs synthesized in a microemulsion ionic liquid system using a high-speed homogenizer and the crosslinker glutaraldehyde (Akdogan et al., 2022). Alternatively, in this thesis, CHL loading was achieved into albumin PEC NPs without the need for organic solvents, crosslinkers and specified equipment, and then their cellular uptake and effects on cell viability were studied (Fig. 3.1).

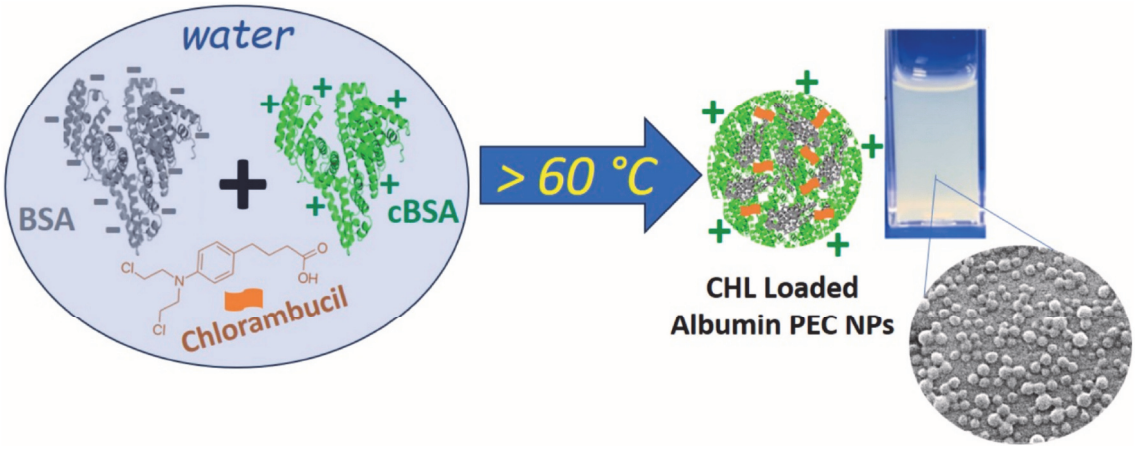

Figure 3.1. Schematic representation of chlorambucil (CHL) loaded albumin polyelectrolyte complex (PEC) nanoparticles (NPs) synthesis in water, without using organic solvents and crosslinkers. BSA: Bovine serum albumin, cBSA: Cationic bovine serum albumin (Sozer-Demirdas, et al. 2025).

3.2. Materials and Methods

3.2.1. Materials

Bovine serum albumin (BSA, Mw: 66.5 kDa lyophilized powder, >96 %), fluorescein isothiocyanate (FTIC) labeled BSA proteins, N-(3-Dimethylaminopropyl)-N′-ethyl carbodiimide hydrochloride (EDC), ethylenediamine (EDA), glutaraldehyde solution (8 % (v/v) in H2O), chlorambucil, dimethyl sulfoxide (DMSO) were purchased from Sigma–Aldrich. Methoxy PEG succimidyl carbonate (m-PEG-SC, 10 K) was purchased from JenKem Technology.

3.2.2. Preparation of cationic bovine serum albumin protein (cBSA)

A solution of 50 mg BSA in 500 µL deionized water was prepared. 650 µL of ethylenediamine was combined with 500 µL deionized water, and the pH was adjusted to 4.75 by adding 9 mL of 6 M HCl. The BSA solution was added to the ethylenediamine solution. Subsequently, 14.5 mg of EDC was dissolved in 15 µL deionized water and slowly introduced into the BSA- ethylenediamine mixture. After two hours of stirring at 750 rpm, the reaction was stopped by adding 4 M acetate buffer (pH 4.75). The resulting cBSA proteins were purified by repeated centrifugation (13,000 rpm for 3 minutes) for three cycles using 0.1 M acetate buffer and deionized water to remove excess EDC and ethylenediamine through an Amicon® Ultra centrifugal filter (molecular cut off: 50 kDa). The final cBSA was collected, and then it was lyophilized and stored at 4 °C. The cBSA yield was 70% wt.

3.2.3. Preparation of albumin PEC NPs

In the formation of albumin-albumin polyelectrolyte complex nanoparticles (PEC NPs), cationic albumin protein (cBSA) and natural albumin protein (BSA) were used as a cationic polyelectrolyte and an anionic polyelectrolyte, respectively. Albumin PEC was rapidly formed by mixing proteins in an aqueous system. In detail, 8 mg of cationic BSA

(cBSA) was dissolved in 0.375 mL of distilled water. Separately, 27 mg of anionic BSA was dissolved in 4.5 mL of distilled water and then added dropwisely to the aqueous cBSA solution at a rate of 1 mL/min. The albumin polyelectrolyte complex was formed under 750 rpm continuous stirring for 5 hours (Fig. 3.2 (A)). The synthesis of PEC NPs was influenced by various factors including the concentration of the albumin in the solution, crosslinking agent, and heating of the solution. These parameters were varied as described below to determine their impact on NP formation.

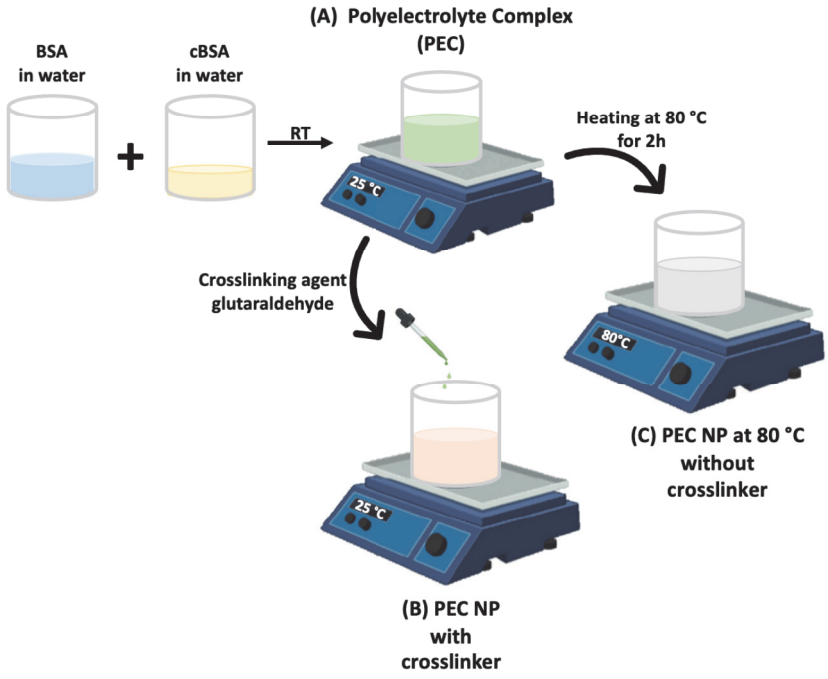

Figure 3.2. Schematic representation of cBSA:BSA polyelectrolyte complex (PEC) formation and PEC nanoparticle (PEC NP) synthesis under different conditions: (A) PEC formation by mixing BSA and cBSA proteins without crosslinking at room temperature (RT), (B) PEC NP synthesis via glutaraldehyde crosslinking at RT, and (C) PEC NP synthesis without crosslinking at 80°C.

3.2.3.1. Concentration Effect

Effects of cBSA:BSA molar ratios were studied in the formation of the cBSA:BSA PEC NPs. Albumin PEC NPs were obtained by using different cBSA:BSA molar ratios as 1:2.5, 1:3, 1:3.5, 1:4 and 1:5. Also, total albumin protein concentration in the water

system was studied. Total albumin concentrations of 3.2, 6.5, 12.2 and 24.6 mg/mL were investigated.

3.2.3.2. Crosslinking Effect

Crosslinking agent effect was studied in the formation of the albumin PEC NPs with glutaraldehyde crosslinking. Albumin PEC NPs were prepared with different amounts of the crosslinking agent glutaraldehyde. After, the mixing of polycation and polyanion solutions, albumin PEC NPs were crosslinked with glutaraldehyde. Then, the mixture was stirred for 5 hours (Fig. 3.2 (B)). Glutaraldehyde was used at concentrations corresponding to 50%, 100%, and 150% of the theoretically required amount for complete crosslinking of the 71 ε-amino groups of lysine residues in the cBSA:BSA matrix. The albumin PEC NPs to be formed were centrifuged at the end of 5 hours and purified from the excess albumin that did not participate in the nanoparticle formation.

3.2.3.3. Heating Effect

After mixing BSA and cBSA proteins at RT for 10 minutes, the temperature of the system was increased to 60 °C, 70 °C, 80 °C and 90 °C. The mixture was kept at high temperatures for 2 hours under stirring at 750 rpm (Fig. 3.2 (C)). Then, the obtained NPs were purified with centrifugation at RT. The final albumin PEC NPs were collected and stored at 4 °C.

3.2.4. Characterization of albumin PEC NPs

Obtained albumin PEC NPs pellets were lyophilized after NP purification for yield calculations. Lyophilized albumin PEC NPs were dissolved in distilled water for size and zeta potential studies. The scanning electron microscope was used to examine the size and form of the albumin PEC NPs (SEM, FEI QUANTA 250 FEG). Samples were prepared by depositing 5 μL of a 1:50 diluted NP suspension put onto aluminum foil and air-drying overnight for SEM analysis. The dried samples were then coated with gold using an EMITECH K550X in a vacuum. The accelerating voltages ranged from 5-7 kV. In addition, the size of albumin PEC NPs was determined using a Malvern dynamic light

scattering (DLS) at a wavelength of 632 nm. The scattering angle was adjusted to 173°. A Malvern dynamic light scattering (DLS) Nano-ZS equipment was used to obtain the zeta potential of albumin PEC NPs (Worcestershire, UK).

3.2.5. Biodegradation test

The enzymatic degradation of albumin PEC NPs was carried out according to the procedure for biodegradability testing of HSA NPs reported by Langer et al (Langer et al., 2008). A suspension of 1000 μg/mL albumin PEC NPs in 0.01 M PBS buffer (pH 7.4) was mixed with trypsin enzymes, with the final trypsin concentration of 50 μg/mL. The degradation of the albumin PEC NPs after the addition of trypsin was assessed by measuring the turbidity of the suspension. The mixture was stirred at 500 rpm and maintained at 37 °C, and turbidity was measured photometrically at 565 nm at different time intervals. For the control experiment, the same procedure was followed for the albumin PEC NPs without trypsin. The remaining albumin PEC NPs in the suspension were quantified using a calibration curve generated from different concentrations of albumin PEC NPs.

3.2.6. Chlorambucil loading into albumin PEC NPs via incorporation method

8 mg of cBSA was dissolved in distilled water and 27 mg of BSA was dissolved in distilled water, separately. Chlorambucil (CHL) stock solutions were prepared in DMSO. CHL was added to each albumin solution at different molar ratios albumin:CHL 1:1, 1:3 and 1:5 while keeping the DMSO content constant at less than 2% (v/v). CHL loaded albumin solutions were mixed for 20 minutes with 750 rpm stirring. After the incorporation of CHL with albumins, CHL loaded BSA aqueous solution was added to CHL loaded cBSA aqueous solution using a syringe pump at a flow rate of 1 mL/min at a 1:3.5 molar ratio of cBSA:BSA. The mixture was stirred for 10 minutes at RT. Then, the mixture was put in a hot bath at 80 °C for 2 hours under stirring. CHL loaded albumin PEC NPs were transported to eppendorf tubes to be centrifuged at 12,000 rpm (9,700 g) for 15 minutes. It was dissolved again in water and was centrifuged to eliminate the unbound drugs.

3.2.7. Chlorambucil loading into albumin PEC NPs via incubation method

4 mg of albumin PEC NPs were dissolved in 2 mL of distilled water. CHL dissolved in DMSO was added to aqueous albumin PEC NPs at different molar ratios of albumin PEC NPs:CHL 1:1, 1:3 and 1:5 while keeping the DMSO content constant at less than 2% (v/v). CHL loaded albumin PEC NPs were stirred at 750 rpm for 5 hours at RT. CHL loaded albumin PEC NPs were transported to eppendorf tubes to be centrifuged at 12,000 rpm (9,700 g) for 15 minutes. It was dissolved again in water and was centrifuged to eliminate the unbound drugs.

3.2.8. Chlorambucil loading into BSA NPs via desolvation method

CHL loading into conventional BSA NPs was studied with the desolvation method. 62.5 mg/mL BSA was dissolved in distilled water. CHL stock solution was prepared in DMSO and dissolved CHL was added to aqueous albumin solution at different molar ratios of albumin:CHL 1:1, 1:3 and 1:5. CHL loaded albumin solutions were mixed for 20 minutes with 750 rpm stirring. Then, ethanol was added dropwise by using a syringe pump with a flow rate of 1 mL/min. The volume ratio of ethanol and water in the system was adjusted to 3:1. CHL loaded BSA NPs were crosslinked with 18 μL of 8% (v/v) glutaraldehyde. The mixture was stirred for overnight at 750 rpm. CHL loaded BSA NPs were transported to eppendorf tubes to be centrifuged at 12,000 rpm (9,700 g) for 15 minutes. It was dissolved again in water and was centrifuged to eliminate the unbound drugs. Bare BSA NPs were also prepared without CHL.

3.2.9. Measuring the percentages of entrapment efficiency and drug loading

CHL loaded NPs were centrifugated at 12,000 rpm (9,700 g) for 15 minutes. Supernatants were collected and analysed by the UV-Vis spectrophotometer to calculate the percentage of drug entrapment efficiency (Eq. (1)) and the percentage of drug loading

(Eq. (2)). For the calibration curve, chlorambucil stock solutions in the water were prepared. The curve was linear and passed through the origin (R^2= 0.9922, n= 6).

$$\text{Entrapment Efficiency (\%)} = \frac{(\text{Initial Drug Weight} - \text{Drug Weight in Supernatant})}{(\text{Initial Drug Weight})} \text{x}100 \quad (3.1)$$

$$\text{Drug Loading (\%)} = \frac{(\text{Weight of Drug in Nanoparticles})}{(\text{Weight of Nanoparticle})} \times 100 \quad (3.2)$$

3.2.10. In vitro release of CHL from albumin PEC NPs

In vitro release of CHL from albumin PEC NPs prepared with incorporation method at molar ratio 1:5 was performed in PBS buffer (0.01 M, pH:7.4). In addition, the same amount of free CHL releasing was performed in PBS. 5 mg of CHL loaded albumin PEC NPs was dissolved in 0.8 mL of distilled water. The solution was then transferred into 0.8 mL D-tube dialysers (Merck, MWCO 6-8 kDa). The dialyzer tube was immersed in a beaker containing 32 mL of PBS at 37 °C and stirred at 550 rpm. At predefined time intervals, 2 mL of sample was collected and analysed with a UV-Vis spectrophotometer to calculate the quantity of CHL released from albumin PEC NPs using the CHL calibration curve. Following measurements, the 2 mL samples were put into the beakers back. Experiments were conducted three times.

3.2.11. PEG Coating of Albumin PEC NPs

PEG coatings (PEGylation) of albumin PEC NPs and drug loaded albumin PEC NPs were carried out by following the procedure for HSA NPs reported by Fahrländer et al. (Fahrländer et al., 2015). Specifically, 2.5 mg of albumin PEC NPs were dispersed in 250 µL of HEPES buffer (pH 8.0) under gentle stirring. A separate solution containing 6.25 mg of m-PEG-SC dissolved in 62.5 µL of distilled water was then added dropwise to the albumin PEC NP suspension over a period of 30 s. The mixtures were stirred for 2 h at RT. The resulting PEGylated albumin PEC NPs were purified by repeated centrifugation (16,000g for 20 min) for 3 cycles using deionized water to remove unbound m-PEG-SC.

3.2.12. Cell Uptake and Imagining

Human hepatocellular carcinoma cell type which is primary liver cancer (Huh-7) was used in cellular uptake assay. Huh-7 cells were cultured in Dulbecco's Modified Eagle Medium (DMEM) at 37 °C incubator with 5 % CO_2. DMEM was prepared with 1 % penicillin/streptomycin, 1 % non-essential amino acid and 10 % fetal bovine serum (FBS). Huh-7 cells stained with CM-Dil were seeded at 70,000 cells/well density on 8-well imaging slides. CM-DiI is a fluorescent membrane dye that enables visualization of the cell boundary, facilitating the assessment of nanoparticle internalization.

For the cell uptake experiments, albumin PEC NPs were prepared by using green fluorophore fluorescein isothiocyanate (FTIC) labeled BSA proteins. Albumin PEC NPs were prepared using a mixture of FITC labeled and unlabeled albumin at a 1:5 ratio (FITC-BSA:BSA) to reduce the cost associated with FITC labeled BSA, reduce fluorescence quenching, and prevent potential alterations in NP formation due to labeling, while still ensuring sufficient fluorescence for detection. CHL loading was achieved via incorporation method (Alb:CHL molar ratio 1:5). Finally, PEG was used to coat the albumin PEC NPs. Cells were incubated with 12.5 μg/mL of CHL loaded or unloaded PEG coated FITC albumin PEC NPs in fresh DMEM at 37 °C for 24 h. In addition, cell uptake experiments were performed using conventional BSA NPs prepared using FITC labeled BSA proteins. A low NP concentration of 12.5 μg/mL was employed to allow visualization of individual particles and to minimize cytotoxicity, particularly when using CHL loaded NPs. Cells were fixed with 4 % formaldehyde for 30 min and post stained with DAPI for 45 min. A drop of 80 % glycerol was added to the 8-well chamber slides before sealing by coverslip. Confocal Microscopy (Zeiss LSM880) with 63× objective were used for imaging. Images were collected as 63×magnification Z-stacks at 2 μm intervals. Images were processed with ImageJ to create overlay images with the same laser and scanning settings for all images.

3.2.13. Cell Viability Assay

Cells (Huh-7, MCF-7 and HEK293T) were seeded 10,000 cells/well in 96-well plates incubated in DMEM at 37 °C with 5 % CO_2 incubator. MCF-7 and HEK293T cells were coated with human fibronectin (F2006, Sigma Aldrich) on a 96-well plate before seeding. 20 µL of fibronectin (0.01 mg/mL) was added to each well, incubated for 1 h in a laminar flow cabinet, and then the fibronectin was removed before adding the cells. MTT (Sigma- Aldrich M5655) assay was performed according to ISO 10993-5 ICH guidelines standards. Dispersions of PEG coated albumin PEC NPs and PEG coated CHL loaded albumin PEC NP (through incorporation) were prepared in DMEM. Then, cells were treated with serial dilutions of these albumin PEC NPs at final concentrations of 50, 12.5, 6.25, 1.6 and 0.4 µg/mL. Also, cells were treated with free CHL at final concentrations of 3.2, 0.8, 0.4, 0.10, 0.025 µg/mL. After 24 h incubation with albumin PEC NPs, CHL loaded albumin PEC NPs and free CHL, the treatment was replaced with DMEM containing 10 µL MTT reagent, incubated at 37 °C for 4 h. Absorbance at 570 nm was measured using a BioTek Synergy H1 microplate reader. The increase in absorbance was used to calculate cell viability relative to control wells, which were considered to have 100 % viability. Each measurement was performed in four replicates, and the percentage viability was determined. Statistical analyses were performed using GraphPad Prism 10.0. Two-way analysis of variance (2-way ANOVA) was used to Tukey comparison test. Error bars represent ±SD, ns: non-significant, *P ≤0.05, **P ≤ 0.01, ***P ≤0.001, ****P ≤0.0001.

3.2.14. mRNA Loading on albumin PEC NPs

The mRNA loading behaviour of albumin PEC nanoparticles was also studied. Briefly, 2 mg of albumin PEC NPs were dissolved in 400 µL of nuclease-free water by vortexing, and sonicated at 21°C for 15 min. For the loading process, mRNA was prepared with albumin PEC nanoparticles at molar ratios of 266:1, 26:1, 13:1, and 2.6:1. For each ratio, equal volumes of mRNA and nanoparticle solutions were mixed to reach the total volume with nuclease-free water. The prepared mRNA-albumin PEC NP mixtures were incubated on an orbital shaker at 500 rpm for 30 min to reinitiate complex formation. The incubated samples were further centrifuged at 14,000 rpm for 15 minutes to obtain mRNA loaded albumin PEC NPs as pellets. They were separated according to

the process steps for nanodrop measurements and DLS characterization and made ready for analysis.

3.3. Results and Discussion

cBSA proteins were prepared by conjugating ethylenediamine to BSA in the presence of N-(3-dimethylaminopropyl)-N′-ethyl carbodiimide hydrochloride (EDC) (Sozer et al., 2020). The net surface charge of BSA protein was changed from −12 mV to +25 mV in distilled water (Fig. 3.3). This shows that ethylenediamine molecules reacted with the carboxylic acid side chains of amino acid residues of Asp and Glu. Upon mixture of cBSA as the polycation and BSA as the polyanion in water, albumin PEC NPs were obtained (Fig. 3.2). The formation of albumin PEC NPs is primarily influenced by the molar ratio of cBSA to BSA, the total albumin concentration, and the temperature.

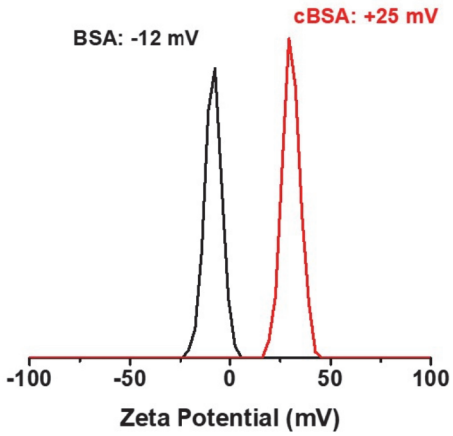

Figure 3.3. The zeta potentials of BSA (black) and cationic BSA (cBSA) (red) proteins were measured in distilled water (Sozer-Demirdas et al., 2025).

Different cBSA:BSA molar ratios were studied at 1:2.5, 1:3, 1:3.5, 1:4 and 1:5 with a total concentration of albumin 6.5 mg/mL. Turbidity was not observed in the cBSA:BSA PEC solution until the molar ratio of cBSA:BSA reached to 1:2.5. Then, turbidity increased with further BSA addition, reaching a maximum at a 1:3.5 M ratio (Fig. 3.4). Therefore, at room temperature, different total albumin concentrations of 3.2, 6.5, 12.2 and 24.6 mg/mL were studied at a 1:3.5 M ratio of cBSA:BSA. SEM results

showed the formation of nonuniform aggregates for all concentrations (Fig. 3.5). But, a limited number of isolated albumin PEC NPs were detected exclusively at a total protein concentration of 6.5 mg/mL, following a brief centrifugation to eliminate aggregates. According to the SEM and DLS results, the particle sizes of these albumin PEC NPs are smaller than 400 nm, exhibiting both spherical and non-spherical shapes (Fig. 3.6 (A) and (B)). The zeta potential of them was found to be +11 mV (Fig. 3.6 (C)), and the formation yield was found to be around 7 %.

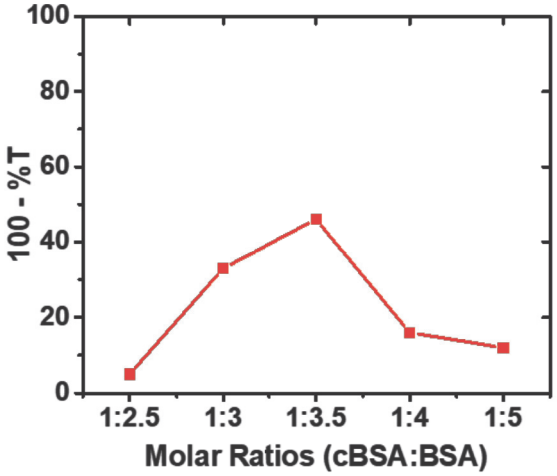

Figure 3.4. Turbidity (100 - T%) versus molar ratios of a system containing cBSA:BSA in different molar ratios (Sozer-Demirdas et al., 2025).

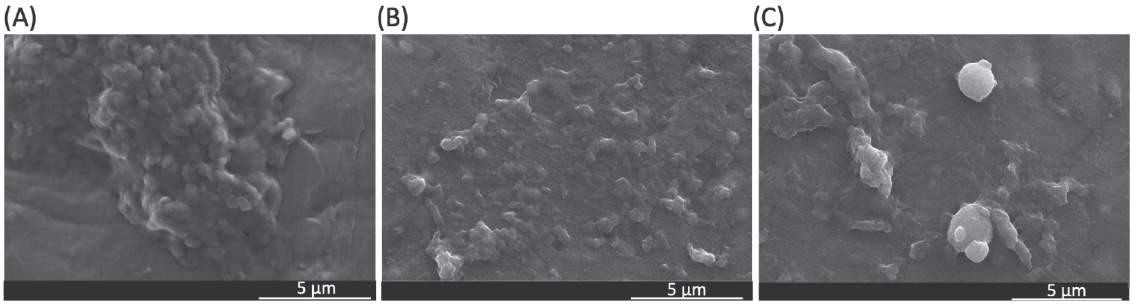

Figure 3.5. SEM images of albumin PEC NPs producing with different albumin concentrations; (A) 3.2 mg/mL, (B) 12.2 mg/mL and (C) 24.6 mg/mL (Sozer-Demirdas et al., 2025).

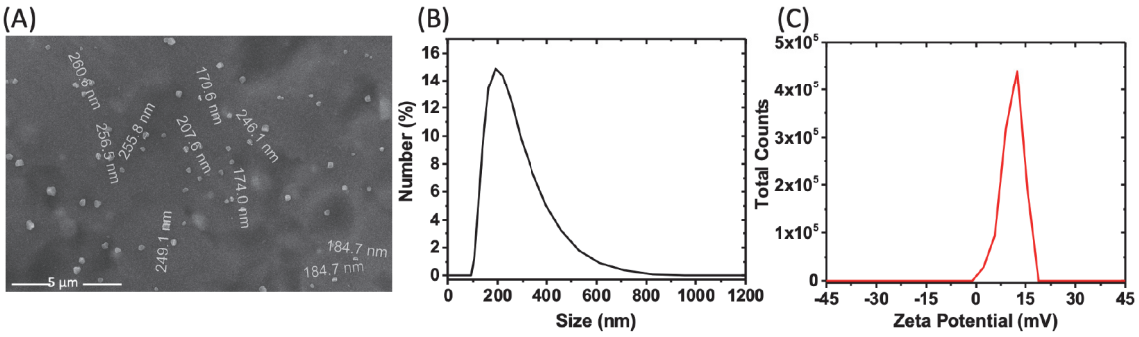

Figure 3.6. (A) SEM image of albumin PEC NPs prepared in water without glutaraldehyde and organic solvents. (B) Hydrodynamic particle size distribution and (C) zeta potential of albumin PEC NPs obtained from DLS measurements. Sample was prepared with 1:3.5 molar ratio of cBSA:BSA at 6.5 mg/mL total albumin concentration (Sozer-Demirdas et al., 2025).

After obtaining maximum albumin complex formation at the 1:3.5 molar ratio of cBSA:BSA, crosslinking agent was added. Effects of crosslinking agents on the resulting albumin PEC were investigated individually by adding glutaraldehyde, citric acid, EDC or glucose crosslinkers. Among used crosslinkers, only glutaraldehyde yielded albumin PEC NPs. Other crosslinkers used as an alternative to glutaraldehyde having low toxicity caused albumin aggregates. BSA proteins are crosslinked with glutaraldehyde via 59 amino groups of lysine found in their structure (Carter and Ho, 1994). However, albumin PEC complex system contains more amino groups due to the presence of ethylenediamines conjugated to BSA in cBSA proteins. In figure 3.7 (A), SEM image shows that albumin PEC NPs crosslinked with glutaraldehyde yielded spherical particles in the range of 300 and 800 nm. The yield of nanoparticle formation was found to be 22.5%. Figure 3.7 (B) shows the hydrodynamic size of albumin PEC NPs obtained by DLS measurements. The average size of albumin PEC NPs was found to be 569 nm with a PDI value of 0.24. The surface charges of albumin PEC NPs were found to be around -15.6 mV (Fig. 3.7 (C)).

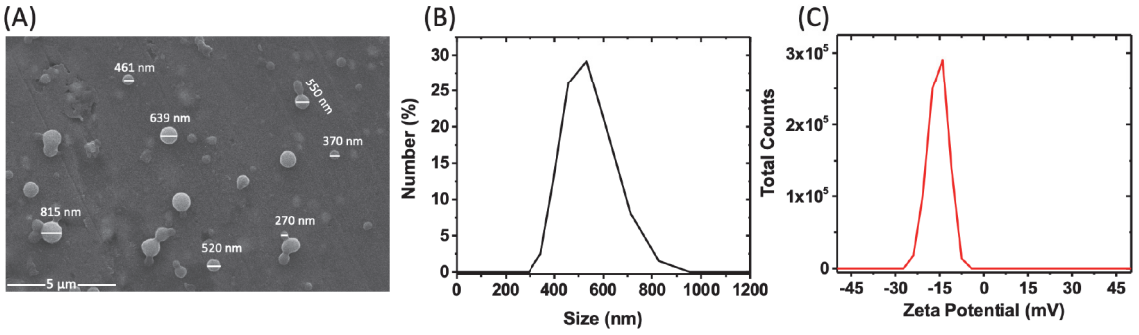

Figure 3.7. (A) SEM image of albumin PEC NPs crosslinked with glutaraldehyde in water system. (B) Particle size distribution and (C) zeta potential results of albumin PEC NPs obtained by DLS measurements. (1:3.5 molar ratio of cBSA:BSA, 6.5 mg/mL albumin concentration).

The temperature effect was evaluated in the formation of albumin PEC NP system to have a higher formation efficiency, more spherical and homogeneously distributed albumin PEC NPs without the use of organic solvents and crosslinkers. The denaturation temperature of BSA protein in aqueous solution typically begins above 65 °C (Nnyigide et al., 2020). Fig. 3.8 shows images of albumin PEC NPs solutions in tubes, obtained at different preparation temperatures. The lowest NP turbidity was observed at 50 °C, suggesting less aggregate formation. However, the turbidity increased significantly when the temperature of mixture was raised to 60 °C and above due to the higher albumin PEC NPs formation yield. The smaller particles with a uniform size distribution and high formation yield (38 wt%) were obtained at 80 °C. Fig. 3.9 (A) shows the SEM image of well-dispersed albumin PEC NPs with sizes below 200 nm. The particle size distribution has a maximum at around 110 nm (Fig. 3.9 (B)). The hydrodynamic size distribution was shown in Fig. 3.9 (C). The narrow size distribution ranging from 80 nm to 250 nm with a maximum at around 122 nm was obtained. The low polydispersity index (PDI) of 0.08 also indicates narrow size distribution.

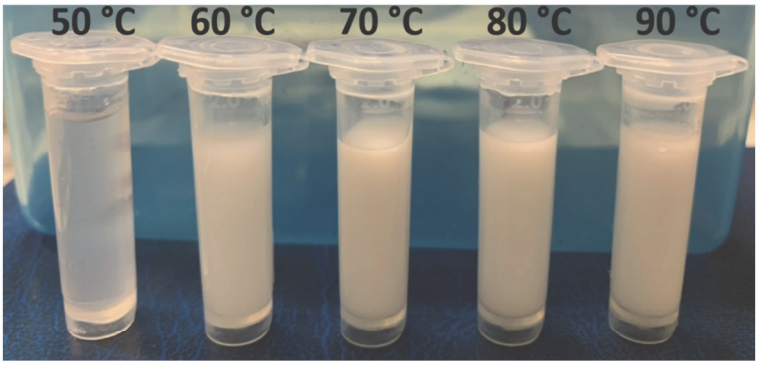

Figure 3.8. Images of albumin PEC NPs produced at different preparation temperatures (Sozer-Demirdas et al., 2025).

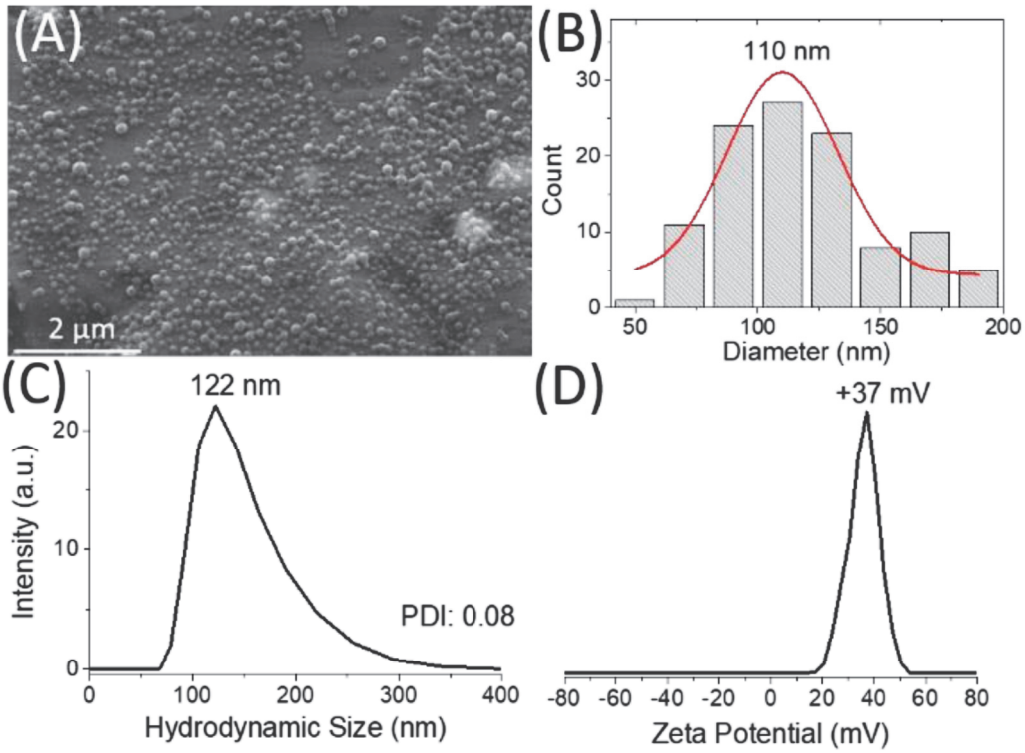

Figure 3.9. (A) SEM image of albumin PEC NPs and (B) particle size distribution obtained from the SEM image (A). (C) DLS results of the hydrodynamic size distribution of albumin PEC NPs in PBS at pH 7.4. (D) Zeta potential of the albumin PEC NPs in water. Albumin PEC NPs were prepared at 80 °C (Sozer-Demirdas et al., 2025).

Albumin PEC NPs were also obtained below and above 80 °C. Fig. 3.10 showed SEM images and DLS results of albumin PEC NPs prepared at 60, 70 and 90 °C. Nonuniform aggregates were detected at 50 °C, while spherical albumin PEC NPs were obtained at 60 °C and above (Fig. 3.10 (A)). Compared to the hydrodynamic sizes of albumin PEC NPs obtained at 80 °C (122 nm), relatively bigger albumin PEC NPs were obtained at 60 °C with a broad size distribution ranging from 150 nm to 700 nm and a peak at 300 nm (Fig. 3.10 (B)). On the other hand, slightly larger albumin PEC NPs were obtained both at 70 °C and 90 °C (190 nm) compared to those formed at 80 °C (122 nm). The formation yields were found to be 7 %, 28 %, 27 %, 38 % and 39 % at temperatures of RT, 60 °C, 70 °C, 80 °C and 90 °C, respectively. In conclusion, at room temperature, mixing anionic and cationic BSA leads to turbidity due to purely electrostatic attractions between the proteins, resulting in aggregation even at this early stage. In contrast, temperatures at or above the denaturation point promote additional interactions, including both intramolecular and intermolecular forces. Protein unfolding in aqueous environments at elevated temperatures exposes hydrophobic regions as well as internal amino and carboxyl groups (Li et al., 2022).

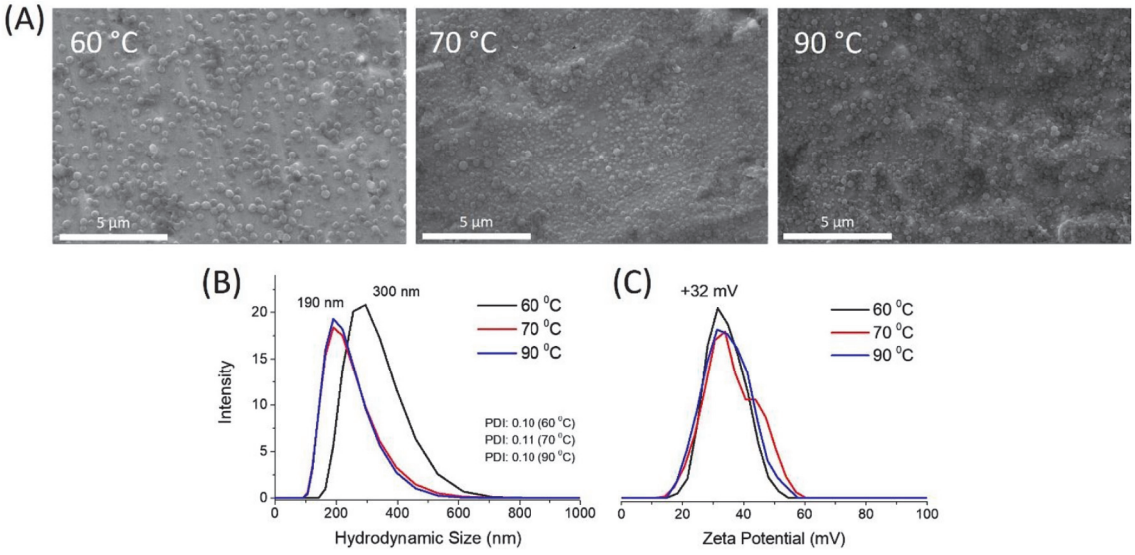

Figure 3.10. (A) SEM images of albumin PEC NPs prepared at 60 °C, 70 °C, and 90 °C. (B) Hydrodynamic particle size distribution and (C) zeta potential of albumin PEC NPs prepared at 60 °C, 70 °C and 90 °C. Samples were prepared with 1:3.5 M ratio of cBSA:BSA at 6.5 mg/mL total albumin concentration (Sozer-Demirdas et al., 2025).

The zeta potentials of albumin PEC NPs prepared at higher temperatures were found to be similar. The zeta potentials of albumin PEC NPs were +32 mV at preparation temperatures of 60, 70, and 90 °C, while it increased to +37 mV at 80 °C. (Figs. 3.10 (C) and 3.10 (D)). It is well known that NPs having surface charges greater than ±30 mV show strong stability (Müller et al., 2004). The hydrodynamic sizes, PDI values and zeta potentials of albumin PEC NPs produced via heating at 80 °C did not change significantly over 4 weeks at pH 3.0, 7.0 and 9.0 indicating the high stability of albumin PEC NPs (Fig. 3.11). At pH 9.0, the zeta potential of albumin PEC NPs became approximately −25 mV. In addition, the degradation of albumin PEC NPs was measured by using trypsin enzyme at 37 °C and pH 7.4. Fig. 3.12 (A) shows that 90 % and 95 % of albumin PEC NPs (1000 µg/mL) were degraded upon interaction with trypsin (50 µg/mL) after 5 and 27 h, respectively. On the other hand, degradation was very limited without the trypsin enzyme, only 15 % and 20 % of albumin PEC NPs were degraded after 5 and 27 h, respectively. These results suggest that the prepared albumin PEC NPs undergo enzymatic degradation quickly at physiological pH and temperature.

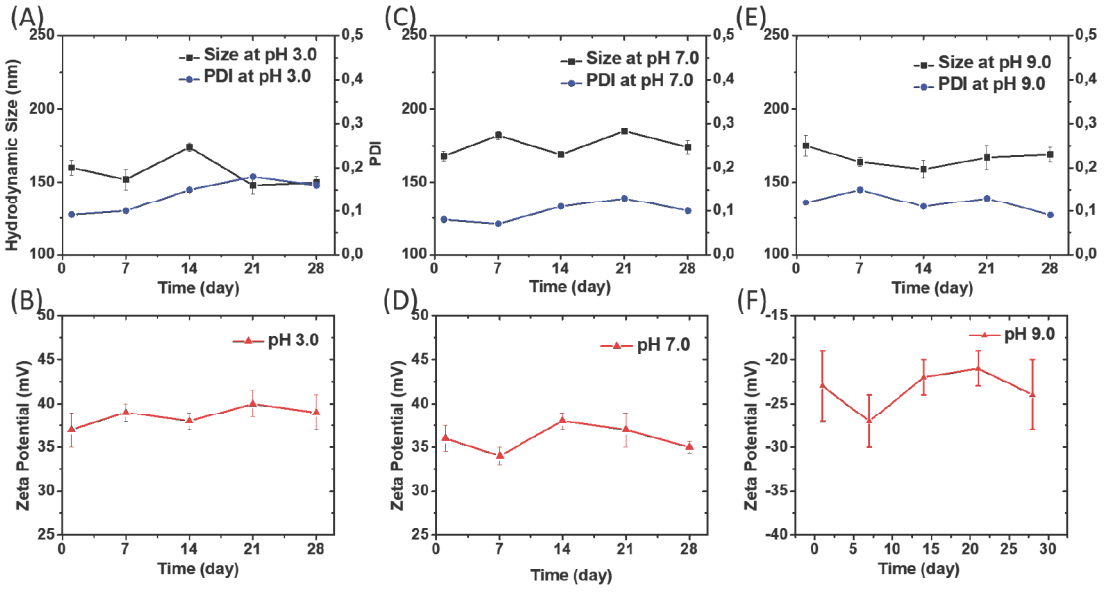

Figure 3.11. DLS results of hydrodynamic size distributions, PDI and zeta potential values of albumin PEC NPs produced at 80 °C in water at different pH values; 3.0 (A, B), 7.0 (C, D) and 9.0 (E, F) within 28 days (Sozer-Demirdas et al., 2025).

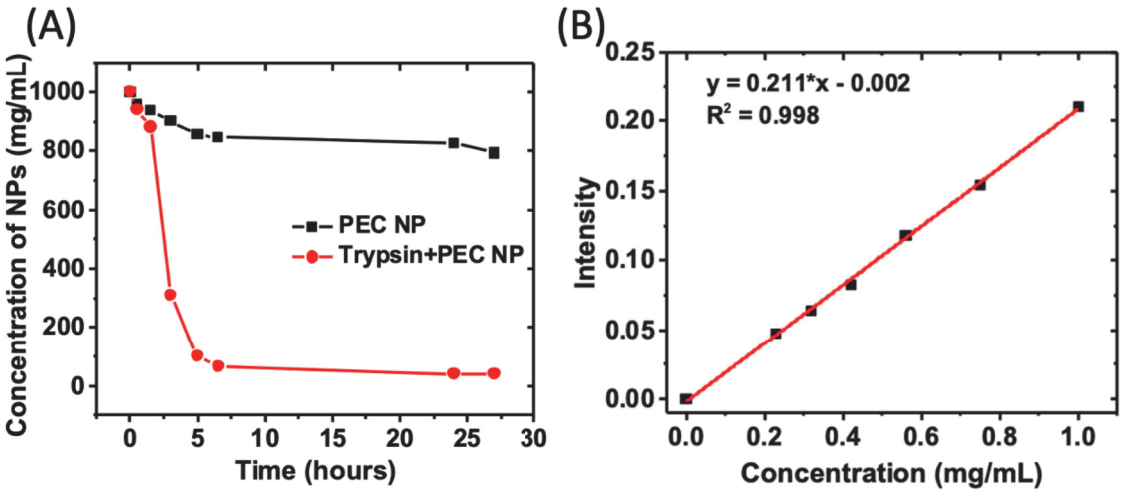

Figure 3.12. (A) The concentrations of the albumin PEC NPs (μg/mL) in PBS (black line) and in trypsin (50 μg/mL) containing PBS (red line) within 27 hours. (B) Calibration curve obtained from the turbidity results of albumin PEC NPs at different concentrations at 565 nm using UV-Vis absorption spectroscopy (Sozer-Demirdas et al., 2025).

The use of PECs not only eliminates the need for toxic solvents or crosslinkers but also enhances drug loading capacity. In emulsification or desolvation methods, water-insoluble drugs tend to remain in the organic solvent rather than incorporating into the albumin NPs, resulting in lower drug entrapment efficiency and reduced drug loading (Akdogan et al., 2022; Sozer et al., 2022).

Here, drug loading and release properties of albumin PEC NPs were investigated with a DNA alkylating agent, chlorambucil (CHL), which is used as a chemotherapeutic. CHL loading was performed using two different methods: incorporation and incubation. Since CHL was insoluble in water, the stock solution was prepared in DMSO. For the incorporation method, CHL was added to both aqueous solutions of cBSA and BSA. The total albumin to CHL mole ratios such as 1:1, 1:3 and 1:5 (albumin:CHL) were performed, while keeping the DMSO content <2 % (v/v). The CHL entrapment efficiencies were found to be 76, 65 and 78 wt% at the albumin:CHL molar ratios of 1:1, 1:3 and 1:5, respectively (Fig. 3.13 (A)). The maximum CHL content in the albumin PEC NPs was found as 6.4 wt% at a molar ratio of 1:5 (Fig. 3.13 (B)). CHL was also loaded using the incubation method, where CHL was added after the formation of albumin PEC NPs. The CHL entrapment efficiencies of albumin PEC NPs at 1:1, 1:3 and 1:5 M ratios (albumin:CHL) were found to be 19.4, 36.5 and 48.3 wt%, respectively (Fig. 3.13 (A)).

The CHL content in albumin PEC NPs increased with higher CHL molar ratios, reaching 1.1 wt% at a 1:5 (albumin:CHL) molar ratio using the incubation method (Fig. 3.13 (B)).

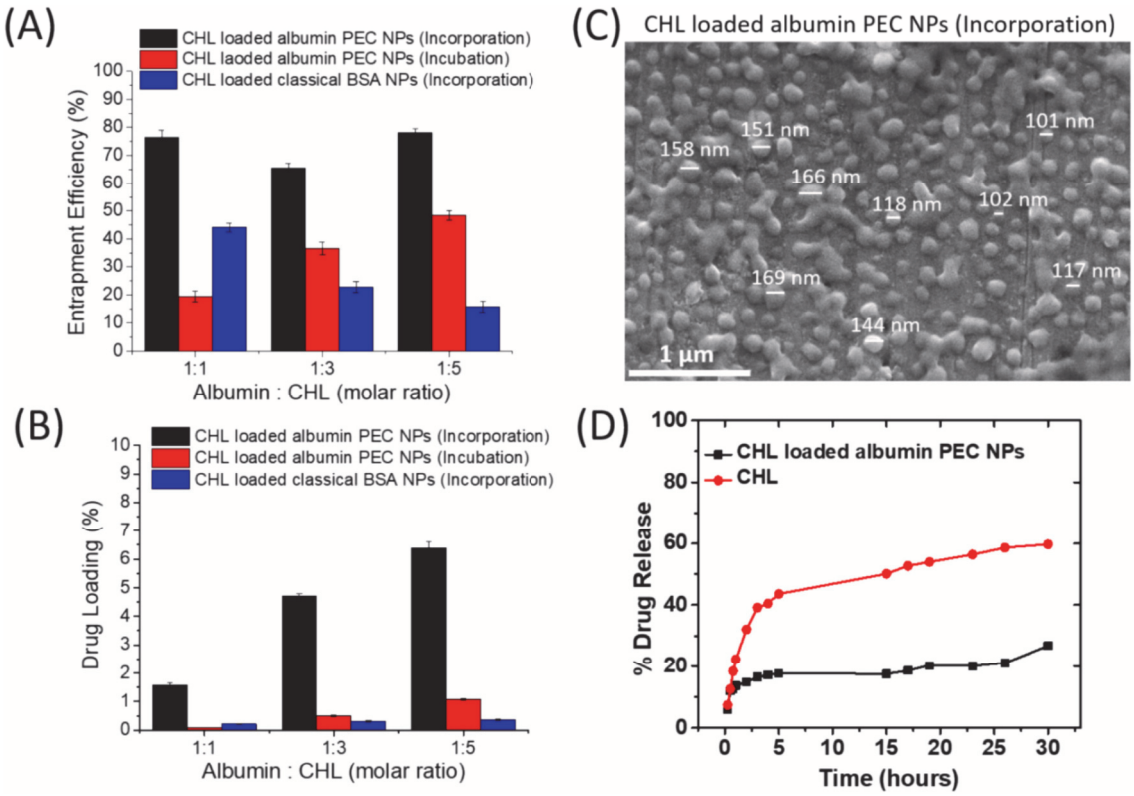

Figure 3.13. (A) CHL encapsulation efficiency (wt%) results and (B) CHL loading (wt%) results of albumin PEC NPs and classical BSA NPs (blue) with respect to the initial mole ratio of albumin:CHL. CHL loading was performed via incorporation (black) or incubation (red) methods. (C) SEM image of CHL loaded albumin PEC NPs prepared via incorporation method at albumin:CHL molar ratio 1:5. (D) The cumulative percentages of CHL released from the albumin PEC NPs (black) prepared via incorporation method with the 1:5 (albumin:CHL) molar ratio and the cumulative percentages of free CHL release (red) after 30 h (Sozer-Demirdas et al., 2025).

The drug-loading behaviour of the resulting albumin PEC NPs was also compared with that of conventional BSA NPs prepared via the desolvation method using ethanol, followed by glutaraldehyde crosslinking. The average hydrodynamic sizes of BSA NPs and CHL loaded BSA NPs were found to be 207 nm (PDI: 0.08) and 252 nm (PDI: 0.06),

respectively, for 1:5 albumin:CHL molar ratio (Fig. 3.14 (A)). Also, the average zeta potentials were found to be − 36 mV and − 41 mV for BSA NPs and CHL loaded BSA NPs, respectively (Fig. 3.14 (B)). Drug loading via incorporation method showed that increasing the albumin:CHL molar ratios from 1:1 to 1:3 and 1:5, the CHL entrapment efficiency decreased from 44 to 22.8 and 15.7 wt%, respectively (Fig. 3.13 (A)). Also, the drug loadings were found to be 0.21, 0.32 and 0.37 wt% at albumin:CHL molar ratios 1:1, 1:3 and 1:5, respectively (Fig. 3.13 (B)). The observed low drug loading suggests that the hydrophobic CHL drug preferentially remains dissolved in the ethanol used during the desolvation process. As a result, CHL loading capacity of albumin PEC NPs (6.4 wt%) is seventeen times higher than that of conventional albumin (BSA) NPs prepared with the desolvation method (0.37 wt%).

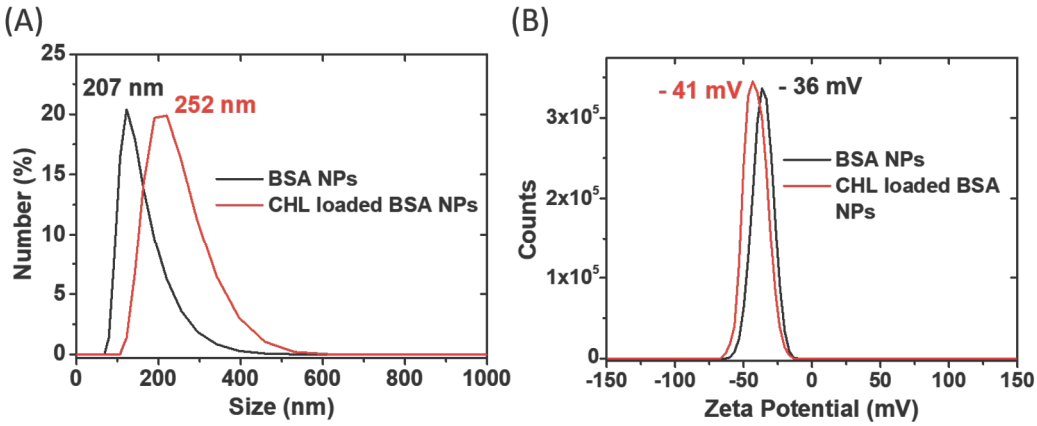

Figure 3.14. (A) Hydrodynamic size distribution and (B) zeta potential value of conventional BSA NPs (black) and CHL loaded conventional BSA NPs (red) produced by desolvation method followed by glutaraldehyde crosslinking (Albumin:CHL molar ratio 1:5) (Sozer-Demirdas et al., 2025).

Quercetin, another hydrophobic compound, has also been studied in the literature for its encapsulation into albumin NPs via the desolvation method. Differently, higher drug encapsulation efficiency (85–96 %) and drug loading capacity (16 %) were achieved when quercetin was encapsulated into BSA NPs in the presence of ethanol and glutaraldehyde (Ebrahimi et al., 2024; Antonio et al., 2016). Higher values, compared to those obtained with CHL, may be attributed to the structural differences between the two drugs. Quercetin is a polyphenolic compound consisting of two benzene rings connected

via an oxygen-containing pyrone ring, and also it possesses five hydroxyl groups that collectively facilitate interactions with albumin. Rathod et al. reported a binding constant of $1.25\times10^{6}\ M^{-1}$ for the interaction between quercetin and BSA protein, whereas Saufi et al. determined the binding constant of CHL to BSA protein to be $5.58\times10^{4}\ M^{-1}$ (Rathod et al., 2025; Saufi et al., 2019). Therefore, CHL, as a smaller molecule with fewer functional groups (a single benzene ring and a carboxyl group), may preferentially remain in the organic solvent phase rather than interact strongly with the albumin during the desolvation method.

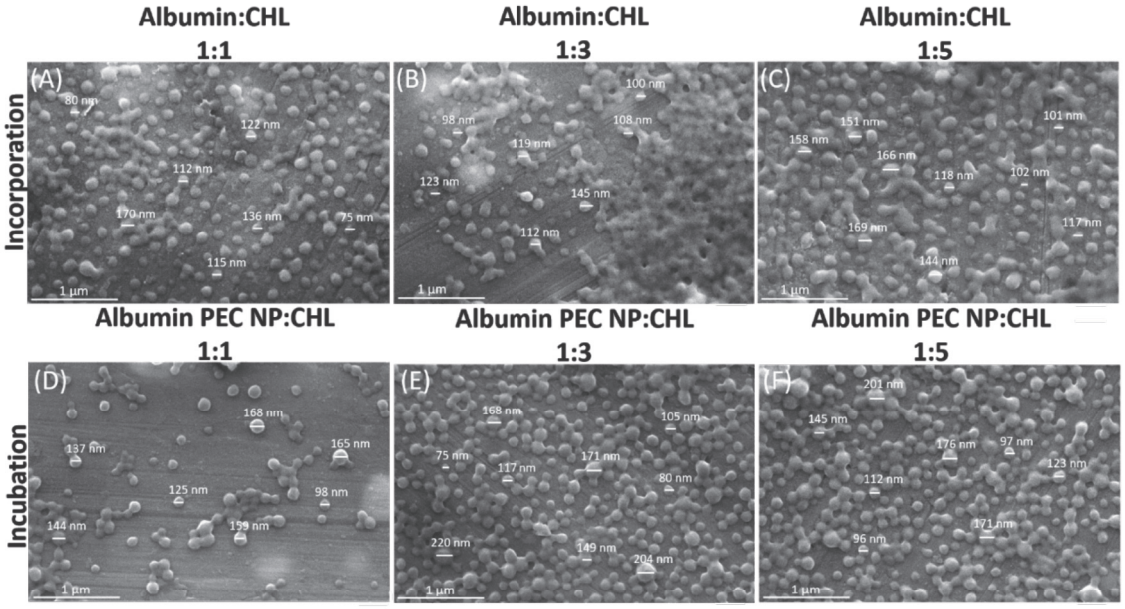

Figure 3.15. SEM images of CHL loaded albumin PEC NP preparation with incorporation method; (A) 1:1 molar ratio, (B) 1:3 molar ratio, (C) 1:5 molar ratio, and with incubation method; (D) 1:1 molar ratio, (E) 1:3 molar ratio, (F) 1:5 molar ratio (Sozer-Demirdas et al., 2025).

SEM images of CHL loaded albumin PEC NPs obtained through incorporation and incubation methods showed that drug loading did not affect the particle size and morphology significantly (Figs. 3.13 (C) and 3.15). Also, DLS results are similar before and after drug loading (Fig. 3.16 (A) and (C)). However, these two drug loading methods yield different zeta potential results (Fig. 3.16 (B) and (D)). The zeta potential of albumin PEC NPs slightly changed from +37 mV to +32 mV upon drug loading via the incorporation method (Fig. 3.16 (B)). This suggests that drugs were loaded mostly inside

the albumin PEC NPs. On the other hand, the surface charges of albumin PEC NPs decreased from +36 mV to +31, +28 and +21 mV after mixing CHL via the incubation method at molar ratios of 1:1, 1:3 and 1:5 (Albumin:CHL), respectively (Fig. 3.16 (D)). This suggests that a higher number of drugs was loaded onto the surface of the albumin PEC NPs using the incubation method compared to the incorporation method.

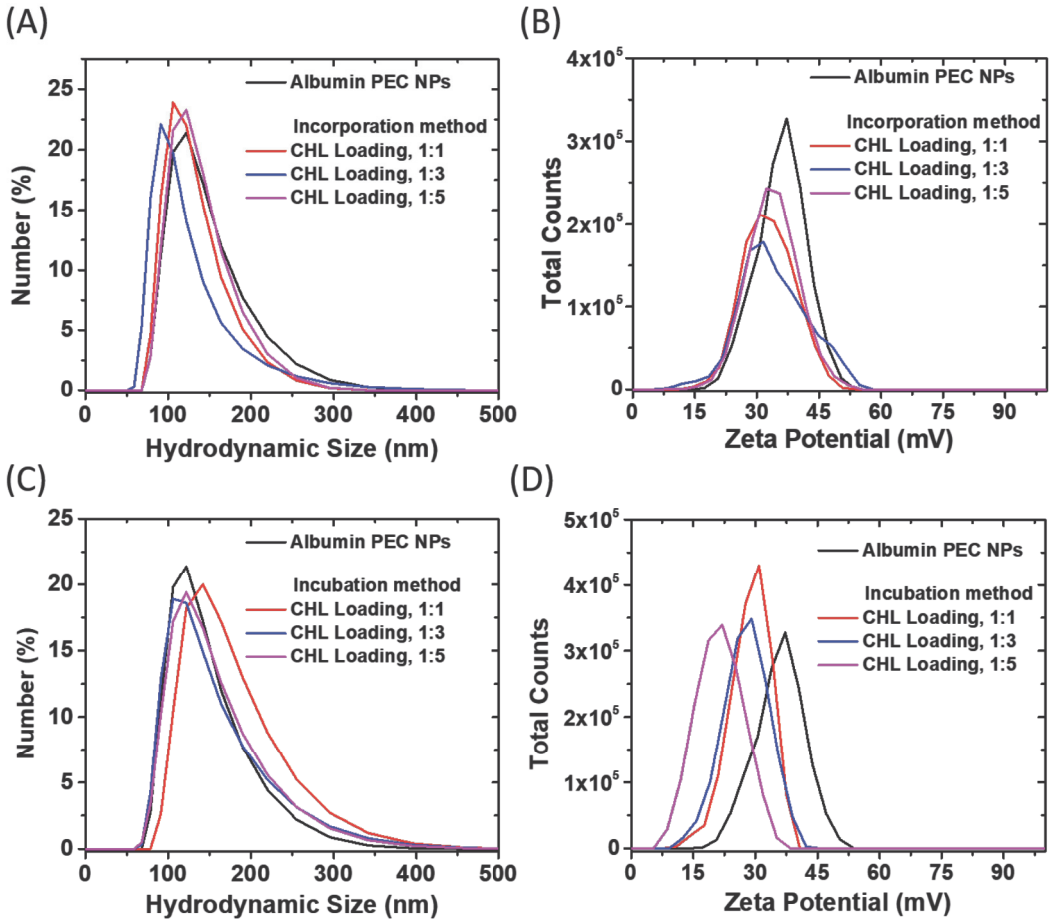

Figure 3.16. DLS results of albumin PEC NPs and CHL loaded albumin PEC NPs prepared with incorporation method (A) and incubation method (C). Zeta potential results of albumin PEC NPs and CHL loaded albumin PEC NPs prepared with incorporation method (B) and incubation method (D) (Sozer-Demirdas et al., 2025).

In vitro release of CHL from the albumin PEC NPs prepared with the 1:5 (albumin:CHL) molar ratio using the incorporation method was investigated at 37 °C in PBS at pH 7.4 (Fig. 3.13 (D)). The CHL release profile of albumin PEC NPs is indicative of a biphasic pattern. An initial burst release of 18% of the loaded CHL occurred within

the first 5 h, followed by a slower release, reaching 27% after 30 h. This suggests that the majority of the drug can be transported over an extended period without being released through diffusion. In contrast, free CHL in PBS diffused from the dialyser tube, reaching 43 % within the first 5 h and 59 % by the end of 30 h.

Human hepatocellular carcinoma (HCC) cell type which is primary liver cancer (Huh-7) was used in the cellular uptake and cell viability assays of albumin PEC NPs and CHL loaded albumin PEC NPs (Krelle et al., 2013). Liver cancer is among the most commonly diagnosed cancers worldwide and ranks as a leading cause of cancer-related deaths (Samant et al., 2021; Siegel et al., 2025). Therefore, Huh-7 cells have been extensively employed as an in vitro model to investigate the therapeutic efficacy of various NPs, including silica, silver, gold and albumin, in cancer treatment (Sozer et al., 2020; Costa et al 2024; Tsai et al., 2019; Kim et al., 2017; Suwannasom et al., 2023) .

Fluorescein isothiocyanate (FTIC) labeled BSA proteins were used to visualize the albumin PEC NPs in cells. For in vitro cellular studies, albumin PEC NPs were coated with poly(ethylene glycol) (PEG). PEGylation has been applied to improve the circulation half-life, and to decrease the NPs aggregation due to its hydrophilic chains (Fahrländer et al., 2015; Suk et al., 2016). Here, PEGylation was also employed to reduce the effective cationic surface charge of albumin PEC NPs, as a high positive charge can lead to cellular toxicity (Frohlich et al., 2012). The hydrodynamic size of albumin PEC NPs after PEG coating increases due to the hydrophilic feature of PEG (Fig. 3.17 (A) and (B)). For example, the peaks of hydrodynamic size distribution increases from 90 nm and 110 nm to 120 nm and 170 nm upon PEG coating for albumin PEC NPs and CHL loaded albumin PEC NPs (via incorporation drug loading), respectively. However, the SEM images obtained from the dried samples showed that PEGylation does not increase the size of albumin PEC NPs significantly (Fig. 3.17 (E) and (F)). The zeta potential of albumin PEC NPs was decreased from +37 mV to +13 mV, and the zeta potential of CHL loaded albumin PEC NPs (via incorporation) was decreased from +33 mV to +19 mV after PEG coverage (Fig. 3.17 (C) and (D)).

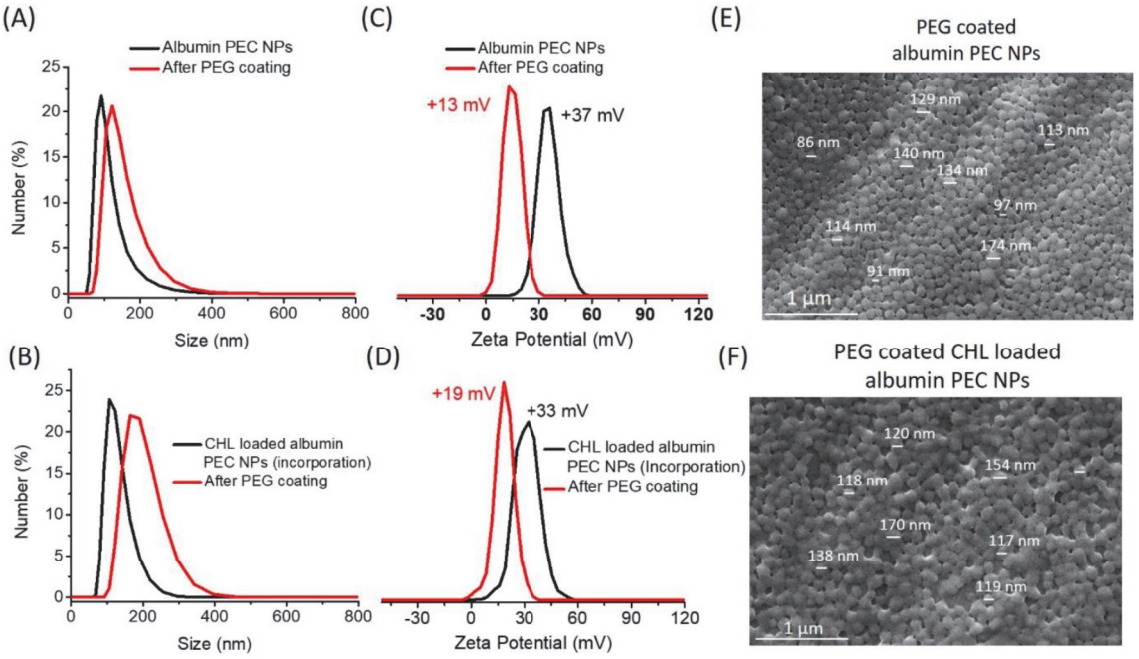

Figure 3.17. DLS results showing the hydrodynamic size distribution of (A) albumin PEC NPs (black) and PEG coated albumin PEC NPs (red), (B) CHL loaded albumin PEC NPs using incorporation method (black) and PEG coated CHL loaded albumin PEC NPs using incorporation method (red), (C-D) Corresponding zeta potential values of (Alb:CHL molar ratio 1:5). SEM images of PEG coated albumin PEC NPs (E) and PEG coated CHL loaded albumin PEC NPs using incorporation method (Albumin:CHL molar ratio 1:5) (F) (Sozer-Demirdas et al., 2025).

Cellular uptake of PEG coated CHL loaded albumin PEC NPs was investigated after incubation with 12.5 µg/mL NPs for 24 h in Huh-7 cells (Fig. 3.18 (A)). CHL was loaded upon the incorporation method which provides higher drug loading (Fig. 3.13 (B)). The confocal microscopy image shows that PEG coated CHL loaded FITC labeled albumin PEC NPs successfully entered the cells and were found in the cytoplasm and the nucleus. Z-stacks were acquired and only the volume that corresponds to the cells were imaged, therefore the green fluorescence in the cytoplasmic area indicates that the albumin PEC NPs have made it inside the cells. This efficient uptake is due to the PEGylated and positively charged surface of the albumin PEC NPs, which helps them interact with the negatively charged cell membrane and get absorbed through endocytosis (Sozer et al., 2020; Fahrländer et al., 2015; Lee et al., 2018; El-Baz et al., 2022). CHL loading did not significantly affect the cellular uptake efficiency of albumin PEC NPs. As

shown in Fig. 3.19 (A), Huh-7 cells internalized 12.5 µg/mL of albumin PEC NPs after 24 h of incubation, indicating effective cellular uptake. In contrast, 12.5 µg/mL of BSA NPs prepared via the desolvation method exhibited relatively lower cellular internalization under the same conditions (Fig. 3.19 (B)). This difference can be attributed to the surface charge of the NPs; BSA NPs possess a negative surface charge (Fig. 3.19 (B)), which may reduce cellular uptake. Previous studies have demonstrated that cationic albumin NPs are more efficiently internalized by cells compared to their anionic counterparts (Sozer et al., 2020; Abbasi et al., 2012).

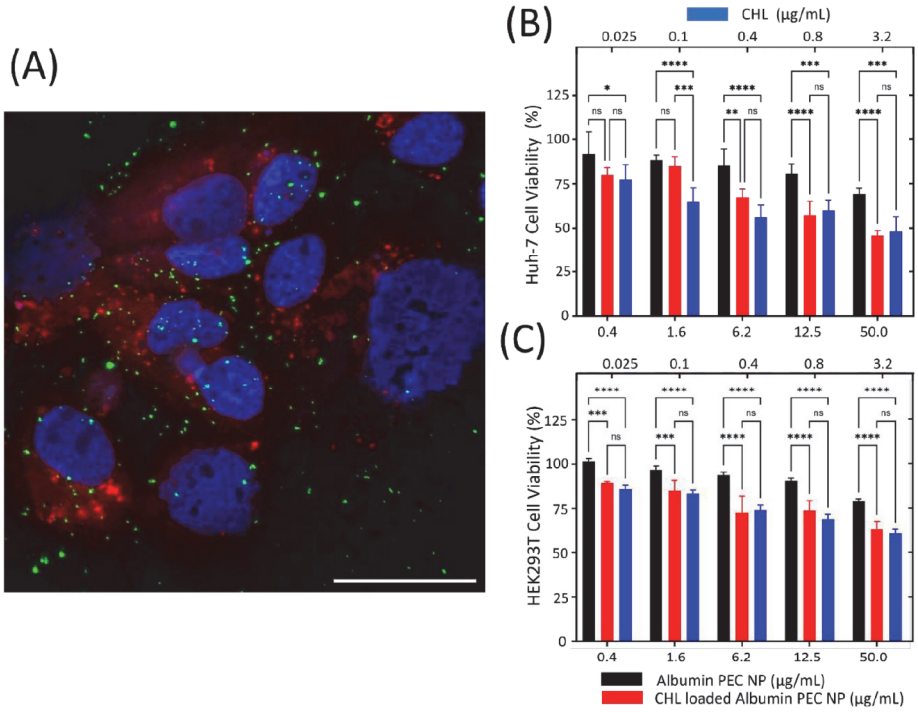

Figure 3.18. (A) Huh-7 cellular uptake of 12.5 µg/mL PEG coated CHL loaded FITC labeled albumin PEC NPs (green) for 24 h of treatment. Huh-7 cells were stained with CM-Dil (red) vital dye. At the end of the treatment, cell nuclei were stained with DAPI (blue). Scale bar = 50 µm. (B) Huh-7 cell viability and (C) HEK293T cell viability upon addition of PEG coated albumin PEC NPs (black), PEG coated CHL loaded albumin PEC NPs via incorporation method (red), or the free CHL in the same amount as that carried by the albumin PEC NPs based on the drug loading efficiency of 6.4 wt% (blue) at different concentrations after 24 h of incubation. Error bars represent ± SD, ns: non-significant, * P ≤0.05, ** P ≤0.01, *** P ≤0.001, **** P ≤0.0001 (Sozer-Demirdas et al., 2025).

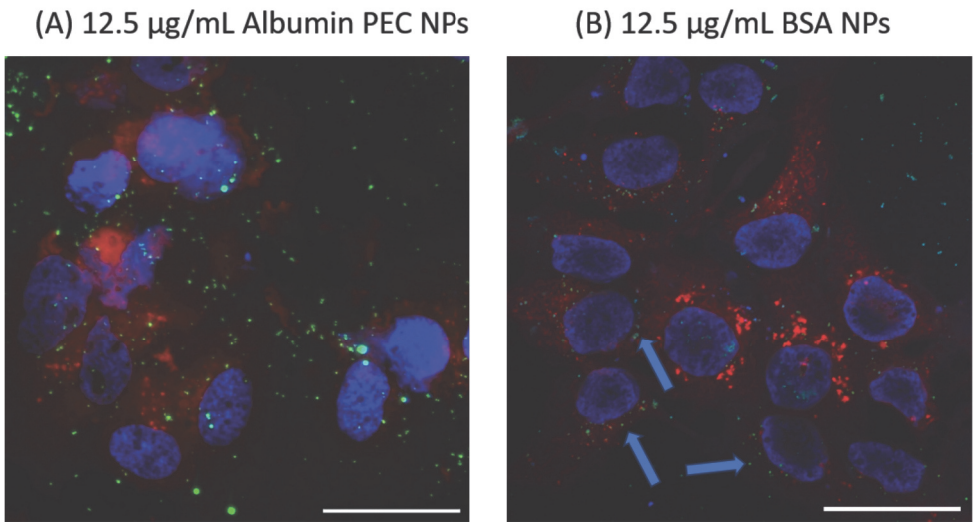

Figure 3.19. (A) Huh-7 cellular uptake of 12.5 µg/mL PEG coated FITC labeled albumin PEC NPs (green) for 24 h of treatment. (B) Huh-7 cellular uptake of 12.5 µg/mL FITC labeled BSA NPs (green) prepared via desolvation method for 24 h of treatment. Huh-7 cells were stained with CM-Dil (red) vital dye. At the end of the treatment, cell nuclei were stained with DAPI (blue). Scale bar = 50 µm. The arrows point the NPs (Sozer-Demirdas et al., 2025).

The effects of PEG coated albumin PEC NPs, CHL loaded PEG coated albumin PEC NPs, and free CHL on survival of Huh-7 cells were investigated after 24 h of treatment (Fig. 3.18 (B)). At low concentrations, PEG coated albumin PEC NPs did not reduce the cell viability significantly, but at 50 µg/mL concentration it reduced to 70 %. On the other hand, CHL loaded PEG coated albumin PEC NPs reduced the cell viability in a more concentration dependent manner, showing a viability of 44 % at a concentration of 50 µg/mL of PEG coated albumin PEC NPs, which include 3.2 µg/mL of CHL. Additionally, the free CHL in the same amount as that carried by the albumin PEC NPs based on the drug loading efficiency of 6.4 wt% was studied. The free CHL reduced cell viability to 48 %, showing a similar effect to that observed with CHL delivered via NPs. It suggests that the drug retained its cytotoxic efficacy after encapsulation in the NPs. These results show that the albumin PEC NPs are an effective drug delivery vehicle with preserved bioactivity.

In addition to Huh-7 cells, the effects of CHL loaded and unloaded PEG coated albumin PEC NPs on MCF-7 breast cancer cell viability were investigated after 24 h of

treatment (Fig. 3.20). MCF-7 cell viability decreased to 75 %, 53 % and 42 % when 50 µg/mL of PEG coated albumin PEC NPs, CHL loaded PEG coated albumin PEC NPs, and corresponding free CHL (3.2 µg/mL) were added, respectively. These findings are comparable to the results observed in Huh-7 cells under the same treatment conditions, where cell viability decreased to 70 %, 44 % and 48 %, respectively.

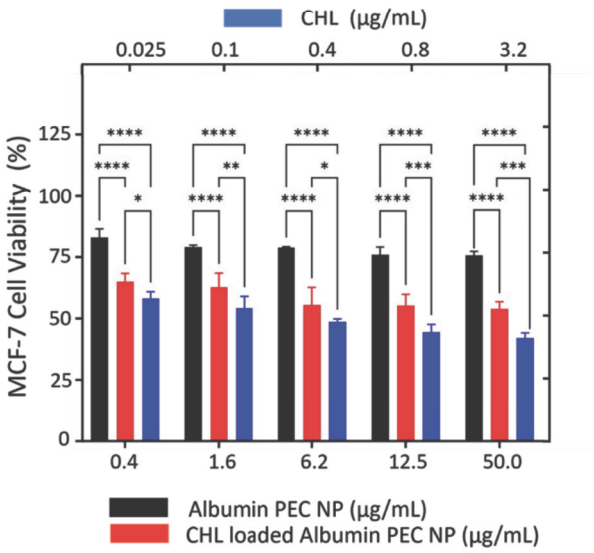

Figure 3.20. MCF-7 cell viability upon addition of PEG coated albumin PEC NPs (black), PEG coated CHL loaded albumin PEC NPs via incorporation method (red), or the free CHL in the same amount as that carried by the albumin PEC NPs based on the drug loading efficiency of 6.4 wt% (blue) at different concentrations after 24 h of incubation. Error bars represent ± SD, ns: non-significant, * P ≤0.05, ** P ≤0.01, *** P ≤0.001, **** P ≤0.0001 (Sozer-Demirdas et al., 2025).

The cytotoxicity of PEG coated albumin PEC NPs was also evaluated using the noncancerous human embryonic kidney cell line, HEK293T (Fig. 3.18 (C)). At low concentrations (<12.5 µg/mL), no significant reduction in HEK293T cell viability was observed. However, at 50 µg/mL, PEG-coated albumin PEC NPs reduced cell viability to 80 %. When CHL loaded albumin PEC NPs were applied at the same concentration (50 µg/mL), containing 3.2 µg/mL of CHL, they reduced HEK293T cell viability further to approximately 60 % a similar decrease was observed with the equivalent amount of free CHL.

Importantly, a comparison of cell viability between the cancerous Huh-7 cell line and the noncancerous HEK293T cell line upon treatment with CHL loaded albumin PEC NPs suggested a relatively higher cytotoxicity toward the cancerous cells. Specifically, Huh-7 cell viability decreased to 44 %, while HEK293T cell viability decreased to 60 % under the same conditions, indicating selective toxicity of the NPs.

Also, this study aimed to load therapeutic mRNA onto albumin polyelectrolyte complex (PEC) nanoparticles and systematically evaluate the effects of different mRNA:PEC NP molar ratios on the physical properties of the nanoparticles. In the first step, the pgc112 plasmid containing the RFP-GPI sequence was linearized with the NotI restriction enzyme, followed by in vitro transcription (IVT) via the SP6 promoter. Following IVT, DNase I digestion and LiCl precipitation steps ensured the removal of impurities, yielding a total of 25 µg of highly pure RFP-GPI mRNA.

An adsorptive binding approach, widely used in the literature (Pardi et al.2018), was used to load pure mRNA onto albumin PEC nanoparticles. The nanoparticles were first dispersed in nuclease-free water (NFW) and homogenized by vortexing and sonication at 21°C for 15 minutes. The samples were then mixed with mRNA in the specified molar ratios and incubated on an orbital shaker for 30 minutes. The amount of free mRNA in the supernatant was analyzed using a Nanodrop Spectrophotometer.

Table 3.1. Encapsulation efficiencies of mRNA loaded albumin PEC NPs obtained by Nanodrop spectrophotometer.

mRNA (µg)	PEC NP (µg)	Mol ratio (mRNA:PEC NP)	Encapsulation Efficiency (%)
10	100	266:1	61
5	100	133:1	97.5
5	500	26:1	94
2.5	500	13:1	100
0.5	500	2.6:1	-

At the beginning of the study, a molar ratio of 266:1 (mRNA:PEC) was tested, and 61% of the mRNA was found to be encapsulated (Table 3.1); however, this high loading ratio was observed to have negative effects on the physical stability of the nanoparticles (Fig. 3.21 (A and B)). Dynamic light scattering (DLS) measurements were

used to evaluate the size and surface charge changes of albumin PEC NPs in the medium (Opti-MEM) and mRNA:PEC NPs at a 266:1 molar ratio. As shown in Figure 3.21 (A), the 266:1 molar ratio caused a significant increase in nanoparticle size and an increased tendency for aggregation. The size of albumin PEC NPs in the medium increased from 344 nm to 2026 nm. Similarly, significant changes were observed in the zeta potential values, indicating a decrease in colloidal stability of the nanoparticles. The surface charge of albumin PEC NPs decreased to -7.60 mV with mRNA loading. These results suggest that high loading rates disrupt particle electrostatic balance due to excessive surface charge accumulation in the albumin PEC NP structure.

Therefore, mRNA loading optimization was repeated at lower molar ratios of 26:1, 13:1, and 2.6:1. Supernatant analysis using Nanodrop spectrophotometry allowed the calculation of loading efficiency at 26:1 and 13:1 ratios. However, the amount of mRNA at 2.6:1 was technically infeasible due to the very low concentration for the determination. Based on the results obtained from the Nanodrop device, the 26:1 and 13:1 molar ratios were found to be 94% and 100% encapsulated in albumin PEC NPs, respectively.

The size of the mRNA loaded albumin PEC NPs were slightly increased from 344 nm to 420 nm at 26:1 molar ratio. The size of the mRNA loaded albumin PEC NPs were found as 346 nm and 354 nm for 13:1 and 2.6:1 molar ratio, respectively. DLS results indicated that the 13:1 and 2.6:1 molar ratios provided the most stable profiles for loading onto albumin PEC NPs. On the other hand, the surface charges of albumin PEC NPs slightly decreased to +28.8 mV, +30 mV and +32.9 mV after mixing mRNA at molar ratios of 26:1, 13:1 and 2.6:1, respectively (Fig. 3.21 (D)). These findings indicate that structural integrity was better preserved at lower loading ratios because the nanoparticle surface was not saturated with excess mRNA.

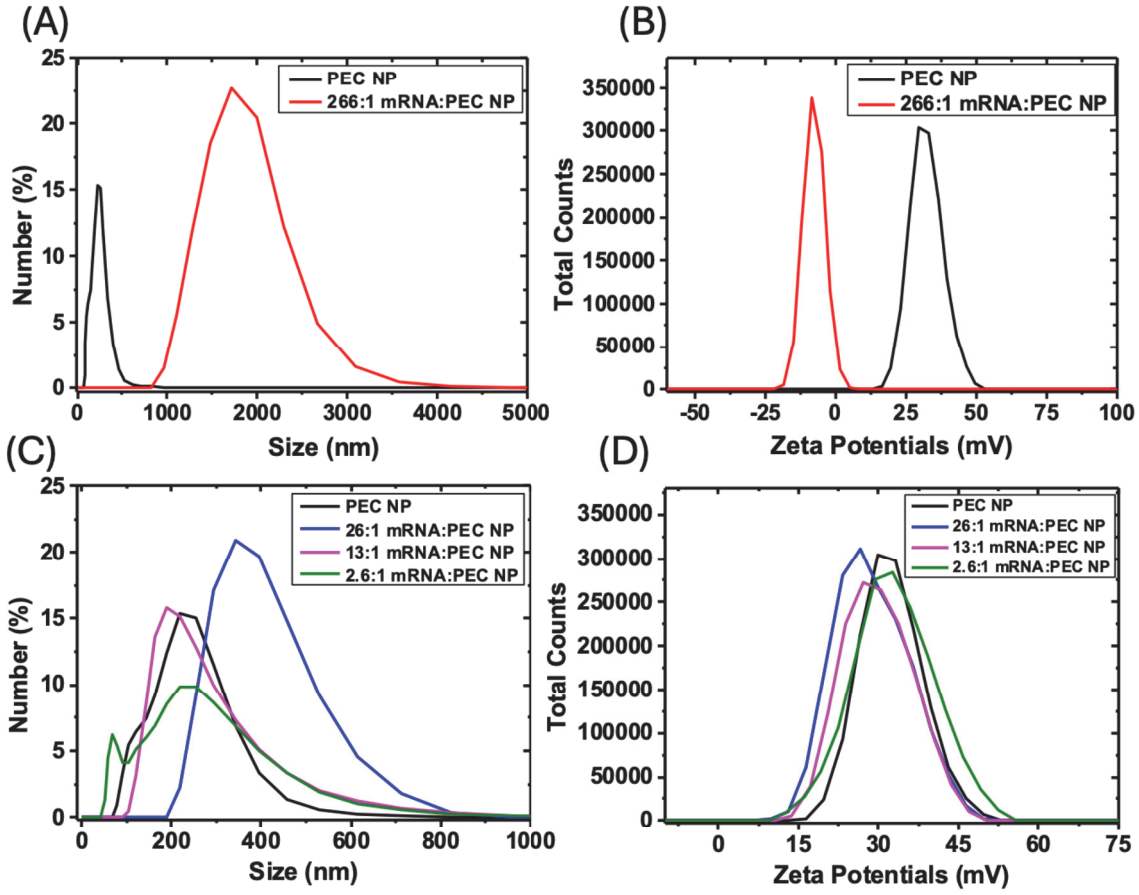

Figure 3.21. DLS results showing the hydrodynamic size distribution of (A) albumin PEC NPs (black) and mRNA loaded albumin PEC NPs (266:1 mol ratio) (red), (C) mRNA loaded albumin PEC NPs at different molar ratios; 26:1 (blue), 13:1 (pink) and 2.6:1 (green), and albumin PEC NPs (black) (B and D) Corresponding zeta potential values.

3.4. Conclusion

Although serum albumin proteins are frequently studied for the preparation of drug nanocarriers, this method, utilizing their polyelectrolyte features, provides a greener method and enables higher drug loading without the use of any specialized instrumentation. Electrostatic interaction between anionic and cationic serum albumin proteins at above 60 °C yielded spherical albumin PEC NPs around 110 nm with a high cationic surface charge of +37 mV. The hydrophobic DNA- alkylating drug of CHL could be loaded into albumin PEC NPs during the preparation of NPs in water. Consequently, albumin PEC NPs demonstrate a CHL loading capacity of 6.4 wt%, which is 17 times

greater than that of traditional albumin NPs (0.37 wt%) produced via the desolvation method involving organic solvents and glutaraldehyde. To reduce the high cationic zeta potential, a PEG coating was applied to the albumin PEC NPs. These PEG-coated NPs were effectively internalized by Huh-7 cells, leading to a reduction in cell viability to approximately 44% due to the delivery of CHL. Although the albumin PEC NPs developed in this study offer a green, efficient, and high-capacity drug loading strategy, the relatively high positive surface charge remains a critical parameter to consider for broader biomedical applications. While PEGylation provided partial attenuation of the high surface charge, further surface modification approaches or adjustments during NP preparation may be needed to achieve a reduced positive charge or even a net negative charge to enhance their potential applicability. Furthermore, this newly obtained albumin PEC NPs offer the successful loading of therapeutic mRNA and their use as a carrier system. Future studies will demonstrate the potential of mRNA loaded albumin PEC NPs in the treatment of ocular diseases associated with protein deficiency by enabling both intracellular activity and intracellular protein expression.

CHAPTER 4

ALBUMIN POLYELECTROLYTE HYDROGEL COMPLEX FORMATION FOR THERAPEUTIC SYSTEMS

4.1. Introduction

Hydrogels are three-dimensional networks formed by the swelling of natural or synthetic polymers in water. The resulting hydrogels can retain large amounts of water in their swollen state (Liu J. et al., 2020). Since the invention of hydrogel contact lenses by Wichterle and Lim in 1960, significant advances have been made in the creation and application of hydrogels for medical applications (Wichterle and Lim, 1960). For example, Sharma and colleagues reported the development of a hydrogel biomaterial that can fragment bone into small pieces during cartilage repair therapy and stimulate bone marrow stem cell production to support new cartilage formation (Sharma et al., 2013). Clinical studies have shown successful coverage of approximately 86% of the new cartilage tissue and significantly reduced postoperative pain. In 2021, a new hydrogel was developed that can effectively deliver to different tumor sites and respond to temperature and pH changes in the tumor environment (Komatsu et al., 2021).

Hydrogels can be composed of natural or synthetic polymers. Natural hydrogels have been frequently investigated for tissue engineering applications due to their biocompatibility and non-toxic degradation. Examples of natural polymers include hyaluronic acid, chitosan, and collagen. However, the mechanical strength of natural hydrogels is relatively weak, and formulation reproducibility and immunogenic risks are limited (Kirchhof et al., 2015).

Synthetic hydrogels are produced from polymers not found in nature; common examples are poly(ethylene glycol) (PEG), poly(vinyl alcohol) (PVA), and poly(hydroxyethyl methacrylate) (PHEMA) (Galante et al., 2015; Jiang et al., 2014; Yu et al., 2014). Synthetic hydrogels are more tunable, more reproducible, and more stable than natural polymers. Their disadvantages include the presence of toxic byproducts and difficulty in cleaning.

Polymer crosslinking can occur by physical or chemical means. Physical crosslinking occurs through chain entanglement, hydrogen bonding, hydrophobic interactions, complexation, or crystal formation (Hoare et al., 2008; Wang et al., 2018). It is reversible and can be degraded by heat, pH, ionic strength, or mechanical stress. Chemical crosslinking, on the other hand, forms permanent hydrogels through covalent interactions between the polymer and crosslinker functional groups. Fine-tuned hydrogels can be produced by chain growth, addition, or condensation reactions. Click chemistry (azide-alkyne cycloaddition, Michael-addition) can also be used in chemical crosslinking (Wang et al., 2017; Xing et al., 2014).

There are numerous hydrogel applications in the biomedical field. This is primarily due to the advantages of hydrogels, such as their simple production processes and low cytotoxicity. However, with the increasing use of hydrogels in biomedical applications, it has been reported that some polymer-based hydrogels can cause allergic and inflammatory reactions. For example, complications associated with polyacrylamide hydrogels are frequently reported, and post-injection reactions such as inflammation, tissue hypertrophy, and pain can occur (Rauso et al., 2019; Ding et al., 2022; Kose et al., 2022). Furthermore, other polymer hydrogels, such as Burnshield®, silicone hydrogel, and Miragel®, have also been reported to occasionally cause adverse reactions (Robertson and Cavanagh, 2005; Storan et al., 2016; Albalawi et al., 2022).

Conventional hydrogels are generally not biodegradable due to their chemical and physical cross-linking networks, which can lead to environmental pollution (Guo et al., 2023). Additionally, the lack of control over the mechanical properties of polymer hydrogels is a significant drawback (Li et al., 2021; Elangwe et al., 2022). Due to these limitations, researchers are continuing to develop new hydrogel types that are more biodegradable, non-immunogenic, and exhibit superior mechanical properties.

Protein-based hydrogels stand out with their tunable and designable biochemical and mechanical properties, superior biocompatibility, and biodegradability (Ong et al., 2019). Furthermore, the unique functional groups and structural features inherent in proteins give protein hydrogels additional advantages over other polymers. Proteins such as collagen, gelatin, elastin, fibrin, silk fibroin, and serum albumin are common sources of protein-based hydrogels; these natural proteins have well-defined sequences, are easily isolated from natural sources, and can serve as crosslinkers or load carriers when needed (Katyal et al., 2020; Zhou et al., 2020)

Collagen is considered an important biomaterial in connective tissue regeneration due to its hydrophilic structure, satisfactory biocompatibility and biodegradability, low antigenicity, and flexibility (Rezvani Ghomi et al., 2021). However, collagen's mechanical strength, the complexity and high cost of isolation and purification processes limit its large-scale application. In contrast, while silk fibroin has attracted interest in the biomedical field due to its superior biocompatibility, controllable degradability, and some properties similar to human tissue, silk-based hydrogels may lack sufficient mechanical properties (Raja et al., 2013; Zheng and Zuo, 2021).

Serum albumin is a preferred protein for many biomedical applications due to its biocompatibility, structural stability, sustainability, non-immunogenicity, and low cost, and has been used in various hydrogel systems. For example, Raghuwanshi et al. (2020) developed a pH-sensitive and reversible hydrogel from BSA, demonstrating its potential for biodiagnostics and controlled drug delivery (Raghuwanshi et al., 2020). Yang et al. (2022) detected IgG concentration in human serum with high accuracy using a BSA based hydrogel sensor (Yang et al., 2022). BSA hydrogels have also yielded successful results in enzyme immobilization (Belgoudi & Fortier, 1999), cancer therapy and bioimaging (Zhao et al., 2019), and injectable hydrogel platforms (Lee et al., 2014; Bai et al., 2019; Liu et al., 2020). Additionally, BSA-based bioconjugate hydrogels developed for wound healing and tissue regeneration have been shown to offer high biocompatibility and biodegradability (Phan et al., 2021; Khanna et al., 2020). In recent years, BSA hydrogels have also been widely investigated in areas such as tissue regeneration, temperature-responsive hydrogel systems, and postoperative adhesion prevention (Arabi et al., 2018; Katarivas Levy et al., 2019; Mao et al., 2021; Yoon et al., 2021). Table 4.1. and 4.2 show some applications of albumin-based hydrogels in cancer therapy and tissue regeneration engineering.

Table 4.1. Areas of use of albumin-based hydrogels in cancer treatment.

Types of Albumins	**Drug**	**Cancer or tumor cells**	**Citations**
BSA	NA	HepG2	(Zhao et al., 2019)
BSA	Ag NP	Skin cancer	(Amatya et al., 2021)

(Cont. on next page)

Table 4.1. (cont'd.)

BSA	Dox	4T1	(Chen et al., 2021)
BSA	PTX	Human brain tumor cells	(Lin et al., 2017)
BSA	PQ912	Inhibiting local tumor recurrence and distal metastasis	(Li et al., 2022)
HSA	TRAIL	MIA PaCa-2	(Kim et al., 2015)
BSA	Dox	A549	(Yamada and Schneider, 2016)
OVA	Anti-tumor vaccines	lymphoma	(Lee et al., 2019)
BSA	Photothermal photodynamic therapy	Breast cancer	(Qui et al., 2022)
HSA	Indocyanine green	Precision cancer surgery	(Lee et al., 2020)

Table 4.2. Areas of use of albumin-based hydrogels in tissue regeneration engineering.

Types of Albumins	**Detailed application types**	**Citations**
BSA	Tibial defect	(Kossover et al., 2020)
BSA	Vascular endothelium	(Layman et al., 2012)
BSA	Alveolar bone	(Areevijit et al., 2020)
BSA	Bone regeneration	(Liu et al., 2020b)
BSA	Wound healing	(Dai et al., 2021)
HSA	Femur defect	(Smith et al., 2014)
HSA	Subcutaneous drug delivery	(Kang et al., 2021)
BSA	Skin regeneration	(Gsib et al., 2020)
BSA	As scaffold materials in tissue engineering	(Berdichevski et al., 2015)
HSA	As a shape memory material in tissue engineering	(Liu et al., 2021)

It is well known that albumin-based hydrogels are generally obtained by thermal induction (Ferry, 1948; Jian et al., 2014; Sun and Holley, 2011). The gelation mechanism of proteins such as BSA protein at high temperatures has been studied for a long time. With increasing temperature, the protein's polypeptide segments are uncoiled, thus changing its structure. This results in the gradual accumulation of the network structure that allows for gel formation upon interaction with another protein. The major disadvantage of this method is the extensive protein denaturation that risks compromising the protein's functionality and biocompatibility due to the high temperatures used (Carter and Ho, 1994). Thermally inducing albumin-based hydrogels at neutral pH using this method results in temperatures exceeding 62°C (albumin denaturation temperature) (Yamasaki et al., 1990). Baler and colleagues have developed a new system as an alternative to this method (Baler et al., 2014). This method aims to induce albumin proteins to form gels in a low pH environment by pH inducing them. The net charge on the protein changes from -16 at pH 7.4 to +100 at pH 3.5 (Baler et al., 2014b). One effect of this charge inversion is that the positively charged protein domains repel each other, causing partial denaturation of the protein and exposure of the buried hydrophobic domains of albumin to the solvent. Then triggers intermolecular self-assembly of the proteins to form a hydrogel at 37 °C. This mechanism has been reported to operate in the pH range of 3.0 to 4.0 for BSA, with an optimum pH of 3.5 (Baler et al., 2014).

Recently, Arabi and colleagues (2018) comprehensively investigated the pH- and temperature-dependent gelation behavior of both BSA and HSA (Arabi et al., 2018). This study enabled the physical characterization of BSA and HSA hydrogels through various phase diagrams. The researchers demonstrated that gelation of BSA and HSA can occur over a wide range of pH and temperature. Specifically, gelation has been determined to occur in the pH range of 1.0–4.3 to pH > 10.6 at 37 °C or in the pH range of 7.0–7.2 at 50–65 °C. However, studies have shown that the production of albumin-based hydrogels can only be achieved under either highly acidic or highly basic conditions or at high temperatures.

In contrast to previous approaches requiring under either highly acidic or highly basic or elevated temperatures, our newly developed polyelectrolyte complex (PEC) system enables the formation of albumin-based hydrogels under mild physiological conditions at pH 6 and 37 °C. In this system, electrostatic interactions between cationized BSA (cBSA) and native BSA molecules promote network formation without the need for thermal denaturation or extreme pH adjustment. This not only preserves the structural

integrity and bioactivity of albumin but also enhances the biocompatibility and safety of the resulting hydrogels. Therefore, our PEC-based approach provides a novel and efficient route for preparing albumin hydrogels under mild and biologically relevant conditions, representing a significant improvement over conventional heat- or pH-induced gelation methods.

In this section, we present a comprehensive investigation of the formation and physicochemical characterization of our novel albumin PEC hydrogels. Firstly, the preparation and optimization of the cBSA:BSA system is described and emphasizing its ability to form stable hydrogels under mild conditions (pH 6, 37 °C) without requiring high temperatures or acidic environments. Subsequently, the rheological behavior of the developed hydrogels, conformational and morphological structures were analyzed of the hydrogels. Collectively, these findings provide valuable insights into the gelation mechanism and structural characteristics of the newly developed albumin PEC hydrogels.

4.2. Materials and Methods

4.2.1. Materials

Bovine serum albumin (BSA, Mw: 66.5 kDa lyophilized powder, >96 %), N-(3-Dimethylaminopropyl)-N′-ethyl carbodiimide hydrochloride (EDC), ethylenediamine (EDA), PBS tablets (0.01 M, pH 7) were purchased from Sigma–Aldrich. Distilled water was used to make all the aqueous solutions.

4.2.2. Preparation of cationic bovine serum albumin protein (cBSA)

A solution of 50 mg BSA in 500 µL deionized water was prepared. 650 µL of ethylenediamine was combined with 500 µL deionized water, and the pH was adjusted to 4.75 by adding 9 mL of 6 M HCl. The BSA solution was added to the ethylenediamine solution. Subsequently, 14.5 mg of EDC was dissolved in 15 µL deionized water and slowly introduced into the BSA- ethylenediamine mixture. After two hours of stirring at 750 rpm, the reaction was stopped by adding 4 M acetate buffer (pH 4.75). The resulting cBSA proteins were purified by repeated centrifugation (13,000 rpm for 3 minutes) for three cycles using 0.1 M acetate buffer and deionized water to remove excess EDC and

ethylenediamine through an Amicon® Ultra centrifugal filter (molecular cut off: 50 kDa). The final cBSA was collected, and then it was lyophilized and stored at 4 °C. The cBSA yield was 70% wt.

4.2.3. Preparation of albumin PEC hydrogels

In the formation of albumin polyelectrolyte complex (PEC) hydrogels, cationic albumin protein (cBSA) and natural albumin protein (BSA) were used as a cationic polyelectrolyte and an anionic polyelectrolyte, respectively. Albumin PEC hydrogels were obtained by using cBSA:BSA molar ratios of 1:1. Also, total albumin protein concentration in the system was studied. Total albumin concentrations of 15, 17.5 and 20 wt% were investigated. In detail, 100 mg of cationic BSA (cBSA) was dissolved in 0.5 mL of PBS buffer (0.01 M, pH:7). Separately, 100 mg of anionic BSA was dissolved in 0.5 mL of same buffer, and then added dropwise to the aqueous cBSA solution under gentle shaking. The pH value of the albumin polyelectrolyte complex was set to pH 6 by the slow addition of HCl. The mixture was subsequently incubated in a water bath at 37 °C for 2 hours to complete the complexation and gelation process.

4.2.4. Characterization of albumin PEC hydrogels

4.2.4.1. Rheological Characterization

The gelation kinetics and viscoelastic behaviour of the albumin PEC hydrogels were characterized rheologically. After the gelation process was completed, the viscoelastic properties of the resulting albumin PEC hydrogels were analyzed. Storage modulus (G′) and loss modulus (G″) were measured to assess the mechanical strength and stability of the resulting hydrogels. These parameters provide information about the elastic and viscous behavior of the material; a G′>G″ value indicates that the material's elastic (solid-like) properties are dominant over its viscous (liquid-like) properties.

The rheological properties of the albumin PEC hydrogels were measured using a rotational rheometer (Hybrid Rheometer Discovery HR-2 DHR series, TA Instruments, USA) equipped with a 20 mm parallel plate geometry and a Peltier steel plate for temperature control. The measurements were performed at 37 ± 0.5 °C. The gap distance

between the plates was set to 1000 μm, and an axial compression force of 1 N was applied to ensure adequate contact between the sample and the plate surfaces.

The viscoelastic properties of the formed hydrogels were evaluated by frequency sweep tests in the linear viscoelastic region. The angular frequency (ω) was varied from 0.1 to 100 rad/s at a constant strain amplitude of 1×10^{-5} rad. During the measurements, the storage modulus (G′), loss modulus (G″), loss tangent (tan (δ)) and complex viscosity (η)* were recorded as a function of frequency. All measurements were carried out under oscillatory mode, with the oscillation torque limit set to 0.1 μN·m and temperature tolerance maintained at ±1 °C. Tan δ, the tangent of the phase angle, is a fundamental parameter that defines the balance between viscous and elastic contributions in a polymer system and is expressed as:

$$Tan\,(\delta) = G''/G' \tag{4.1}$$

Tan δ reflects the overall viscoelastic character of the sample. It is a measure of the energy lost per cycle compared to the energy stored. When Tan δ < 1, the system exhibits a gel-like behavior dominated by the elastic component, while values of Tan δ > 1 indicate a liquid-like behavior. Therefore, a decrease in Tan δ means an increase in the material's elasticity and a decrease in the dominance of the viscous component (Delanne-Cuménal et al., 2024).

The Young's modulus (E) values were calculated from the storage modulus (G′) obtained by oscillatory frequency sweep tests according to equation 4.1 where the Poisson's ratio (ν) was assumed to be 0.45 (Caliari et al., 2016), considering the slightly compressible nature of the protein-based hydrogel network.

$$E = 2G'(1 + \nu) \tag{4.1}$$

4.2.4.2. Fourier Transform Infrared Spectroscopy Measurements

Perkin Elmer Fourier Transform Infrared Spectrophotometer (FTIR) equipped with attenuated total reflectance accessory was used for the analyze of synthesized cBSA, BSA and albumin PEC hydrogel. cBSA proteins and albumin PEC hydrogels were

lyophilized for the FTIR measurements. The spectra of the samples were recorded between 4000-400 cm^{-1} wavenumber range with a resolution of 4 cm^{-1}.

4.2.4.3. Scanning Electron Microscopy

Scanning electron microscopy (SEM) was used to examine the morphology of albumin PEC hydrogels (SEM, FEI QUANTA 250 FEG). Lyophilized albumin PEC hydrogels were put into aluminum foil and then lyophilized hydrogels coated with gold in a vacuum using an EMITECH K550X for SEM imaging. The accelerating voltages ranged between 5 and 7 kV.

4.3. Results and Discussion

Hydrogel formation behavior was evaluated using solutions prepared at different cBSA:BSA molar ratios of 0.8:1, 1:1, 2:1, 3:1, and 4:1. According to the experimental results, hydrogel formation was observed in all ratios except 0.8:1 at pH 6 and 37 °C. However, in order to avoid systems requiring high cBSA amounts, subsequent studies were carried out on samples prepared at a 1:1 molar ratio.

To determine the effect of pH on hydrogel formation, the same ratios were examined at pH 7 and pH 8. Gelation was not observed after incubation at 37 °C at pH 7 and 8. This suggests that optimal electrostatic interactions and complexation occur around pH 6. In the control experiment, no gel formation was observed when a solution containing only BSA or cBSA was incubated at 37 °C and pH 6; however, the 1:1 cBSA:BSA complex formed a distinct gel structure. This result supports the conclusion that gel formation occurs as a result of polyelectrolyte complexation between BSA and cBSA.

Furthermore, mixtures were prepared at 15, 17.5, and 20 wt% total protein ratios to evaluate the effect of total protein concentration on gelation. Figure 4.3.1 presents a visual comparison of these samples. Figure 4.1(A) shows the appearance of the 20 wt% cBSA:BSA (1:1) complex solution in an eppendorf tube at room temperature and pH 6 in liquid form. Figure 4.1(B) shows that the same sample transformed into a solid hydrogel after 2 hours of incubation at 37°C. Figure 4.1(C) compares the gelation behaviors of samples at 15, 17.5, and 20 wt% concentrations after 2 hours of incubation at 37°C. These

images demonstrate that gelation did not occur in the sample at a concentration as low as 15 wt%, but a three-dimensional hydrogel network structure was formed above a certain limit concentration of 17.5 wt%. Based on these findings, all characterization and further analyses (including morphological, mechanical, and drug release studies) were conducted on the sample at a 1:1 cBSA:BSA ratio, pH 6, and a total protein concentration of 20 wt%.

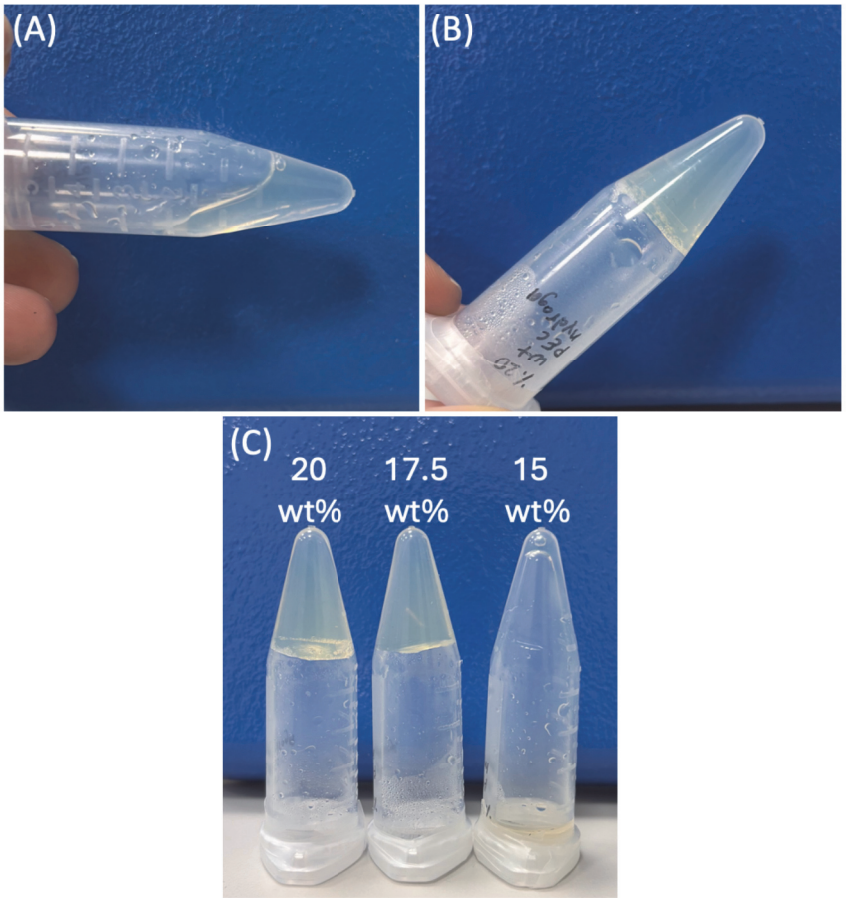

Figure 4.1. Gelation behavior of cBSA:BSA (1:1, pH 6) complex solutions under different conditions; (A) Liquid form of 20 wt% albumin PEC sample at room temperature, (B) Hydrogel form of the same sample after 2 hours of incubation at 37 °C, (C) Comparison of gelation of samples prepared at 15, 17.5 and 20 wt% total protein ratios after 2 hours of incubation at 37 °C.

The viscoelastic properties of the albumin PEC hydrogel were investigated by oscillatory frequency sweep tests performed in the frequency range of 0.1–100 Hz at 37 ° C. The storage modulus (G′), loss modulus (G″), tan (δ) and complex viscosity (η*), and Young's modulus (E) values obtained were analyzed to evaluate the mechanical behavior of the hydrogel and its suitability for biomedical applications. As seen in Figure

4.2 (A), G′ values were higher than G″ values across the entire frequency range. This indicates that the hydrogel exhibited a predominantly elastic (solid-like) behavior (Qu et al., 2025; Amdursky et al., 2018). Both moduli slightly increased with increasing frequency, indicating a physical network structure formed by electrostatic and hydrophobic interactions between protein chains (Arabi et al., 2018, Maria et al., 2019; Shi et al., 2024). Despite not using an external chemical crosslinker, the hydrogel exhibited a physically stabilized network character due to the interactions of cBSA and BSA proteins, along with their inherent structural stability and multiple interaction sites. The plateau region observed at low frequencies indicates that the cBSA:BSA PEC system forms a stable polymer network that resists the applied strain (Fan et al., 2022). Figure 4.2 (B) shows that loss tangent (Tan δ) values are around 0.1 across the entire frequency range. Since Tan δ is defined as the G″/G′ ratio, a value below 1 indicates that the elastic component dominates the viscous component in the system and that the hydrogel exhibits a solid-like behavior (Delanne-Cuménal et al., 2024). These low Tan δ values also indicate that the hydrogel has a high energy storage capacity and a physically strong three-dimensional network structure. Such low loss tangents are a desirable property, especially for injectable or tissue-compatible viscoelastic biomaterials.

Figure 4.2 (C) shows that the complex viscosity (η*) values of the albumin PEC hydrogel change with frequency. The complex viscosity of albumin PEC hydrogel decreases with frequency, which is attributed to the weakening and breaking of attractive forces, resulting in a shear-thinning behaviour similar to that of viscoplastic systems. However, complex viscosity increases at higher frequencies due to the dynamic stiffening of the hydrogel structure. Because deformation occurs too rapidly for these interactions to relax, resulting in a dynamically constrained network. Therefore, the hydrogel behaves more viscously at low frequencies and becomes dynamically stiffer (more elastic) at high frequencies (Shah et al., 2022). This is a desirable property in injectable or topically applicable (skin/eye) systems because the material easily deforms during application and can resume its gel structure upon cessation (Chen et al., 2021; Hu et al., 2022). Similar behavior has been reported in protein-polysaccharide-based hydrogels for drug delivery (Bercea et al., 2023). Therefore, this result supports the viscoelastic profile of the albumin PEC hydrogel, suitable for injectable or mucosal applications.

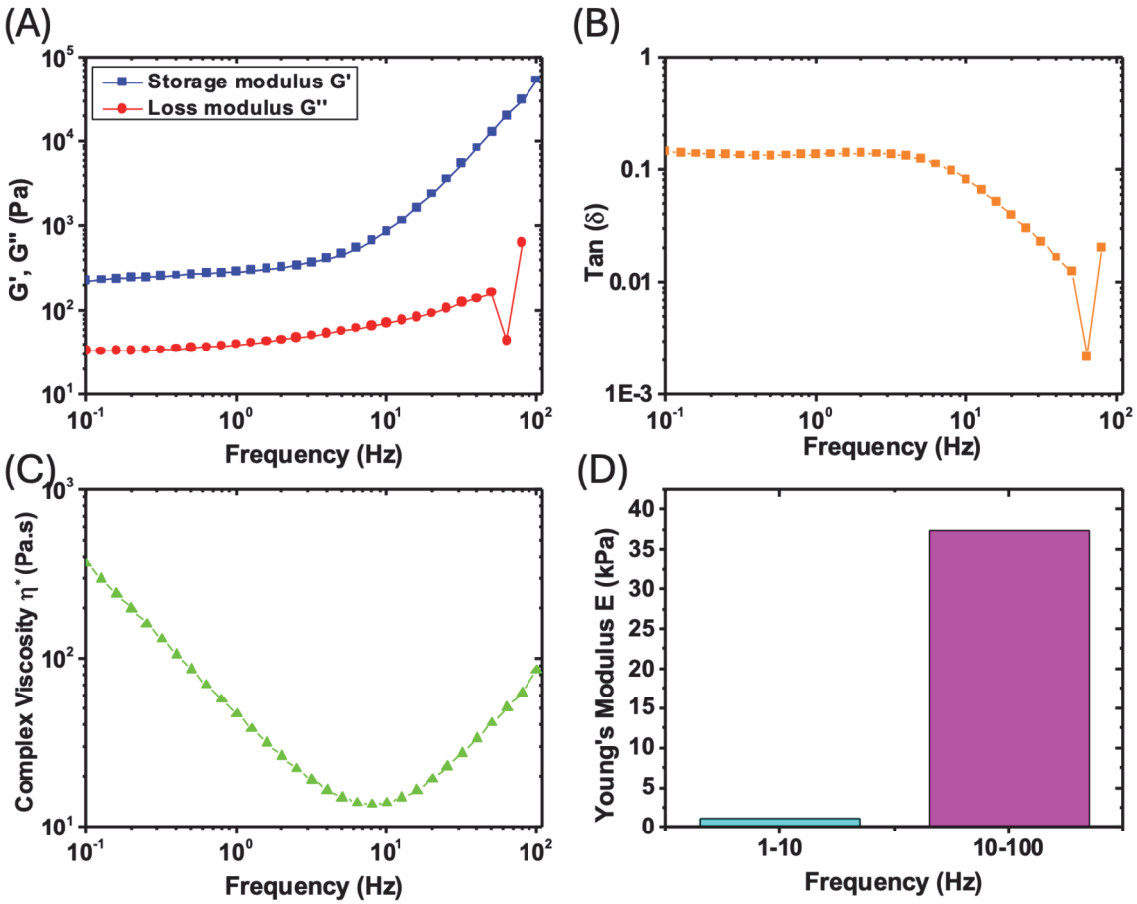

Figure 4.2. (A) Frequency-dependent variation of storage modulus (G′) and loss modulus (G″) of 20 wt% albumin PEC hydrogel, plotted as a function of logarithmic frequency (Hz). (B) The loss ratio, tan(δ) and (C) Complex viscosity (η*) as a function of logarithmic frequency. (D) Comparison of average Young's modulus values in the 1-10 Hz and 10–100 Hz logarithmic frequency ranges.

Young's modulus (E) values were calculated from the storage modulus using equation 4.1. In this calculation, the Poisson's ratio (ν) was set at 0.45 to reflect the partially compressible nature of protein-based hydrogels (Chippada et al.,2019). As seen in Figure 4.2 (D), the E value increases with frequency, reaching approximately 2 kPa at low frequencies (1-10 Hz) and approximately 38 kPa at high frequencies (10-100 Hz). This increase reflects the network stiffening tendency with increasing frequency, a characteristic behavior of physical hydrogels. In the literature, target E for ophthalmic applications is generally reported to be in the range of a few kPa (≈1–6 kPa), while for topical/dermal applications and some tissue engineering applications, the target E is typically in the higher range (≈5–40 kPa) (Wu et al. 2024; Mark et al., 2017; Bovone et

al. 2021). In soft tissue engineering and injectable systems, a range of approximately 2–40 kPa is frequently reported (e.g., 2.7 kPa – over 40 kPa) (Orbach et al., 2024). Additionally, moduli for skin applications have been reported to be around 10–18 kPa (Xie et al., 2024). In this context, the ~38 kPa value we obtained is consistent with the upper limits in the literature and demonstrates that it is a hydrogel with high mechanical strength.

SEM and FTIR analyses were performed to determine the surface morphology and functional groups of the obtained albumin PEC hydrogel, respectively. The surface morphology of the resulting albumin PEC hydrogels at different magnifications were examined by SEM analysis (Fig. 4.3). The images reveal that the resulting hydrogel has a three-dimensional network structure composed of irregular but interconnected pores. In low-magnification images (Fig. 4.3 (A, B)), it was observed that the pore diameters varied on the micrometer scale, were distributed intermittently, and the pore walls exhibited a tortuous and rough morphology in some places. This irregular but continuous structure suggests that the gel has a high water retention capacity and that ionic and molecular diffusion can easily occur. Furthermore, it is thought that during gelation, the albumin chains organize through electrostatic interactions to form a heterogeneous network structure. This morphology is consistent with similar porous and irregular structural features reported in the literature for BSA and other protein-polysaccharide-based hydrogels (Bercea et al.,2023). Image obtained at higher magnifications (Fig. 4.3 (C)) demonstrate that the hydrogel has a multi-scale organization at the micro- and nanoscale. In Figure 4.3 (C), the white arrows highlight the pore structures within the albumin PEC hydrogel, indicating the porous three-dimensional network formed as a result of PEC structuring. Fine interconnected fibril-like connections are also noticeable in these same regions. These fibrils represent network-like transition zones formed by the partially unfolded conformations of the protein chains, held together by physical bonds.

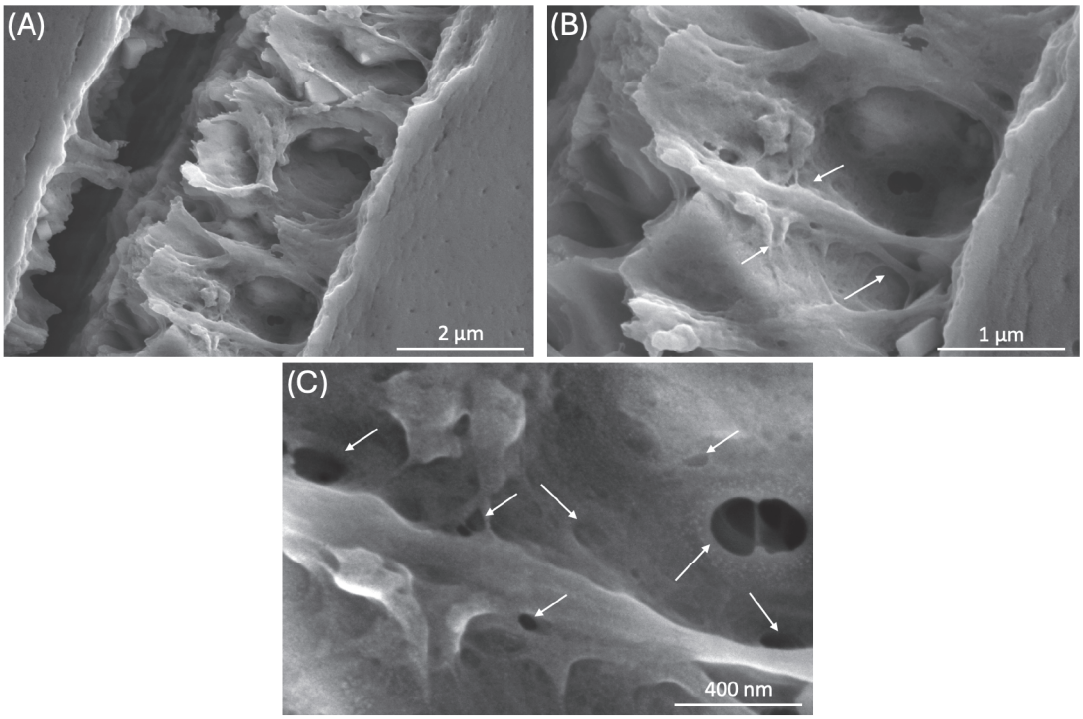

Figure 4.3. SEM images obtained from 20 wt% albumin PEC hydrogel solution at pH 6 and incubated for 2 hours at 37 °C. (A, B) Microstructure showing the porous and layered morphology of the hydrogel (C) nanometer-scale smooth surface regions and transitional pore structure (A portion of the sample was cut and dried at RT for 24h).

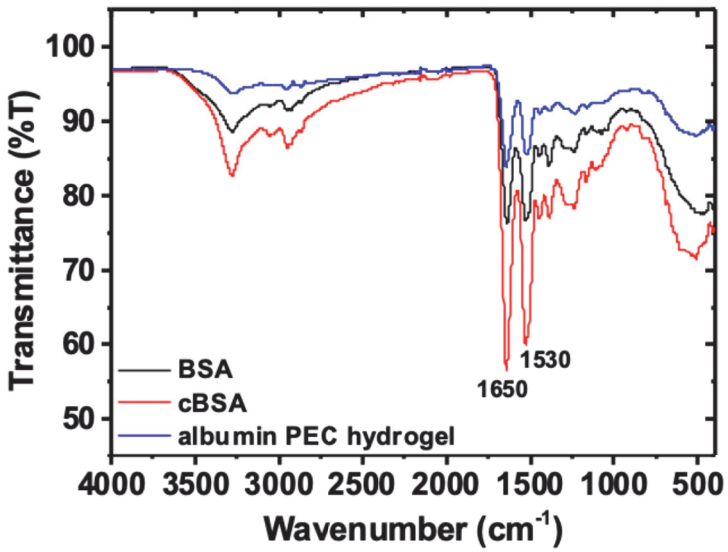

Figure 4.4. The FTIR spectra of BSA (black), cBSA (red) and albumin PEC (blue) hydrogel powder.

For the FTIR study, a freeze-dried 20 wt% albumin PEC hydrogel sample and the native BSA and cBSA powders were used. As shown in Fig. 4.4., both the BSA, cBSA powder and the albumin PEC hydrogel exhibited very similar FTIR profiles, particularly around 1650 and 1530 cm^{-1}, which correspond to the characteristic amide I and amide II bands of BSA (Lad et al., 2006; Subia et al., 2013). The absence of a new peak in the FTIR spectra of the albumin PEC hydrogels indicates that no new covalent bonds are formed during complexation, but rather that the structures are brought together by electrostatic interactions. Furthermore, in this study, a decrease in the intensity of the amide I (≈1650 cm^{-1}) and amide II (≈1530 cm^{-1}) bands was observed after hydrogel formation. This weakening of the amide bands is attributed to partial unfolding of the albumin secondary structure, especially in the α-helix regions, the formation of more disordered conformations, and the relaxation of the protein chain as a result of the polyelectrolyte complex structure. Teir and colleagues similarly reported a decrease in the intensity of the amide I and II bands resulting from protein–polyelectrolyte interactions, correlating this decrease with the partial unfolding of the protein chain and the loss of its ordered structure (Teir et al., 2012). Taken together, these findings support that albumin PEC hydrogel formation induces a rearrangement of albumin chains, leading to a noncovalently assembled, electrostatically stabilized, and flexible PEC hydrogel network rather than a covalently crosslinked structure.

4.4. Conclusion

Although albumin hydrogels are frequently studied by using high temperatures or very low pH conditions, this method achieved a stable hydrogel structure at pH 6 and the physiological temperature of 37°C, thanks to the PEC interactions formed by cationic and anionic albumin proteins. Rheological analyses of the cBSA:BSA polyelectrolyte complex (PEC) hydrogel showed that the elastic component dominates the entire frequency range of the system. The storage modulus (G′) being consistently higher than the loss modulus (G″) and Tan δ values around 0.1 confirm that the hydrogel forms a physically strong three-dimensional network structure capable of storing energy, and the hydrogel exhibited a predominantly elastic (solid-like) behavior. The shear-thinning behavior observed in the complex viscosity analysis, which shows hydrogel complex viscosity decreases with frequency. This feature makes the hydrogel a highly suitable

candidate for injectable or mucosal applications. SEM images also revealed distinct porous regions within the gel, organized by PEC interactions between protein chains. Overall, the rheological and morphological findings demonstrate that the albumin-based PEC hydrogel forms a stable, elastic, and physiologically compatible network structure, demonstrating that this material is a promising candidate for drug delivery and soft tissue-focused biomedical applications.

CHAPTER 5

CONCLUSION AND FUTURE DIRECTIONS

This thesis aims to evaluate serum albumin proteins (BSA and cBSA) in various structural forms (protein, nanoparticle, and hydrogel) to increase the water solubility of hydrophobic drugs, elucidate drug-carrier interactions, develop new non-toxic carrier platforms, and adapt polyelectrolyte complex (PEC)-based biomaterials for therapeutic applications. The findings from the three main sections, taken together, demonstrate that albumin-based nanostructures and PEC systems have high potential for both drug and biomacromolecule delivery.

In the first section of the thesis, the binding behavior of drugs with different hydrophobic properties to albumin proteins and nanoparticles derived from these proteins, their solubility states, and the distinction between free and bound forms were investigated using EPR spectroscopy using spin-labeled drugs. Thanks to the high sensitivity of EPR to spin-spin interactions and spin rotational correlation time (freedom) in solution, it was possible to directly distinguish between dissolved and undissolved drugs and whether they are bound to the carrier, respectively. The findings demonstrated that albumin nanoparticles are more effective than albumin proteins in increasing the water solubility of hydrophobic drugs. Furthermore, the positive surface charge of cBSA significantly increased the loading capacity of anionic drugs. EPR, which allows for both drug loading and release to be monitored directly from nanoparticle pellets, makes this method a powerful characterization tool alternative to traditional techniques.

In the second part, albumin PEC nanoparticles were developed for the first time in the literature by utilizing the opposite charges of BSA and cBSA proteins, without the use of toxic solvents or chemical cross-linkers. These nanoparticles, approximately 110 nm in size and possessing a high positive surface charge, exhibited a loading capacity of 6.4% of the hydrophobic CHL drug, approximately seventeen times higher than albumin nanoparticles produced by the conventional desolvation method. PEG coating enhanced the biocompatibility of the nanoparticles, and CHL-loaded PEC NPs were shown to have a significant therapeutic effect in Huh-7 cells. Furthermore, this new albumin PEC NP

platform was demonstrated for mRNA loading, demonstrating strong potential for use as a genetic material carrier.

Based on the PEC system formed by the resulting albumin proteins, a stable PEC hydrogel was obtained under physiological conditions of pH 6 and 37°C, requiring no high temperature, low or high pH, or chemical crosslinkers. Rheological measurements showed that the storage modulus (G′) of the hydrogel dominated the loss modulus (G″) across the entire frequency range, with Tan δ values of ~0.1. This confirmed that the material formed a physically stabilized, strong, and elastic three-dimensional network structure. Its shear-thinning behavior made the developed hydrogel a suitable candidate for injectable applications. SEM analyses confirmed the rheological findings by revealing a porous morphology organized by PEC interactions.

Overall, this thesis demonstrates that albumin-based nanostructures and polyelectrolyte complex-based biomaterials are reliable, non-toxic, and effective platforms that can be used in a wide range of biomedical applications, including hydrophobic drug delivery, controlled release, mRNA delivery, and soft tissue applications. It also demonstrates that EPR spectroscopy can be used as a powerful and complementary analysis method for assessing drug solubility and carrier interactions.

In future studies, it is important to more comprehensively evaluate the potential of the developed carrier systems, particularly in gene therapy applications. In this context, the successful loading of mRNA into PEC NPs demonstrates the platform's adaptability to nucleic acid-based therapies. The use of albumin PEC NPs for mRNA delivery is advantageous because they can be synthesized in a green way without using organic solvents and chemical crosslinkers. Further, parameters such as mRNA stability, in vivo expression efficiency, and target tissue-specific distribution require detailed investigation. Furthermore, adapting the resulting PEC hydrogel structure to controlled release applications will enable optimization of the hydrogel for different biomedical targets, such as local drug delivery, protein delivery, or cell delivery. Finally, evaluating the in vivo biocompatibility of both PEC nanoparticles and PEC hydrogels, and examining tissue response, inflammatory processes, biodistribution, and elimination profiles in animal models are critical requirements for the translation of these materials into clinical applications.

REFERENCES

Abbasi, S.; Paul, A.; Shao, W.; Prakash, S. Cationic albumin nanoparticles for enhanced drug delivery to treat breast cancer: preparation and in vitro assessment. *J. Drug Deliv*. **2012**, 686108.

Akdogan, Y.; Emrullahoglu, M.; Tatlidil, D.; Ucuncu, M.; Cakan-Akdogan, G. EPR studies of intermolecular interactions and competitive binding of drugs in a drug–BSA binding model. *Phys. Chem. Chem. Phys*. **2016**, *18*, 22531-22539.

Akdogan, Y.; Junk, M. J. N.; Hinderberger, D. Effect of Ionic liquids on the solution structure of human serum albumin. *Biomacromolecules*. **2011**, *12*, 1072-1079.

Akdogan, Y.; Sozer, S. C.; Akyol, C.; Basol, M.; Karakoyun, C.; Cakan-Akdogan, G. Synthesis of albumin nanoparticles in a water-miscible ionic liquid system, and their applications for chlorambucil delivery to cancer cells. *J. Mol. Liq*. **2022**, *367*, 120575.

Albalawi, H. B.; Asharari, K. S.; Alali, N. M.; Alraddadi, O.; Magliyah, M.; and Alanazi, G. B. Hydrogel (Miragel®) scleral explant, late orbital complication. *Int. J. Surg. Case Rep*. **2022**, *98*, 107583.

Amatya, R.; Hwang, S.; Park, T.; Chung, Y. J.; Ryu, S.; Lee, J.; et al. BSA/Silver nanoparticle-loaded hydrogel film for local photothermal treatment of skin cancer. *Pharm. Res*. **2021**, *38*, 873–883.

Amdursky, N.; Mazo, M. M.; Thomas, M. R.; Humphrey, E. J.; Puetzer, J. L.; St-Pierre, J. P.; Skaalure, S. C.; Richardson, R. M.; Terracciano, C. M.; Stevens, M. M. Elastic serum-albumin based hydrogels: mechanism of formation and application in cardiac tissue engineering. *J Mater Chem B*. **2018**, *6* (35), 5604-5612.

Andrianov, A.K.; Marin, A.; Roberts, B.E. Polyphosphazene polyelectrolytes: a link between the formation of noncovalent complexes with antigenic proteins and immunostimulating activity. *Biomacromolecules*. **2005**, *6*, 1375–1379.

Antonio, E.; Khalil, N. M.; Mainardes, R. M. Bovine serum albumin nanoparticles containing quercetin: characterization and antioxidant activity, *J. Nanosci. Nanotechnol*. **2016**, *16* (2), 1346–1353.

Arabi, S. H.; Aghelnejad, B.; Schwieger, C.; Meister, A.; Kerth, A.; and Hinderberger, D. Serum albumin hydrogels in broad pH and temperature ranges: Characterization of their self-assembled structures and nanoscopic and macroscopic properties. *Biomaterials Sci*. **2018**, *6*, 478–492

Areevijit, K.; Dhanesuan, N.; Luckanagul, J. A.; and Rungsiyanont, S. Biocompatibility study of modified injectable hyaluronic acid hydrogel with mannitol/BSA to alveolar bone cells. *J. biomaterials Appl.* **2020**, *35*, 1294–1303.

Argitekin, E.; Erez, O.; Cakan-Akdogan, G.; Akdogan, Y. Periodate-mediated cross-linking for the preparation of catechol conjugated albumin nanoparticles used for in vitro drug delivery, *ACS Appl. Bio Mater*. **2025**, *8* (3), 2182–2193.

Argitekin, E.; Ersoz-Gulseven, E.; Cakan-Akdogan, G.; Akdogan, Y. Dopamine-conjugated bovine serum albumin nanoparticles containing pH-responsive catechol-V(III) coordination for in vitro and in vivo drug delivery. *Biomacromolecules*. **2023**, *24* (8), 3603–3618.

Babcock, N. S. and Kattnig, D. R. Electron–Electron Dipolar Interaction Poses a Challenge to the Radical Pair Mechanism of Magnetoreception. *The Journal of Physical Chemistry Letters.* **2020,** *11* (7), 2414-2421

Bai, Y.; Li, S.; Li, X.; Han, X.; Li, Y.; Zhao, J.; et al. An injectable robust denatured albumin hydrogel formed via double equi librium reactions. *J. biomaterials Sci. Polym. Ed*. **2019**, *30*, 662–678.

Baler, K.; Martin, O. A.; Carignano, M. A.; Ameer, G. A.; Vila, J. A.; and Szleifer, I. Electrostatic Unfolding and Interactions of Albumin Driven by pH Changes: A Molecular Dynamics Study. *The Journal of Physical Chemistry B*. **2014b,** *118* (4), 921-930.

Baler, K.; Michael, R.; Szleifer, I.; and Ameer, G. A. Albumin Hydrogels Formed by Electrostatically Triggered Self-Assembly and Their Drug Delivery Capability. *Biomacromolecules*. **2014,** *15* (10), 3625-3633

Belgoudi, J.; and Fortier, G. Poly(Ethylene glycol)-bovine serum albumin hydrogel as a matrix for enzyme immobilization. in vitro biochemical characterization. *J. Bioact. Compatible Polym*. **1999**,*14*, 31–53.

Bercea, M.; Plugariu, I.-A.; Dinu, M.V.; Pelin, I.M.; Lupu, A.; Bele, A.; Gradinaru, V.R. Poly(Vinyl Alcohol)/Bovine Serum Albumin Hybrid Hydrogels with Tunable Mechanical Properties. *Polymers*. **2023**, *15*, 4611.

Berdichevski, A.; Shachaf, Y.; Wechsler, R.; and Seliktar, D. Protein composition alters in vivo resorption of PEG-based hydrogels as monitored by contrast-enhanced MRI. *Biomaterials*. **2015**, *42*, 1–10.

Bergström, C. A.; Norinder, U.; Luthman, K.; Artursson, P. Experimental and computational screening models for prediction of aqueous drug solubility. *Pharm Res*. **2002**, *19* (2), 182-8.

Bielawski, K.; Bielawska, A.; Muszynska, A.; Poplawska, B.; Czarnomysy, R. Cytotoxic activity of G3 PAMAM-NH2 dendrimer-chlorambucil conjugate in human breast cancer cells, Environ. *Toxicol. Pharmacol*. **2011**, *32*, 364–372.

Bovone, G.; Dudaryeva, O. Y.; Marco-Dufort, B.; and Tibbitt, M. W. Engineering Hydrogel Adhesion for Biomedical Applications via Chemical Design of the Junction. *ACS Biomaterials Science & Engineering*. **2021**, *7* (9), 4048-4076.

Bronze-Uhle, E. S.; Costa, B. C.; Ximenes, V. F.; Lisboa-Filho, P. N. Synthetic nanoparticles of bovine serum albumin with entrapped salicylic acid. *Nanotechnology Sci Appl*. **2017**, *10*, 11-21.

Buriuli, M.; Verma, D. *Polyelectrolyte complexes (PECs) for biomedical applications*, in: a. Tripathi, J. Melo (Eds.), Advances in Biomaterials for Biomedical Applications, Advanced Structured Materials. 2017, *66*, Springer, Singapore.

Byeon, H. J.; Thao, le Q.; Lee, S.; Min, S. Y.; Lee, E. S.; Shin, B. S.; Choi, H. G.; Youn, Y. S. Doxorubicin-loaded nanoparticles consisted of cationic- and mannose-modified-albumins for dual-targeting in brain tumors. *J Control Release*. **2016**, *225*, 301-13.

Cakan-Akdogan, G.; Ersoz, E.; Sozer, S.C.; Gelinci, E. An in vivo zebrafish model reveals circulating tumor cell targeting capacity of serum albumin nanoparticles. *J. Drug Deliv. Sci. Technol*. **2022**, *75*, 103658.

Caliari, S. R.; Burdick, J.A. A practical guide to hydrogels for cell culture. *Nat Methods*. **2016**, *13* (5), 405-14.

Carter, D. C. and Ho, J. X. Structure of Serum Albumin. *Advances in Protein Chemistry*. **1994**, *45*, 153-203.

Chaniotakis, N.A. Enzyme stabilization strategies based on electrolytes and polyelectrolytes for biosensor applications. *Anal. Bioanal. Chem*. **2004**, *378*, 89–95.

Chaux-Gutiérrez, A. M.; Pérez-Monterroza, E. J.; Mauro, M. A. Rheological and structural characterization of gels from albumin and low methoxyl amidated pectin mixtures. *Food Hydrocolloids*. **2019**, *92*, 60-68.

Chen, Y.; Wang, X.; Huang, Y.; Kuang, P.; Wang, Y.; Liu, Y.; et al. In situ- forming cellulose/albumin-based injectable hydrogels for localized antitumor therapy. *Polym. (Basel)* **2021**, *13*.

Chen,Y.; Wang, X.; Huang, Y.; Kuang, P.; Wang, Y.; Liu, Y.; Yin, W.; Zan, J.; Liu, Y.; Yin, C.; et al. In Situ-Forming Cellulose/ Albumin-Based Injectable Hydrogels for Localized Antitumor Therapy. *Polymers.* **2021**, *13*, 4221.

Chippada, U.; Langrana, N.; Yurke, B. Complete mechanical characterization of soft media using nonspherical rods. *J Appl Phys.* **2009**, *106* (6), 63528.

Cisneros, J. A.; Robertson, M. J.; Valhondo, M.; Jorgensen, W. L. A Fluorescence Polarization Assay for Binding to Macrophage Migration Inhibitory Factor and Crystal Structures for Complexes of Two Potent Inhibitors. *Journal of the American Chemical Society.* **2016,** *138* (27), 8630-8638.

da Costa, T. S.; da Silva, M. R.; Barbosa, J. C. J.; Neves, U. D. S. D.; de Jesus, M. B.; Tasic, L. Biogenic silver nanoparticles' antibacterial activity and cytotoxicity on human hepatocarcinoma cells (Huh-7). *RSC Adv.* **2024**, *14,* 2192.

Dai, Z.; Zhang, Y.; Chen, C.; Yu, F.; Tian, J.; Cai, H.; et al. An antifouling and antimicrobial zwitterionic nanocomposite hydrogel dressing for enhanced wound healing. *ACS biomaterials Sci. Eng.* **2021**, *7*, 1621–1630.

Das, S.; Banerjee, R.; Bellare, J. Aspirin Loaded Albumin Nanoparticles by Coacervation: Implications in Drug Delivery. *Trends Biomater. Artif. Organs* **2005**, *18*, 203–212.

Delanne-Cuménal, A.; Lainé, E.; Hoffart, V.; Verney, V.; Garrait, G.; Beyssac, E. Effect of Molecules' Physicochemical Properties on Whey Protein/Alginate Hydrogel Rheology, Microstructure and Release Profile. *Pharmaceutics* **2024**, *16*, 258.

Demirkurt, B.; Akdogan, Y. Development of an ionic liquid based method for the preparation of albumin nanoparticles. *ChemistrySelect.* **2018**, *3*, 9940-9445.

Demirkurt, B.; Cakan-Akdogan, G.; Akdogan, Y. Preparation of albumin nanoparticles in water-in-ionic liquid microemulsions. *Journal of Molecular Liquids.* **2019**, *295*, 111713.

Di Antonio, M.; McLuckie, K. I. E.; Balasubramanian, S. Reprogramming the mechanism of action of chlorambucil by coupling to a G-quadruplex ligand. *J. Am. Chem. Soc*. **2014**, *136*, 5860–5863.

Di, L.; Fish, P. V.; Mano, T. Bridging solubility between drug discovery and development. *Drug Discov Today*. **2012**, *17* (9-10), 486-95.

Din, F.; Aman, W.; Ullah, I.; Qureshi, O. S.; Mustapha, O.; Shafique, S.; Zeb, A. Effective use of nanocarriers as drug delivery systems for the treatment of selected tumors. *Int J Nanomedicine*. **2017**, *12*, 7291-7309.

Ding, F.; Zhao, F.; Jin, R.; Rao, Y.; Yang, G.; Lu, L.; et al. Management of complications in 257 cases of breast augmentation with polyacrylamide hydrogel, using two different strategies: A retrospective study. *Aesthetic Plast. Surg*. **2022**, *46*, 2107–2121.

Dubin, P.L.; Gao, J.; Mattison, K. Protein purification by selective phase separation with polyelectrolytes. *Sep. Purif. Methods*. **1994**, *23*, 1–16.

Durmaz, E.N.; Baig, M.I.; Willott, J.D.; de Vos, W.M. Polyelectrolyte complex membranes via salinity change induced aqueous phase separation. *ACS Appl. Polym. Mater*. **2020**, *2* (7), 2612–2621.

Ebrahimi, B.; Mokhtari, T.; Ghaffari, N.; Adabi, M.; Hassanzadeh, G. Acellular spinal cord scaffold containing quercetin-encapsulated nanoparticles plays an anti-inflammatory role in functional recovery from spinal cord injury in rats. I*nflammopharmacology*. **2024**, *32* (4), 2505–2524.

Eisele, K.; Gropeanu, R. A.; Zehendner, C. M.; Rouhanipour, A.; Ramanathan, A.; Mihov, G.; Koynov, K.; Kuhlmann, C. R.; Vasudevan, S. G.; Luhmann, H. J.; Weil, T. Fine-tuning DNA/albumin polyelectrolyte interactions to produce the efficient transfection agent cBSA-147. *Biomaterials.* **2010**, *31* (33), 8789–8801.

El-Baz, N.; Nunn, B. M.; Bates, P. J.; O'Toole, M. G. The impact of PEGylation on cellular uptake and in vivo biodistribution of gold nanoparticle MRI contrast agents. *Bioengineering*. **2022**, *9* (12), 766.

Elangwe, C. N.; Morozkina, S. N.; Olekhnovich, R. O.; Krasichkov, A.; Polyakova, V. O.; and Uspenskaya, M. V. A review on chitosan and cellulose hydrogels for wound dressings. *Polymers*. **2022**, *14*.

Elzoghby, A. O.; Samy, W. M.; Elgindy, N. A. Albumin-based nanoparticles as potential controlled release drug delivery systems. *J Control Release*. **2012**, *157* (2), 168-82.

Fahrländer, E.; Schelhaas, S.; Jacobs, A. H.; Langer, K. PEGylated human serum albumin (HSA) nanoparticles: preparation, characterization and quantification of the PEGylation extent, *Nanotechnology*. **2015**, *26*, 145103.

Fan, Z.; Cheng, P.; Zhang, P.; Zhang, G.; Han, J. Rheological insight of polysaccharide/protein based hydrogels in recent food and biomedical fields: A review. *International Journal of Biological Macromolecules*. **2022**, *222*, Part B, 1642-1664.

Ferreira, L. O.; Santos, M. B.; Garcia-Rojas, E. E. Complex coacervates between bovine serum albumin and anionic polysaccharides: formation and characterization. *Braz. J. Food Technol*. **2021**, *24*, e2021070.

Ferry, J.D. Protein gels. *Adv Protein Chem*. **1948**, *4*, 1-78.

Freedman, B. R.; Kuttler, A.; Beckmann, N.; Nam, S.; Kent, D.; Schuleit, M.; et al. Enhanced tendon healing by a tough hydrogel with an adhesive side and high drug-loading capacity. *Nat. Biomed. Eng*. **2022**, *6*, 1167–1179.

Frohlich, E. The role of surface charge in cellular uptake and cytotoxicity of medical nanoparticles. *Int. J. Nanomedicine*. **2012**, *7*, 5577–5591.

Fürst, W.; Banerjee, A. Release of glutaraldehyde from an albumin-glutaraldehyde tissue adhesive causes significant in vitro and in vivo toxicity. *Ann. Thorac. Surg.* **2005**, *79* (5), 1522–1528.

Galante, R.; Paradiso, P.; Moutinho, M. G.; Fernandes, A. I.; Mata, J. L. G.; Matos, A. P. A.; Colaco, R.; Saramago, B.; Serro, A. R. About the effect of eye blinking on drug release from pHEMA-based hydrogels: an in vitro study. *J. Biomat. Sci. Polym. Ed.* **2015**, *26*, 235–251.

Ghobril, C.; Grinstaff, M. W. The chemistry and engineering of polymeric hydrogel adhesives for wound closure: a tutorial. *Chem. Soc. Rev.* **2015**, *44*, 1820–1835.

Ghorbani, M.; Hamishehkar, H.; Tabibiazar, M. BSA/chitosan polyelectrolyte complex: a platform for enhancing the loading and cancer cell-uptake of resveratrol. *Macromol. Res.* **2018**, *26* (9), 808–813.

Ghosh, S.; Das, P.; Nayak, B. High potency EDC-crosslinked bovine serum albumin nanoencapsulation of berberine enhances in vitro anticancer efficacy against glioblastoma by inducing ROS mediated cell apoptosis. *New J. Chem.* **2022**, *46*, 23254–23267.

Ghuman, J.; Zunszain, P. A.; Petitpas, I.; Bhattacharya, A. A.; Otagiri, M.; Curry, S. Structural basis of the drug-binding specificity of human serum albumin. *J Mol Biol.* **2005**, *353* (1),38-52.

Glomme, A.; März, J.; Dressman, J. B. Comparison of a miniaturized shake-flask solubility method with automated potentiometric acid/base titrations and calculated solubilities. *J Pharm Sci.* **2005**, *94* (1), 1-16.

Goder Orbach, D.; Roitman, I.; Coster Kimhi, G.; Zilberman, M. Formulation-Property Effects in Novel Injectable and Resilient Natural Polymer-Based Hydrogels for Soft Tissue Regeneration. *Polymers,* **2024**, *16*, 2879.

Gsib, O.; Eggermont, L. J.; Egles, C.; and Bencherif, S. A. Engineering a macroporous fibrin-based sequential interpenetrating polymer network for dermal tissue engineering. *Biomaterials Sci*. **2020**, *8*, 7106–7116.

Gulsun, T.; Gursoy, R. N.; Oner, L. Nanocrystal technology for oral delivery of poorly water-soluble drugs. *Fabad J Pharm Sci*. **2009**, *34* (1), 55-65.

Guo, B.; Zhong, Y.; Chen, X.; Yu, S.; and Bai, J. 3D printing of electrically conductive and degradable hydrogel for epidermal strain sensor. *Compos. Commun*. **2023**, *37*, 101454.

Hao, H. X.; Hou, B. H.; Wang, J. K.; Zhang, M. J. Solubility of erythritol in different solvent. *J.Chem. Eng.Data.* **2005**, *50*, 1454–1456.

Hauenschild, T.; Reichenwallner, J.; Enkelmann, V.; Hinderberger, D. Characterizing Active Pharmaceutical Ingredient Binding to Human Serum Albumin by Spin-Labeling and EPR Spectroscopy. *Chem. Eur. J.* **2016**, *22*, 12825.

Hoare, T.R.; Kohane, D. S. Hydrogels in drug delivery: progress and challenges. *Polymer.* **2008**, *49*,1993–2007.

Hu, L.; Xu, Y.; & Meng, H. Development and Evaluation of Puerarin Loaded-Albumin Nanoparticles Thermoresponsive in situ Gel for Ophthalmic Delivery. *Drug Design, Development and Therapy*. **2022**, 3315-3326.

Hwang, D.; Ramsey, J.D.; Kabanov, A. V. Polymeric micelles for the delivery of poorly soluble drugs: From nanoformulation to clinical approval. *Adv Drug Deliv Rev*. **2020**, *156*, 80-118.

Jian, H.; Xiong, Y. L.; Guo, F.; Huang, X.; Adhikari, B.; Chen, J. Gelation enhancement of soy protein isolate by sequential low- and ultrahigh-temperature two-stage preheating treatments. *International Journal of Food Science and Technology*. **2014**, *49* (12), 2529–2537

Jiang, H.; Zuo, Y.; Zhang, L.; Li, J. D.; Zhang, A. M.; Li, Y. B.; Yang, X. C. Property-based design: optimization and characterization of polyvinyl alcohol (PVA) hydrogel and PVA-matrix composite for artificial cornea. *J. Mat. Sci. Mat. Med.* **2014,** *25*, 941–952.

Kang, N.-W.; Yoon, S.-Y.; Kim, S.; Yu, N.-Y.; Park, J.-H.; Lee, J.-Y.; et al. Subcutaneously injectable hyaluronic acid hydrogel for sustained release of donepezil with reduced initial burst release: Effect of hybridization of microstructured lipid carriers and albumin. *Pharmaceutics*. **2021**, *13*, 864.

Kanikkannan, N. Technologies to Improve the Solubility, Dissolution and Bioavailability of Poorly Soluble Drugs. *J Anal Pharm Res.* **2018**, *7* (1), 00198.

Kanwar, R.; Rathee, J.; Salunke, D. B.; Mehta, S. K. Green nanotechnology-driven drug delivery assemblies. *ACS Omega*. **2019,** *4* (5), 8804–8815.

Katarivas Levy, G.; Ong, J.; Birch, M. A.; Justin, A. W.; and Markaki, A. E. Albumin-enriched fibrin hydrogel embedded in active ferromagnetic networks improves osteoblast differentiation and vascular self-organisation. *Polymers*. **2019**, *11*, 1743.

Katyal, P.; Mahmoudinobar, F.; Montclare, J. K. Recent trends in peptide and protein-based hydrogels. *Curr. Opin. Struct. Biol*. **2020**, *63*, 97-105.

Khanna, S.; Singh, A. K.; Behera, S. P.; and Gupta, S. Thermoresponsive BSA hydrogels with phase tunability. *Mater. Sci. Eng. C, Mater. Biol. Appl. Ons*. **2020**, *119*, 111590.

Kim, E. H.; Kim, M. S.; Song, H. S.; Yoo, S. H.; Sai, S.; Chung, K.; Sung, J.; Jeong, Y. K.; Jo, Y. H.; Yoon, M. Gold nanoparticles as a potent radiosensitizer in neutron therapy. *Oncotarget*. **2017**, *8* (68), 112390–112400.

Kim, I.; Choi, J. S.; Lee, S.; Byeon, H. J.; Lee, E. S.; Shin, B. S.; et al. In situ facile-forming PEG cross-linked albumin hydrogels loaded with an apoptotic TRAIL protein. *J. Control Release*. **2015**, *214*, 30–39.

Kirchhof, S.; Goepferich, A. M.; Brandl, F. P. Hydrogels in ophthalmic applications. *Eur. J. Pharm. Biopharm.* **2015**, *95*, 227–238.

Kokufuta, E. Functional immobilized biocatalysts. *Prog. Polym. Sci.* **1992**, *17*, 647–697.

Komatsu, S.; Tago, M.; Ando, Y.; Asoh, T. A., and Kikuchi, A. Facile preparation of multi-stimuli-responsive degradable hydrogels for protein loading and release. *J. Control Release*. **2021**, *331*, 1–6.

Kose, A. A.; Ekinci, C.; and Kocman, A. E. Abscess formation after tooth extraction: A long-term complication of polyacrylamide hydrogel filler. *Cureus*. **2022**, *14*, e28180.

Kossover, O.; Cohen, N.; Lewis, J. A.; Berkovitch, Y.; Peled, E.; and Seliktar, D. Growth factor delivery for the repair of a critical size tibia defect using an acellular, biodegradable polyethylene glycol–albumin hydrogel implant. *ACS Biomaterials Sci. Eng.* **2020**, *6*, 100–111.

Krelle, A.; Okoli, A.; Mendz, G. Huh-7 human liver cancer cells: a model system to understand hepatocellular carcinoma and therapy. *J. Cancer Ther*. **2013**, *4* (2), 606–631.

Kumar, G.; Wang, Y.C.; Co, C.; Ho, C.C. Spatially controlled cell engineering on biomaterials using polyelectrolytes. *Langmuir*. **2003**, *19*, 10550–10556.

Lad, M. D.; Birembaut, F.; Matthew, J. M.; Frazier, R. A. & Green, R. J. The adsorbed conformation of globular proteins at the air/water interface. *Physical Chemistry Chemical Physics*. **2006**, *8*, 2179–2186.

Langer, K.; Anhorn, M. G.; Steinhauser, I.; Dreis, S.; Celebi, D.; Schrickel, N.; Faust, S.; Vogel, V. Human serum albumin (HSA) nanoparticles: reproducibility of preparation process and kinetics of enzymatic degradation. *Int. J. Pharm*. **2008**, *347*, 109–117.

Langer, K.; Balthasar, S.; Vogel, V.; Dinauer, N.; Von Briesen, H.; Schubert, D. Optimization of the preparation process for human serum albumin (HSA) nanoparticles. *Int. J. Pharm*. **2003**, *257*, 169–180.

Lankalapalli, S.; Kolapalli, V.R. Polyelectrolyte complexes: a review of their applicability in drug delivery technology. In*dian J. Pharm. Sci*. **2009**, *71* (5), 481.

Layman, H.; Li, X.; Nagar, E.; Vial, X.; Pham, S. M.; and Andreopoulos, F. M. Enhanced angiogenic efficacy through controlled and sustained delivery of FGF-2 and G-CSF from fibrin hydrogels containing ionic-albumin microspheres. *J. Biomaterials Sci. Polym. Ed*. **2012**, *23*, 185–206.

Lee, A. L. Z.; Yang, C.; Gao, S.; Hedrick, J. L.; and Yang, Y. Y. Subcutaneous vaccination using injectable biodegradable hydrogels for long-term immune response. *Nanomedicine*. **2019**, *21*, 102056.

Lee, J. E.; Kim, M. G.; Jang, Y. L.; Lee, M. S.; Kim, N. W.; Yin, Y.; Lee, J. H.; Lim, S. Y.; Park, J. W.; Kim, J.; Lee, D. S.; Kim, S. H.; Jeong, J. H. Self-assembled PEGylated albumin nanoparticles (SPAN) as a platform for cancer chemotherapy and imaging. *Drug Deliv*. **2018**, *25* (1), 1570–1578.

Lee, K.-J.; Lee, M.-H.; Shih, Y.-H.; Wang, C.-P.; Lin, H.-Y.; and Jian, S.-R. Fabrication of carboxylated carbon nanotube buckypaper composite films for bovine serum albumin detection. *Coatings*. **2014**, *12*, 810.

Lee, S. H.; Heng, D.; Ng, W. K.; Chan, H. K.; Tan, R. B. Nano spray drying: a novel method for preparing protein nanoparticles for protein therapy. *Int J Pharm*. **2011**, *403* (1-2), 192-200.

Lee, S. S.; Kim, H.; Sohn, D. K.; Eom, J. B.; Seo, Y. S.; Yoon, H. M.; et al. Indocyanine green-loaded injectable alginate hydrogel as a marker for precision cancer surgery. *Quant. Imaging Med. Surg.* **2020**, *10*, 779–788.

Li, C.; Liu, Y.; Li, D.; Wang, Q.; Zhou, S.; Zhang, H.; et al. Promising alternatives of CD47 monoclonal antibody: An injectable degradable hydrogel loaded with PQ912 for postoperative immunotherapy effectively blocks CD47-sirpα signal. *Theranostics.* **2022**, *12*, 4581–4598.

Li, F.; Yeh, S.; Shi, Q.; Wang, P.; Wu, H.; Xin, J. A. A novel thermal-driven self-assembly method to prepare albumin nanoparticles: formation kinetics, degradation behavior and formation mechanism. *AAPS PharmSciTech.* **2022**, *23* (7), 250.

Li, S.-N.; Yu, Z.-R.; Guo, B.-F.; Guo, K.-Y.; Li, Y.; Gong, L.-X.; et al. Environmentally stable, mechanically flexible, self-adhesive, and electrically conductive Ti3C2TX MXene hydrogels for wide-temperature strain sensing. *Nano Energy.* **2021**, *90*, 106502.

Li, X.; Yin, Q.; Chen, A. W.; Wang, J. Solubility of hydroquinone in different solvents from 276.65 K to 345.10 K. *Journal of Chemical & Engineering Data.* **2006**, *51*, 127-129.

Lin, F.-W.; Chen, P.-Y.; Wei, K.-C.; Huang, C.-Y.; Wang, C.-K.; and Yang, H.-W. Rapid in situ MRI traceable gel-forming dual-drug delivery for synergistic therapy of brain tumor. *Theranostics.* **2017**, *7*, 2524–2536.

Liu, J.; Qu, S.; Suo, Z.; and Yang, W. Functional hydrogel coatings. *Natl. Sci. Rev.* **2020**, *2*, 254.

Liu, W.; Sun, J.; Sun, Y.; Xiang, Y.; Yan, Y.; Han, Z.; et al. Multifunctional injectable protein-based hydrogel for bone regeneration. *Chem. Eng. J.* **2020b**, *394*, 124875.

Liu, Y.; Wang, L.; Lu, H.; and Huang, Z. Double-network shape memory organohydrogel prepared by one-pot polymerization. *Mater. Chem. Front.* **2021**, *5*, 8056–8065.

Mao, S.-Y.; Peng, H.-W.; Wei, S.-Y.; Chen, C.-S.; and Chen, Y.-C. Dynamically and spatially controllable albumin-based hydrogels for the prevention of postoperative adhesion. *ACS Biomaterials Sci. Eng.* **2021**, *7*, 3293–3305.

Migneault, I.; Dartiguenave, C.; Bertrand, M. J.; Waldron, K. C. Glutaraldehyde: behavior in aqueous solution, reaction with proteins, and application to enzyme crosslinking, *Biotechniques*. **2004**, *37* (5). 790–802.

Müller, R. H.; Jacobs, C.; Kayser, O. Nanosuspensions as particulate drug formulations in therapy. Rationale for development and what we can expect for the future. *Adv. Drug Deliv*. Rev. **2004**, *47* (1), 3–19.

Nnyigide, O. S.; Hyun, K. The protection of bovine serum albumin against thermal denaturation and gelation by sodium dodecyl sulfate studied by rheology and molecular dynamics simulation. *Food Hydrocoll*. **2020**, *103*, 105656.

Okuda, K.; Urabe, I.; Yamada, Y.; Okada, H. Reaction of glutaraldehyde with amino and thiol compounds. *J. Ferment. Bioeng*. **1991**, *71*, 100–105.

Onafuye, H;, Pieper, S.; Mulac, D.; Cinatl, J. Jr.;, Wass, M. N.; Langer, K.; Michaelis, M. Doxorubicin-loaded human serum albumin nanoparticles overcome transporter-mediated drug resistance in drug-adapted cancer cells. *Beilstein J Nanotechnol*. **2019**, *10*, 1707-1715.

Ong, J.; Zhao, J.; Justin, A. W.; Markaki, A. E. Albumin-based hydrogels for regenerative engineering and cell transplantation. *Biotechnol. Bioeng*. **2019**, *116* (12), 3457–3468.

Pardi, N., Hogan, M., Porter, F. *et al.* mRNA vaccines — a new era in vaccinology. *Nat Rev Drug Discov.* **2018**, *17*, 261–279.

Patra, J. K.; Das, G.; Fraceto, L. F.; Campos, E. V. R.; Rodriguez-Torres, M. D. P.; Acosta-Torres, L. S.; Diaz-Torres, L. A.; Grillo, R.; Swamy, M. K.; Sharma, S.;

Habtemariam, S.; Shin, H. S. Nano based drug delivery systems: recent developments and future prospects. *J Nanobiotechnology*. **2018**, *16* (1), 71.

Phan, V. H. G.; Le, T. M. D.; Janarthanan, G.; Ngo, P.-K. T.; Lee, D. S.; and Thambi, T. Development of bioresorbable smart injectable hydrogels based on thermo-responsive copolymer integrated bovine serum albumin bioconjugates for accelerated healing of excisional wounds. *J. Industrial Eng. Chem.* **2021**, *96*, 345–355.

Qi, Y.; Yuan, Y.; Qian, Z.; Ma, X.; Yuan, W.; and Song, Y. Injectable and self-healing polysaccharide hydrogel loading molybdenum disulfide nanoflakes for synergistic photothermal-photodynamic therapy of breast cancer. *Macromol. Biosci.* **2022**, *22*, e2200161.

Qu, N.; Song, K.; Ji, Y.; Liu, M.; Chen, L.; Lee, R. J.; Teng, L. Albumin nanoparticle-based drug delivery systems. *Int. J. Nanomedicine*. **2024**, *10* (19), 6945–6980.

Qu, Y.; Li, J.; Jia, X.; Yin, L. Schiff Base-Crosslinked Tetra-PEG-BSA Hydrogel: Design, Properties, and Multifunctional Functions. *J Funct Biomater*. **2025,** *16* (2), 69.

Raghuwanshi, V. S.; Yu, B.; Browne, C.; and Garnier, G. Reversible pH responsive bovine serum albumin hydrogel sponge nanolayer. *Front. Bioeng. Biotechnol.* **2020**, *8*, 573.

Raja, W. K.; Maccorkle, S.; Diwan, I. M.; Abdurrob, A.; Lu, J.; Omenetto, F. G.; Kaplan, D. L. Transdermal delivery devices: fabrication, mechanics and drug release from silk. *Small*. **2013**, *9* (21), 3704–3713.

Rathod, A. G.; Tiwari, P.; Shaily, J.; Tiwari, S. Stabilizing effect of quercetin upon bovine serum albumin as a model protein. *Colloids Surf. B: Biointerfaces*. **2025**, *252*, 114663.

Rauso, R.; Albani, G.; Salini, C.; Rugge, L.; Chirico, F.; and Tartaro, G. Continuum: Late onset complications secondary to polyacrylamide hydrogel-based filler for

rehabilitation of HIV-related facial lipoatropy. *Aesthetic Surg. J.* **2019**, *39*, 152–155.

Rezvani Ghomi, E.; Nourbakhsh, N.; Akbari Kenari, M.; Zare, M.; Ramakrishna, S. Collagen-based biomaterials for biomedical applications. *J. Biomed. Mater. Res. B.* **2021**, *109* (12), 1986–1999.

Robertson, D. M.; and Cavanagh, H. D. Pseudomonas aeruginosa keratitis in an atopic silicone hydrogel lens wearer with rosacea. *Eye Contact Lens*. **2005**, *31*, 254–256.

Saha, B.; Choudhury, N.; Seal, S.; Ruidas, B.; De, P. Aromatic nitrogen mustard-based autofluorescent amphiphilic brush copolymer as pH-responsive drug delivery vehicle. *Biomacromolecules*. **2019**, *20*, 546–557.

Sahoo, S. K.; Jain, T. K.; Reddy, M. K.; Labhasetwar, V. *Nano-sized carriers for drug delivery, in: O. Shoseyov, E. Levy* (Eds.), *NanoBioTechonology: BioInspired Devices and Materials of the Future*, Humana Press, Totowa, NJ. **2007**, 329–348.

Samant, H.; Amiri, H. S.; Zibari, G. B. Addressing the worldwide hepatocellular carcinoma: epidemiology, prevention and management. *J. Gastrointest. Oncol.* **2021**, *12*, 361–373.

Saufi, A. N. M.; Ridzwan, N. F. W.; Mohamad, S. B.; Tayyab, S.; Halim, A. A. A. Fluorometric and docking analysis of the complex formation between an anti-cancer drug, Chlorambucil and bovine serum albumin. *Indian J. Pharm. Educ. Res*. **2019**, *53*, 682–687.

Savjani, K. T.; Gajjar, A. K.; Savjani, J. K. Drug Solubility: Importance and Enhancement Techniques. *ISRN Pharmaceutics*. **2012**, 195727.

Serajuddin, A. T. M. Salt formation to improve drug solubility. *Advanced Drug Delivery Reviews*. **2007**, *59* (7), 603-616.

Shah, A.; Aftab, S.; Nisar, J.; Ashiq, M. N.; Iftikhar, F. J. Nanocarriers for targeted drug delivery. *Journal of Drug Delivery Science and Technology*. **2021**, *62*, 102426.

Shah, L.A.; Gul, K.; Ali, I. *et al.* Poly (*N*-vinyl formamide-*co*-acrylamide) hydrogels: synthesis, composition and rheology. *Iran Polym J*. **2022**, *31*, 845–856.

Sharma, B.; Fermanian, S.; Gibson, M.; Unterman, S.; Herzka, D. A.; Cascio, B.; et al. Human cartilage repair with a photoreactive adhesive-hydrogel composite. *Sci. Transl. Med*. **2013**, *5*, 1676.

Shi, C.; Li, S.; Li, C.; Liu, H.; Wang, Z.; Li, Y.; Li, M.; Zhang, X.; Mu, W.; Han, X. Bovine serum albumin-based hydrogels: Preparation, properties and biological applications. *Chemical Engineering Journal*. **2024**, *498,* 154651.

Siegel, R. L.; Kratzer, T. B.; Giaquinto, A. N.; Sung, H.; Jemal, A. Cancer statistics, 2025. *CA Cancer J. Clin*. **2025**, *75* (1), 10–45.

Smith, E. L.; Kanczler, J. M.; Gothard, D.; Roberts, C. A.; Wells, J. A.; White, L. J.; et al. Evaluation of skeletal tissue repair, part 1: Assessment of novel growth factor releasing hydrogels in an ex vivo chick femur defect model. *Acta biomater*. **2014**, *10*, 4186–4196.

Solanki, R.; Rostamabadi, H.; Patel, S.; Jafari, S. M. Anticancer nano-delivery systems based on bovine serum albumin nanoparticles: a critical review. *Int. J. Biol. Macromol*. **2021**, *193*, 528–540.

Solanki, R.; Srivastav, A. K.; Patel, S.; Singh, S. K.; Jodha, B.; Kumar, U.; Patel, S. Folate conjugated albumin as a targeted nanocarrier for the delivery of fisetin: in silico and in vitro biological studies. *RSC Adv*. **2024**, *14,* 7338–7349.

Sozer, S. C.; Akdogan, Y. Characterization of Water Solubility and Binding of Spin Labeled Drugs in the Presence of Albumin Nanoparticles and Proteins by Electron Paramagnetic Resonance Spectroscopy. *ChemistrySelect.* **2022**, *7*, e202103890.

Sozer, S. C.; Egesoy, T. O.; Basol, M.; Cakan-Akdogan, G.; Akdogan, Y. A simple desolvation method for production of cationic albumin nanoparticles with improved drug loading and cell uptake. *J. Drug Delivery Sci. Technol.* **2020**, *60*, 101931.

Sozer-Demirdas, S. C.; Erez, O.; Cakan-Akdogan, G.; Akdogan, Y. A green route to albumin/albumin polyelectrolyte complex nanoparticles in water with high drug loading for drug delivery. *International Journal of Biological Macromolecules*. **2025**, *322*, 3, 146978.

Spada, A.; Emami, J.; Tuszynski, J. A.; Lavasanifar, A. The Uniqueness of Albumin as a Carrier in Nanodrug Delivery. *Mol Pharm*. **2021**, *18* (5), 1862-1894.

Srivastava, A.; Prajapati, A. Albumin and functionalized albumin nanoparticles: production strategies, characterization, and target indications. *Asian Biomed.* **2020**, *14* (6), 217–242.

St Clair, M. B.; Bermudez, E.; Gross, E. A.; Butterworth, B. E. Recio, L. Evaluation of the genotoxic potential of glutaraldehyde. *Environ. Mol. Mutagen*. **1991**, *18* (2), 113–119.

Storan, E. R.; Nolan, U.; and Kirby, B. Allergic contact dermatitis caused by the tea tree oil-containing hydrogel Burnshield®. *Contact Dermat*. **2016**, *74*, 309–310.

Storp, B.; Engel, A.; Boeker, A.; Ploeger, M.; Langer, K. Albumin nanoparticles with predictable size by desolvation procedure. *J Microencapsul*. **2012**, *29* (2), 138-46.

Subia, B. & Kundu, S. Drug loading and release on tumor cells using silk fibroin–albumin nanoparticles as carriers. *Nanotechnology*. ***2013***, *24*, 035103.

Sudlow, G.; Birkett, D. J.; Wade, D. N. The characterization of two specific drug binding sites on human serum albumin. *Mol Pharmacol*. **1975**, *11* (6), 824-32.

Suk, J. S.; Xu, Q.; Kim, N.; Hanes, J.; Ensign, L. M. PEGylation as a strategy for improving nanoparticle-based drug and gene delivery. *Adv. Drug Deliv. Rev.* **2016**, *99*, 28–51.

Sun, X. D. and Holley, R. A. Factors influencing gel formation by myofibrillar proteins in muscle foods. *Comp. Rev. Food Sci. Food Saf.* **2011**, *10*, 33–51.

Suwannasom, N.; Sriaksorn, N.; Thepmalee, C.; Khoothiam, K.; Prapan, A.; Baumler, H.; Thephinlap, C. Curcumin-loaded albumin submicron particles with potential as a cancer therapy: an in vitro study. *Beilstein J. Nanotechnol.* **2023**,*14,* 1127–1140.

Tang, X.; Wang, G.; Shi, R.; Jiang, K.; Meng, L.; Ren, H.; Wu, J.; Hu, Y. Enhanced tolerance and antitumor efficacy by docetaxel-loaded albumin nanoparticles. *Drug Deliv.* **2016**, *23*, 2686–2696.

Tatlidil, D.; Ucuncu, M.; Akdogan, Y. Physiological concentrations of albumin favor drug binding. *Physical Chemistry Chemical Physics.* **2015**, *17* (35), 22678-22685.

Teir, M. M. A.; Ghithan, J.; Darwish, S.; Abu-Hadid, M. M. Multi-Spectroscopic Investigation of the Interactions between Cholesterol and Human Serum Albumin. J*ournal of Applied Biological Sciences.* **2012**, *6* (3), 45-55.

Thapa, R. K.; Choi, H. G.; Kim, J. O.; Yong, C. S. Analysis and optimization of drug solubility to improve pharmacokinetics. *J. Pharm. Investig.* **2017**, *47*, 95–110.

Torricella, F.; Pierro, A.; Mileo, E.; Belle, V.; Bonucci, A. Nitroxide spin labels and EPR spectroscopy: A powerful association for protein dynamics studies. *Biochimica et Biophysica Acta (BBA) - Proteins and Proteomics.* **2021**, *1869* (7), 140653.

Tsai, P. H.; Wang, M. L.; Chang, J. H.; Yarmishyn, A. A.; Nguyen, P. N. N.; Chen, W.; Chien, Y.; Huo, T. H.; Mou, C. Y.; Chiou, S. H. Dual delivery of HNF4α and cisplatin by mesoporous silica nanoparticles inhibits cancer pluripotency and tumorigenicity in hepatoma derived CD133-expressing stem cells. *ACS Appl. Mater. Interfaces.* **2019**, *11*, 19808–19818.

Tuinier, R.; de Kruif, C.G. Stability of casein micelles in milk. J. *Chem. Phys.* **2002**, *117*, 1290–1295.

Verma, D.; Gulati, N.; Kaul, S.; Mukherjee, S.; Nagaich, U. Protein based nanostructures for drug delivery. *J. Pharm*. **2018**, 9285854.

Von Storp, B.; Engel, A.; Boeker, A.; Ploeger, M.; Langer, K. Albumin nanoparticles with predictable size by desolvation procedure. *J. Microencapsul*. **2012**, *29*, 138–146.

Wang, J.; He, H. L.; Cooper, R. C.; Yang, H. In situ-forming polyamidoamine dendrimer hydrogels with tunable properties prepared via Aza-Michael addition reaction. *ACS Appl. Mater. Interfaces.* **2017**, *9*,10494–10503.

Wang, J.; Williamson, G. S.; Yang, H. Branched polyrotaxane hydrogels consisting of alpha-cyclodextrin and low-molecular-weight four-arm polyethylene glycol and the utility of their thixotropic property for controlled drug release. *Colloids Surf. B Biointerfaces.* **2018**, *165*,144–149.

Wang, L. C.; Ding, H.; Zhao, J. H.; Song, C. Y.; Wang, J. S. Solubility of Isonicotinic Acid in 4-Methylpyridine + Water from (287.65 to 361.15) K. *Journal of Chemical & Engineering Data.* **2008**, *53* (11), 2544-2546.

Wichterle, O.; and Lím, D. Hydrophilic gels for biological use. *Nature*. **1960**, *185*, 117–118.

Willcox, M. D. P.; Argueso, P.; Georgiev, G. A.; Holopainen, J. M.; Laurie, G. W.; Millar, T. J.; Papas, E. B.; Rolland, J. P.; Schmidt, T. A.; Stahl, U.; Suarez, T.; Subbaraman, L. N.; Ucakhan, O. O.; Jones, L. TFOS DEWS II Tear Film Report. *The Ocular Surface*. **2017**, *15* (3), 366-403.

Williams, H. D.; Trevaskis, N. L.; Charman, S. A.; Shanker, R.; Charman, W. N.; Pouton, C. W.; Porter, C. J. H. Strategies for Enhancing Oral Bioavailability of Poorly Water-Soluble Drugs. *Pharmacol. Rev.* **2013**, *65* (2), 315–499.

Wu, D.; Zhu, L.; Li, Y.; Zhang, X.; Xu, S.; Yang, G.; Delair, T. Chitosan-based colloidal polyelectrolyte complexes for drug delivery: a review. *Carbohydr. Polym.* **2020**, *238*, 116126.

Wu, K. Y.; Qian, S. Y.; Faucher, A.; Tran, S. D. Advancements in Hydrogels for Corneal Healing and Tissue Engineering. *Gels.* **2024**, *10*, 662.

Xie, C.; Liu, G.; Wang, L.; Yang, Q.; Liao, F.; Yang, X.; Xiao, B.; Duan, L. Synthesis and Properties of Injectable Hydrogel for Tissue Filling. *Pharmaceutics.* **2024**, *16*, 430.

Xing, L.; Dorrepaal, S. J.; Gale, J. Survey of intravitreal injection techniques and treatment protocols among retina specialists in Canada. *J. Can. D Ophtalmol.* **2014**, *49*, 261–266.

Yamada, Y.; and Schneider, J. P. Fragmentation of injectable bioadhesive hydrogels affords chemotherapeutic macromolecules. *Biomacromolecules.* **2016**, *17*, 2634–2641.

Yamasaki, M.; Yano, H.; Aoki, K. Differential scanning calorimetric studies on bovine serum albumin: I. Effects of pH and ionic strength. *Int J Biol Macromol.* **1990**, *12* (4), 263-8.

Yang, H.; Hou, Q.; and Ding, C. Denatured bovine serum albumin hydrogel- based electrochemical biosensors for detection of IgG. *Mikrochim. Acta.* **2022**, *189*, 400.

Yoon, H.; Lee, H.; Shin, S. Y.; Jodat, Y. A.; Jhun, H.; Lim, W.; et al. Photo- cross-linkable human albumin colloidal gels facilitate in vivo Vascular integration for regenerative medicine. *ACS omega.* **2021**, *6*, 33511–33522.

Yordanov, G. G.; Bedzhova, Z. A.; Dushkin, C. D. Preparation and physicochemical characterization of novel chlorambucil-loaded nanoparticles of poly (butylcyanoacrylate), *Colloid Polym. Sci.* **2010**, *288*, 893–899.

Yu, J.; Xu, X.; Yao, F. L.; Luo, Z. C.; Jin, L.; Xie, B. B.; Shi, S.; Ma, H. X.; Li, X. Y.; Chen, H. In situ covalently cross-linked PEG hydrogel for ocular drug delivery applications. *Int. J. Pharm*. **2014**, *470*, 151–157.

Zhang, H.; Ye, Z. W.; Lou, Y. J. Metabolism of chlorambucil by rat liver microsomal glutathione S-transferase. *Chem. Biol. Interact*. **2004**, *149*, 61–67.

Zhang, Q.; Zhang, L.; Zemin, L.; Xie, X.; Gao, X.; Xu, X. Inducing controlled release and increased tumor-targeted delivery of chlorambucil via albumin/liposome hybrid nanoparticles. *AAPS PharmSciTech*. **2017**, *18*, 2977–2986.

Zhao, Z.; Hu, R.; Shi, H.; Wang, Y.; Ji, L.; Zhang, P.; et al. Design of ruthenium-albumin hydrogel for cancer therapeutics and luminescent imaging. *J. Inorg. Biochem*. **2019**, *194*, 19–25.

Zheng, H.; Zuo, B. Functional silk fibroin hydrogels: preparation, properties and applications, *J. Mater. Chem. B*. **2021**, *9* (5),1238–1258.

Zhou, X.; Luo, Z.; Baidya, A.; Kim, H. J.; Wang, C.; Jiang, X.; Qu, M.; Zhu, J.; Ren, L.; Vajhadin, F.; Tebon, P.; Zhang, N.; Xue, Y.; Feng, Y.; Xue, C.; Chen, Y.; Lee, K.; Lee, J.; Zhang, S.; Xu, C.; Ashammakhi, N.; Ahadian, S.; Dokmeci, M. R.; Gu, Z.; Sun, W.; Khademhosseini, A. Biodegradable beta-cyclodextrin conjugated gelatin methacryloyl microneedle for delivery of water-insoluble drug. *Adv. Healthc. Mater*. **2020**, *9* (11), e2000527

VITA

Name and Surname: Sümeyra Çiğdem SÖZER DEMİRDAŞ

EDUCATION

2021-2025	Doctor of Philosophy *Department of Materials Science and Engineering, IZTECH*
2019-2021	Master of Science *Department of Materials Science and Engineering, IZTECH*
2014-2019	Bachelor of Science *Department of Chemistry, IZTECH*

WORK EXPERIENCE

2023-	Research Assistant *Department of Materials Science and Engineering, IZTECH*

CONFERENCES

21-23.08.2025	Oral Presentation *16th International Conference on Nanotechnology: Fundamentals and Applications (ICNFA 2025), Paris/France*
19-21.09.2023	Oral Presentation *22nd International Metallurgy and Materials Congress (IMMC 2024), Istanbul/Türkiye*

PUBLICATIONS

Sozer-Demirdas, S. C.; Akdogan, Y. "Albumin Polyelectrolyte Hydrogel Complex Formation for Therapeutic Systems". (In preparation)

Sozer-Demirdas, S. C.; Erez, O.; Cakan-Akdogan, G.; Akdogan, Y. A green route to albumin/albumin polyelectrolyte complex nanoparticles in water with high drug loading for drug delivery. *International Journal of Biological Macromolecules*. **2025**, *322* (3), 146978.

Akdogan, Y.; Sozer, S. C.; Akyol, C.; Basol, M.; Karakoyun, C.; Cakan-Akdogan, G. Synthesis of albumin nanoparticles in a water-miscible ionic liquid system, and their applications for chlorambucil delivery to cancer cells. *J. Mol. Liq*. **2022**, *367*, 120575.

Cakan-Akdogan, G.; Ersoz, E.; Sozer, S.C.; Gelinci, E. An in vivo zebrafish model reveals circulating tumor cell targeting capacity of serum albumin nanoparticles. J. *Drug Deliv. Sci. Technol*. **2022**, *75*, 103658.

Sozer, S. C.; Akdogan, Y. Characterization of Water Solubility and Binding of Spin Labeled Drugs in the Presence of Albumin Nanoparticles and Proteins by Electron Paramagnetic Resonance Spectroscopy. *ChemistrySelect*. **2022**, *7,* e202103890.

Sozer, S. C.; Egesoy, T. O.; Basol, M.; Cakan-Akdogan, G.; Akdogan, Y. A simple desolvation method for production of cationic albumin nanoparticles with improved drug loading and cell uptake. *J. Drug Delivery Sci. Technol*. **2020**, *60*, 101931.